Mathematical models for atherosclerotic plaque evolution

Proefschrift

ter verkrijging van de graad van doctor
aan de Technische Universiteit Delft,
op gezag van de Rector Magnificus prof. ir. K.C.A.M. Luyben,
voorzitter van het College voor Promoties,
in het openbaar te verdedigen op maandag 09 december 2013 om 12.30 uur

door

Muhammad Atif Khan BULELZAI,
Master of Science in Mathematics, University of Sindh, Pakistan

geboren te Hyderabad, Pakistan.

Dit proefschrift is goedgekeurd door de promotor:
Prof. dr. ir. A. W. Heemink

Copromotor:
Dr. J.L.A. Dubbeldam

Samenstelling promotiecommissie:

Rector Magnificus	voorzitter
Prof. dr. ir. A. W. Heemink	Technische Universiteit Delft, promotor
Dr. J.L.A. Dubbeldam	Technische Universiteit Delft, copromotor
Prof. dr. ir. C. Vuik	Technische Universiteit Delft
Prof. dr. J. Molenaar	Wageningen UR
Prof. dr. ir. J. Westerweel	Technische Universiteit Delft
Dr. S.M. Wieczorek	University of Exeter, UK
Dr. F. Gijsen	Erasmus Medical University
Prof.dr.ir. H.X. Lin	Technische Universiteit Delft, reservelid

This thesis has been completed in fulfillment of the requirements of the Delft University of Technology for the award of the Ph.D. degree. The research described in this thesis was carried out in the Delft Institute of Applied Mathematics, Delft University of Technology, The Netherlands.

ISBN 978-94-6186-241-9

To my parents

Contents

List of Figures

List of Tables

Chapter 1

Introduction

The fundamental cause of trouble in the world is that the stupid are cocksure while the intelligent are full of doubt.

Bertrand Russell

The main idea of this dissertation is to examine complex dynamics associated with the plaque growth in human arteries which leads to fatal consequences to human life. It is a chronic disease better known as *Atherosclerosis*, and its accurate clinical and mathematical understanding is essential to unravel the important risk factors in its development and offer a cure. This disease is very complex as it involves many chemical agents, complicated blood flow profiles, genetic make-up of an individual etc. Many of them influence each other via chemical reactions or biomechanical interactions. To date, atherosclerosis is still only partly understood by physiological and clinical methods. From the mathematical modeling point of view, it is a challenge to contribute to the understanding of this disease. In recent times, many studies are conducted *in vivo* (experiments in living organisms), *in vitro* (experiments in laboratory) and *in silico* (experiments using computers), in order to determine the salient features that might affect and control the biochemical and biomechanical reactions in the arteries. Mathematical models, on one hand, could provide deeper insight into such complex phenomena and assist in predicting their evolution. Essentially, various techniques for mathematical analysis are utilized, such as the theory of dynamical systems, bifurcation analysis, numerical analysis etc. Fluid mechanics is another discipline, which is a prerequisite to determine the interactions between blood flow and artery walls. In this thesis, we present the mathematical and computational analyses on the formation of plaques in arteries. We consider atherosclerosis as a coupled problem for both blood flow conditions and biochemical evolution of the plaque constituents involved. We explore the interaction of different important plaque constituents on short time scales, and its accumulation into the artery on a longer time scale to clearly distinguish which factors are the most relevant and what can be inferred from a mathematical perspective.

In this Introduction, we explain the fundamentals of the development of atherosclerosis by reviewing the early and most prominent theories available in literature. We want to emphasize that all the previous work can be unified into a single framework commonly called the *stages of development* for atherosclerotic plaques (Libby et al. 2002). Furthermore, we dis-

cuss the basic vascular dynamics and its impact on evolution of this disease. Finally, we conclude this chapter with a brief outline for this thesis.

1.1 Background

Arteriosclerosis is the hardening of human arteries. One of its variant is atherosclerosis, which is hardening of arteries due to plaque deposition. It is the most prevalent form of cardiovascular disease and is characterized by the progressive accumulation of lipids and fibrous elements in large arteries. It is believed that atherosclerosis is one of leading causes of death in the industrialized world by 2020 (Mach 2005). The main causes for this disease known are high blood pressure, diabetes, high levels of cholesterol, smoking, age and genetic make-up (Kuvin and Kimmelstiel 1999). People with a parent or sibling who has had atherosclerosis or cardiovascular diseases, have a much higher risk of developing atherosclerosis than others.

During the 1970s, atherosclerosis was believed to be caused by deposition of lipids on arterial walls due to a strong correlation between hypercholesterolaemia and atheroma (Ross and Harker 1976). The advancements in vascular biology and rapid clinical investigations have suggested that the disease is initialized by the dysfunction of internal elastic lamina. Several theories have been proposed regarding the pathogenesis of atherosclerosis (Schwartz and Reidy 1987, Davis 1986, Libby et al. 2002). The most prominent is 'response-to-injury' theory, proposed by Ross and Glomset (Ross and Glomset 1976a, Ross and Glomset 1976b) that essentially predicts that the injury of endothelium is responsible for platelet adhesion and aggregation. They proposed that the growth factors released from the platelets are responsible for smooth muscle migration into the intima as they secrete components of extra cellular matrix. Another aspect was presented by (Ross 1986) that the monocytes and macrophages also contribute to the pathogenesis of atherosclerosis due to the inflammatory response. Uptill now numerous *in vivo* and *in vitro* studies have been performed to understand the mechanisms responsible for atherogenesis. It is quite well established that atherosclerosis is a multifocal, smoldering, immuno-inflammatory disease of medium-sized and large arteries fuelled by lipids. Endothelial cells, leukocytes, and intimal smooth muscle cells are the major players in the development of this disease (Falk 2006). Furthermore, (Libby et al. 2002, Hansson and Libby 2006, Gotlieb 2007) have reviewed previous existing research clinically and explained that the theories of origin of atherosclerosis are not mutually exclusive and are all linked. They have explained that all the hypotheses/theories can be combined into one by understanding the progression of atherosclerosis in different stages. Many of their experiments both, *in-vivo* and *in-vitro* have suggested that plaque evolution can be divided into mainly four stages of atherosclerosis. These stages of development of

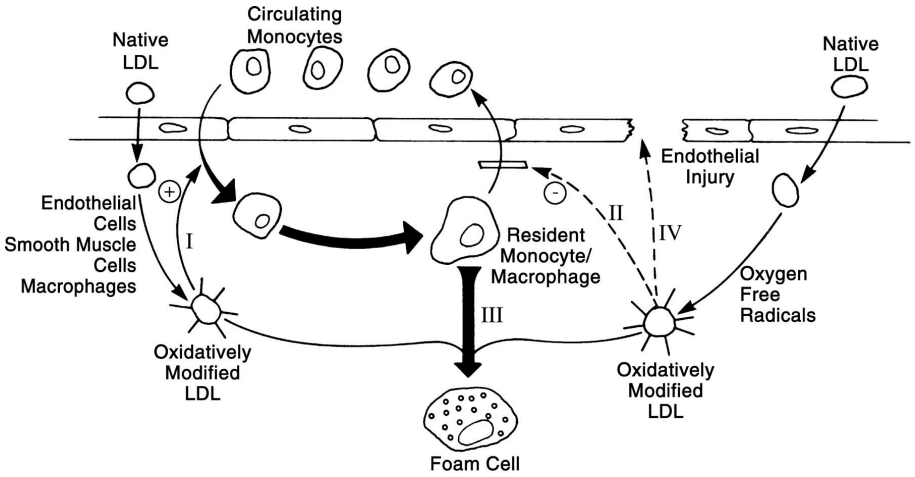

Figure 1.1: *The pathogenesis of atherosclerosis: Endothelial injury triggers the complex mechanism shown in the form of a diagram.*

plaques are explained below and also depicted in Figure 1.2. As such, the development of plaque is divided into four stages viz., 'Endothelial injury', 'Oxidation of LDL', 'Inflammatory process' and 'Calcification'. We explain each of them in next subsections.

1.1.1 Endothelial injury

The 'response to injury' hypothesis proposes that the primary event in atherogenesis is endothelial damage and dysfunction which disrupts properties resulting in platelet and leukocyte adhesion (resulting in recruitment of monocytes), thrombosis (formation of blood clots), smooth muscle proliferation, vasospasm (causing ischemia), lipid accumulation and ultimately atheroma (Ross 1986). Endothelial derived nitric oxide regulates vessel tone, inhibits platelet activation, adhesion and aggregation (Upchurch et al. 1996). It also limits smooth muscle proliferation and modulates endothelial leukocyte interactions (Luscher et al. 1996). On the other hand, It was observed that the wall shear stress can change the morphology and orientation of endothelial cell layer (Shaaban and Deurinckx 2000). Endothelial cells are subjected to elevated levels of wall shear stress tend to elongate and align in the direction of flow, whereas those experiencing low or oscillatory wall shear stress remain more rounded and have no preferred alignment pattern (Levesque and Nerem 1985). This implies that the endothelial dysfunction is directly associated with the flow regions. In Figure 1.1, the dysfunction of endothelial layer is depicted. As it is a complex phenomena involving a lot of secretion of signaling molecules, we assume a constant supply of LDL through this barrier and consider it as a parameter in the first part of the thesis. Later, we consider the endothelial

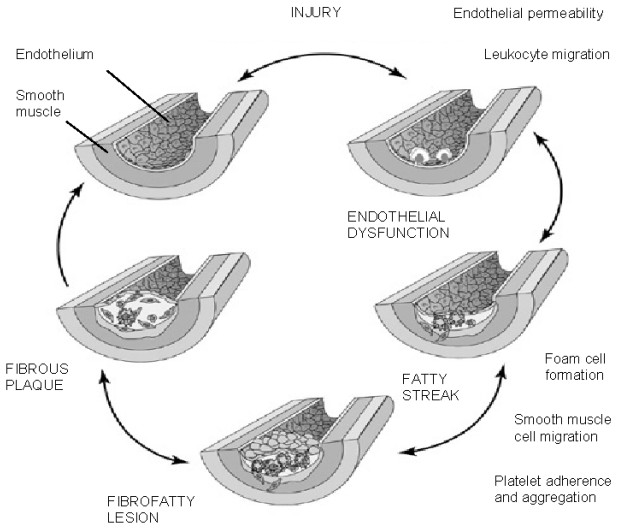

Figure 1.2: *Four different stages of development of atherosclerosis.*

shear stress dependence on the evolution of radius of the artery.

1.1.2 Oxidation of LDL

Low-density lipoproteins (LDL) are one out of five different groups of lipoproteins that stream through the blood and are supplied to other parts of the human body (others include Chylomicrons, VLDL, IDL and HDL). The LDL particles are the aggregates of lipids and proteins. The most abundant lipid constituents are triacylglycerols, free cholesterol, cholesterol esters and phospholipids (especially phosphatidylcholine and sphingomyelin). These LDL particles are formed in the liver and gut, and carry cholesterol, which they transfer to different cells and tissues to provide lipid for the use of cellular metabolism. High density lipoprotein (HDL) on the other hand, performs the reverse role of transporting lipids to the liver for excretion. That is why, it is very common to call LDL a bad cholesterol and HDL a good cholesterol. HDL particles are small and dense and have the same structure as LDL, although LDL is more dense (Cobbold et al. 2002). LDL consists of a lipid core, a surface protein and some antioxidant defences such as ubiquinol-10 and α-tocopherol (vitamin E) (Bowry et al. 1992). Both LDL and HDL can diffuse through the endothelium (the layer of the artery) and enter into the intima while being transported into the blood. The endothelium takes the role of a selectively permeable barrier between blood and intima, and consists of

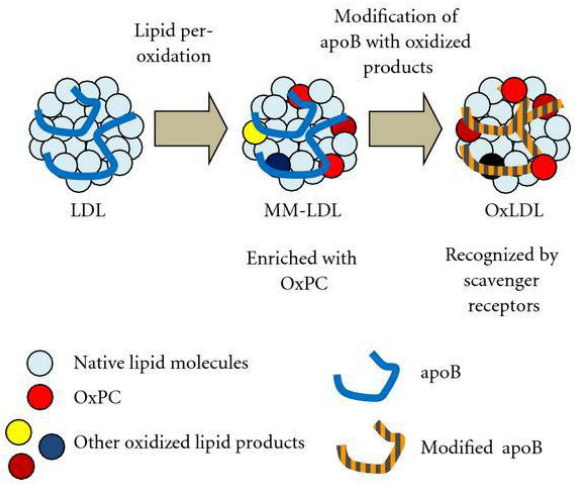

Figure 1.3: *The oxidation of LDL particles after it enters into the intima. The modified ox-LDL being the potential threat to the defence system.*

tightly packed endothelial cells (Mckay et al. 2005). Endothelial cells adopt to the flow conditions. For laminar and uniform blood flow in the artery, their shape remains ellipsoidal. Regions where the flow conditions are not normal, for example, turbulent or stagnant, the endothelial cells are more polygonal in their shape. For the later regions, the permeability for LDL becomes higher and thus more LDL can enter the intima. In the lumen, antioxidants are present that is why the LDL/HDL do not oxidize; but as these particles enter the intima, which is not a protected environment, the free radicals penetrate into the LDL particle and destroy the antioxidant (vitamin E). Later, they do the same with surface protein and then to the lipid in the core. The oxidized-LDL particles are recognized by the scavenger receptors (Parthasarathy et al. 1990). This triggers the immune system response and recruitment of monocytes takes place later on (See Figure 1.2).

1.1.3 Inflammatory process

After oxidation of LDL (formation of ox-LDL), being recognized by the scavenger receptors, the endothelial cells display adhesion molecules to the blood at the permeable interface. Blood containing the immune system (monocytes, T-cells etc.) recognizes the threat and thus these monocytes enter into the intima. This initiates leukocyte locomotion (chemotaxis) and so the monocytes and T-cells squeeze through gaps between endothelial cells and migrate up the chemo-attractant gradient (Mckay et al. 2005). A series of reactions take place within

the intima in order to attract ox-LDL to the site. Monocytes multiply themselves to become macrophages. These macrophages digest ox-LDL and simultaneously smooth muscle cells begin migrating from the media and fatty streak is formed. After macrophages digest the ox-LDL content, their size increases and they do not survive in the vasculature. These macrophages are called foam cells after they digested the lipid core. A fibrous cap starts forming by the smooth muscle cells and collagen in the vasculature. Artery starts expanding by the elastic wall (media) as the necrotic core grows further. This phenomenon is called remodeling. There is a limit to the expansion of arterial wall, when it reaches its maximum point, the plaque formation bulges into the lumen (Davis 2005).

1.1.4 Plaque Growth and Calcifications

At this stage a change in the geometry of vasculature is clearly witnessed (See Figure 1.2). The plaque growth is attributed to a combination of debris of cellular apoptosis (such as macrophages and foam cells), and migration of smooth muscle cells and collagen. The majority of plaque is found in areas of high density of macrophages and foam cells. Unlike the natural cell death, apoptosis is the main contributor in the evolution of atherosclerotic plaques. It is believed that the foam cell apoptosis is the specific cause of lipid core in the atherosclerotic plaque (Mckay et al. 2005).

1.2 Blood Vessels

There are mainly two kind of arteries which are classified as being muscular and elastic. Elastic arteries are the largest, ranging from 1cm to 2.5cm in diameter. They have more significance as they can adopt to the applied blood pressure and other bodily mechanisms. The majority of elastic arteries reside near the heart. They include the aorta, carotid, illiac and pulmonary. Arteries are designed to minimize internal friction and flow resistance, and to maximize the strength of the wall. This is very simple to understand: arteries, which are near the heart, are organized in a fashion that they are quite elastic containing the fibers of collagen and elastin. Once they gather the blood out to the major regions of the body, there is a transition in the structure of the arterial wall. The collagen and elastic fibers get reduced in number and all that remains is smooth muscle cells (which is what makes an artery more muscular). Figure 1.2 shows a healthy elastic artery.

On a microscopic level, arteries are divided into three layers, which are known as *Intima*, *Media* (tunica media) and *Adventitia* (tunica externa). The intima is nearest to the lumen where endothelial layer separates it with flow of blood. The intima has a lining of endothelial cells which are polygonal, oval or fusiform and have very distinct round or oval nuclei. It is an elastic structure that thickens with age, disease and topography. In atherosclerosis, en-

dothelial cells play a vital role as they are closest cells (within intima) that adapt to the blood pressure, shear stresses and other mechanical factors of animal species. It is known that pathological changes of the intimal components may be associated with atherosclerosis; the most common disease of arterial walls. It involves deposition of fatty substances, calcium, collagen fibers, cellular waste products and fibrin (a clotting material in the blood). The resulting build-up is called atherosclerotic plaque, and it may be very complex in geometry and biochemical composition. In later stages, the media is also affected. These pathological changes are associated with significant alterations in the mechanical properties of the arterial wall. Hence, the mechanical behavior of atherosclerotic arteries differs significantly from that of healthy arteries (Holzapfel and Gasser 2000).

The tunica media is the second layer of arteries consisting of smooth muscle cells and in the case of elastic arteries, they also consist of elastin and collagen fibers. This layer is separated from the intima and the adventitia both by internal elastic lamina and external elastic lamina. When smooth muscle cells contract (*vasoconstriction*), the lumen gets smaller and blood pressure rises. When it expands (*vasodilation*), the lumen gets bigger, lowering the blood pressure. The adventitia being the outermost layer, contains fibroblasts and fibrocytes which produce elastin and collagen. This layer provides the reinforcement to the artery. For atherosclerosis, its importance lies in the fact that it produces collagen fibers, which contributes to atherosclerotic plaques.

1.3 Vascular Dynamics

Vascular dynamics is an important factor in the pathogenesis of atherosclerosis. It involves the laws of fluid dynamics applied to the tissue response of the blood vessels. Continuous blood flow governed by the laws of fluid mechanics is instrumental to the development and evolution of biological tissues in the vaso vasorum (network of blood vessels). The mechanical blood properties at the site of atherosclerotic lesions are found to be different compared to the sites with no such lesions. The motion of blood in the vessels can be in the form of laminar streamlines or turbulent flow. In turbulent motion, the blood flows irregularly in eddying motion at different sites of the vessel during various instances. In laminar flow, the motion of blood is in straight streamlines. In the presence of atherosclerotic plaques, the flow characteristics at sites of turbulent motion change drastically, causing flow disturbances and high pressure gradients. The blood flow is governed by the pulsation of the heart muscle which provides pressure to drive the blood into the whole body (circulatory system). The recurring pulsation of the heart provides arteries to adopt themselves on a given time in a way that the blood is transferred to all parts of the body. Thus, this pressure-flow relationship governs the

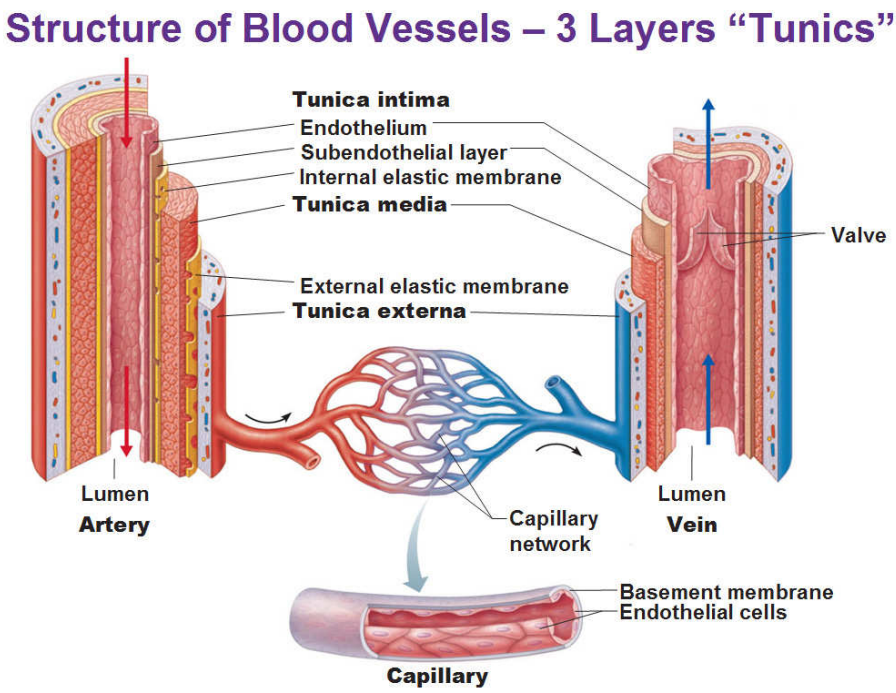

Figure 1.4: *The layers within an artery: Intima, Media and Externa along with their sublayers.*

arterial movement of the blood. The blood viscosity plays a vital role in the ongoing flow behavior. It is known that in small arteries, the viscosity is not constant, implying that blood behaves in non-newtonian fashion, but in medium and large arteries, the shear stresses are smaller and the blood viscosity can be regarded as constant (Dormandy 1970).

One of the most important consequences of the blood flow profile in vessels is the shear stress applied at their walls. The shear stress is the parallel or tangential force onto the wall of the arteries, the endothelium. The wall shear stress, or endothelial shear stress, is the product of blood viscosity and the shear rate. The shear rate is the velocity gradient normal to the boundary (the wall). It is widely confirmed that atherosclerosis in adult human beings develops preferentially in arterial regions where wall shear stress is low (Caro 2009). Furthermore, the arterial wall mass transport is more complicated and appears to be a very important factor in atherogenesis.

1.4 Outline and motivation of the thesis

As described in (Hansson and Libby 2006, Libby et al. 2002, Mckay et al. 2005), there are mainly four stages in the development of atheroma in the arteries (as shown in Figure 1.2). These stages being: (1). Lipoproteins entering the intima and their oxidation, (2). The inflammatory process, (3). Plaque growth: SMC migration and apoptosis in the vasculature and (4). Plaque instability: SMC and EC apoptosis and cap degradation. Though comprehensive guidelines are given in (Mckay et al. 2005) for the modeling of atherosclerosis as a biochemical process, a detailed analysis is not carried out. After a careful review of literature, we came across with the following objectives and recommendations.

- There is need for all four stages of atherosclerosis to be fully understood and modeled more realistically. In recent times, there have been many mathematical models (Cobbold et al. 2002, Khatib et al. 2007, Khatib et al. 2009, Ibragimov et al. 2005, Ougrinovskaia et al. 2010, Calvez et al. 2009) that have studied certain aspects of atherosclerosis. But all of them, somehow, lack the analysis of the time scale these biological processes evolve and concentrated mainly on the initial stage of atherosclerosis. In the wake of these models, a long term analysis of atherosclerosis is desirable as mentioned in (Zohdi et al. 2004).

- It is also desirable to take into account, the blood flow and its coupling to the biological evolution of species (LDL, ox-LDL and others).

- In models like (Cobbold et al. 2002, Khatib et al. 2007, Khatib et al. 2009, Ibragimov et al. 2005, Ougrinovskaia et al. 2010, Calvez et al. 2009), monocytes and macrophages are not distinguished. Furthermore, there is no model yet to our knowledge, which has separate equations for monocytes, macrophages, ox-LDL, radius of the artery and foam cells. It is desirable to understand the key roles each of these particles play in time evolution of atherosclerotic plaques.

In this thesis, we consider the evolution of the main constituents of plaques which include, LDL, ox-LDL, monocytes, macrophages and foam cells. We assume a constant supply of LDL particles from the lumen to the intima and denote it with the dimensionless parameter d and later on, we consider its evolution as a convection-diffusion process in the lumen. We further take the advantage of a previous study (Lantz and Karlsson 2012), and impose shear dependent transfer of LDL into the intima. This further elaborates on the role of LDL transfer depending upon the flow conditions. The evolution of foam cells which is coupled to monocytes, macrophages and ox-LDL concentrations, is obtained in time. Broadly speaking, the human plaque is composed of necrotic core, the fibrous content and calcium. In this

thesis, we consider the necrotic core as the plaque itself since the fibrous part and the calcium accumulation into the plaque are found at a very late stage. Thus we can safely approximate plaque with the necrotic core which is made up of foam cells. The models presented in this thesis consist of several parameters, some of which are clinically well-known (Mckay et al. 2005), whereas the others are not known due to insufficient clinical data.

In chapter 2, we present two models, which we call model A and model B, differing in approach that, in model A, there is no coupling of blood flow while in model B, blood flow is coupled to it. The analysis is time-dependent and it gives sufficient approximation of the reduction of the radius of the artery and increase in the volume of the plaque. In Chapter 3, we present the bifurcation analysis of codimension two by considering two most important parameters that largely affect the plaque growth. Chapter 3 presents the slow-fast dynamics of the model we presented in Chapter 2. In Chapter 4, we consider the full version of Navier-Stokes equation coupled to the transfer of LDL particles and thus understanding the consequence of different flow conditions on transfer of LDL into the intima. We consider the plaque growth as a time-dependent moving boundary problem to explore the temporal influence which has never been performed to the best of our knowledge. This results in many new parameters introduced in our proposed models, and they are discussed in detail in this thesis. After several simulations, we found two threshold values, one for LDL intake and the other for shear stress, which in turn gives the idea of the importance of these two. Calculations also show that the regions, where the flow profile is not laminar, is subjected to a higher amount of infiltration of particles from the blood to the wall of the artery. We present all the conclusions in Chapter 5.

Published as M.A.K. Bulelzai, J.L.A. Dubbeldam – *"Long time evolution of atheroscelrotic plaques"*, J. Theor. Biol. 297, pp. 1-10, 2012.

Chapter 2

Long time evolution of atherosclerotic plaques

The question is not what you look at, but what you see.

Henry David Thoreau

Abstract

The evolution of atherosclerosis in general, and the influence of wall shear stress on the growth of atherosclerotic plaques in particular, is an intricate phenomenon which is still only partly understood. We therefore propose a qualitative mathematical model which consists of a number of ordinary differential equations for the concentrations of the most relevant constituents of the atherosclerotic plaque. These equations were studied both for the case that the wall shear stress is a parameter (model A), and for the case in which the plaque evolution is coupled to the blood flow (model B) which results in a time dependent wall shear stress. We find that both models exhibit a class of marginally stable equilibria, all reflecting states in which the plaque only grows for a short period of time after a perturbation. The uncoupled model A, however, shows bi-stability between this class of equilibria and another equilibrium state in which the plaque experiences unlimited growth in time, if the LDL cholesterol intake exceeds a threshold value. In model B the bi-stability vanishes, but we find that there is still a critical value of the LDL cholesterol intake beyond which the lumen radius drastically decreases. We show that this decrease is quite sensitive to the value of the wall shear stress.

2.1 Introduction

Atherosclerosis is a vascular disease caused by inflammation of the intima, a layer in the arterial wall, which results in the accumulation of LDL (low density lipoprotein) cholesterol, monocytes, macrophages and fat-laden foam cells at the place of the inflammation. This process is commonly referred to as plaque formation. A large number of clinical investigations (Malek et al. 1999, Li et al. 2006, Gijsen et al. 2008, Hansson and Libby 2006) have been performed on plaque formation and growth of atheromatous plaque. From these investigations is was inferred that after accumulation of LDL particles in the intima, the LDL molecules can get oxidized causing an inflammatory reaction. This oxidation process is mediated by the monocytes (Xing et al. 1998). The immune response following the penetration

and oxidation of LDL cholesterol urge the endothelial cells near the inflammatory area to recruit monocytes from the blood, which subsequently enter the intima. The monocytes on their turn, are converted into macrophages, which digest (or phagocytose) the oxidized LDL particles. These macrophages are eventually transformed in inert fat-laden foam cells, which again trigger the immune system. The cycle of recruitment of monocytes and production of more foam cells then starts again from the beginning. In this biological process the inflammatory response is transmitted by cytokines (Hansson and Libby 2006), which increase the endothelial cell activation leading to an enhanced rate of monocyte recruitment.

Once a plaque is formed, it is covered by a fibrous cap, consisting of elastin/collagen and smooth muscle cells (SMCs). Rupture of this cap leads to serious events like myocardial infarction or stroke. Therefore it is of crucial importance to find criteria which help to determine the vulnerability of the cap, in order to predict which caps are eventually prone to rupture (Li et al. 2006, Koskinas et al. 2009, de Korte and van der Steen 2002, Fan and Wanatabe 2003). No adequate diagnostic strategy to identify vulnerability is available yet. Since plaques typically evolve on timescales as long as 10 to 15 years, clinical investigations are very time consuming and expensive. Consequently, mathematical models have been developed to address a number of questions associated with atherosclerosis. So far, most models either concentrate on explaining a specific clinical trial result about the growth and rupture of atherosclerotic plaques (Wang 2001), or focus on the initiation of atherosclerosis (Cobbold et al. 2002, Khatib et al. 2007, Khatib et al. 2009, Ibragimov et al. 2005, Ougrinovskaia et al. 2010, Calvez et al. 2009). In the paper by Cobbold *et al.* (Cobbold et al. 2002), for example, a model for the oxidation process of LDL cholesterol and the protective effects of vitamins has been put forward. Their findings give results that are consistent with clinical studies that vitamin E does not lead to significant reduction of atherosclerotic plaques, contrary to the expectations. More recently, in the work of Ougrinovskaia *et al.* (Ougrinovskaia et al. 2010) the uptake of cholesterol by different scavenger receptors of macrophages during early stage atherosclerosis was investigated, using an ODE model. It was found that macrophage proliferation rather than an increased influx of LDL particles drives lesion instability. Another interesting model was studied by Ibragimov *et al.* in Ref. (Ibragimov et al. 2005), where a sophisticated partial differential equation model for the first stages in the atherosclerosis process was examined. In Ref. (Mckay et al. 2005) a very clear introduction of models that may be applied during different stages in the evolution of atherosclerotic plaques and an extensive list of parameter values are provided.

Although atherosclerosis is in the first place an inflammatory phenomenon, its evolution can be influenced by mechanical stimuli. It has long been known, for example, that shear stresses can influence plaque formation in a beneficial way (Wang 2001, Malek et al. 1999). Higher shear stress generally leads to reduced plaque formation and growth. This is generally believed to be due to the endothelial cells (Gijsen et al. 2008), which are capable of sensing the wall shear stresses exerted by the flowing blood. It follows that, in general, the growth

of the plaque region into the lumen is dependent on the flow profile of the blood in the lumen. The interaction between blood flow and the progression of atherosclerotic plaques has, however, not yet received much attention from the mathematical modeling prospective.

One of the few papers addressing this phenomenon is a recent paper by Zohdi *et al.* (Zohdi et al. 2004) in which it was attempted to construct a simple model taking into account the growth of the monocyte concentration in the plaque, by calculating the adhesion of monocytes to the endothelial layer. In their seminal work Zohdi *et al.* developed a numerical scheme to deal with the long term evolution of atherosclerotic plaques. The goal of this paper is to extend the model put forward in Refs. (Zohdi et al. 2004) and (Zohdi 2005) by taking explicitly into account the reactions that occur in the intima as well as the effect of shear stress exerted by the blood flow and discerned by the endothelial cells. As recent findings have indicated that shear stress not only critically affects plaque formation and growth, but also the transition of a developing plaque to a rupture-prone phenotype (Chatzisis et al. 2008), the need for mathematical models that incorporate such features is evident.

We do not intend to give a quantitative model in this paper, but rather report on the consequences of shear stress on plaque evolution on long time scales, for a generic model describing the development of atherosclerosis. We therefore use a system of ordinary differential equations (ODEs) to describe the evolution of the main constituents of the plaque. We do not take any spatial-dependence or stochastic processes into account, but rather focus on the coupling between flow and plaque growth. We believe that it is important to understand the consequences of the ODE model, before generalizing the model to higher spatial dimensions or including stochastic effects. Modeling features that are not robust under small changes of assumptions in the ODE systems are likely to remain non-robust in more complicated scenarios. The basis for our model is the interaction between the endothelial cells and the wall shear stress. We first consider the case that the shear rate is an adjustable control parameter (model A) and subsequently develop a more sophisticated model in which the wall shear stress is calculated in a self-consistent way from the flow profile (model B). We find that system A, in which the shear stress is treated as a control parameter, exhibits bi-stability between the class I equilibria, in which the plaque is marginally stable and a state in which the plaque grows indefinitely. The self-consistent model B possesses only the (marginally) stable equilibrium states. In these marginally stable states the radius of the lumen can still be significantly reduced. We show that this reduction depends rather strongly on the size of the wall shear stress that was exerted by the blood on the arterial wall.

This paper is organized as follows. In section 2, we introduce two mathematical models: model A and model B; each consisting of a system of ordinary differential equations (ODEs) for the constituents of the plaque. However, whereas the wall shear stress in *model A* is simply a parameter whose value can be controlled, in *model B*, also referred to as the *self-consistent system (SCS)*, the flow is coupled in a self-consistent way to the plaque evolution. That is, the Navier-Stokes equations for an incompressible fluid are solved in the

axisymmetric case, from which then the wall shear stress can be calculated. On the one hand this value of the wall shear stress enters the evolution equations of plaque constituents and on the other hand the plaque volume determines the wall shear stress by occluding part of the artery. For this reason we coin model B the SCS model. Next, in section 3, we discuss our numerical findings for the two different models and report on how the lumen radius depends on the LDL-intake. Finally, in section 4 we summarize our results. We also discuss necessary generalizations of the model in order to make long term predictions about cap tissue vulnerability.

2.2 The models A and B

As the main objective of this paper is to investigate the effects of wall shear stress on the progression of atherosclerotic plaques, we consider two different models: model A and model B. The first model (A) we develop consists of four differential equations for the constituents of the plaque. In this model there is *no coupling between the blood flow in the artery and the growth of the atherosclerotic plaque*. Rather the wall shear stress is simply considered an adjustable parameter. This allows a bifurcation analysis to be performed to determine the stability of the plaque for varying shear rates; the model is described in detail in subsection 2.2.1.

As the blood flow through an artery is obviously dependent on the plaque volume, since a larger occlusion implies by incompressibility higher blood velocities, we also develop a second model, model B, in which the wall shear stress is calculated from the velocity profile in the partially occluded artery. This wall stress influences on its turn the volume of the plaque and therefore the cross sectional area available for blood flow; this model is derived in subsection 2.2.2.

2.2.1 Model A

Our model is inspired by that of Ref. (Zohdi et al. 2004), but differs from it in the way the volume of the plaque evolves. The ODE model proposed by Ougrinovskaia *et al.* (Ougrinovskaia et al. 2010) has similar evolution equations of some plaque constituents, but does not incorporate any effects of wall shear stress. Also the models described in Ref. (Mckay et al. 2005) are akin to our model, although there are differences in the details. In Fig. 2.1 we present a sketch of the configuration we consider in this paper. The problem is reduced to essentially one-dimension, by considering a cylindrical geometry with translational symmetry in the z-direction and axial symmetry along the z-axis. The plaque is presumed to consist of monocytes, macrophages, LDL cholesterol, and fat-laden foam cells. The model is supposed to give qualitative results and it offers the opportunity to investigate the influence of shear stress on the progression of atherosclerosis. It has long been known that shear stresses influence the

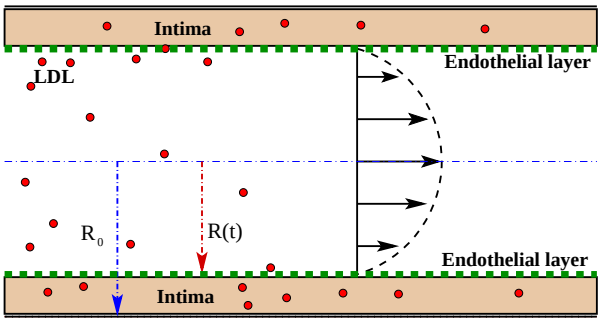

Figure 2.1: *Schematic representation of the blood flow in the lumen. The LDL-particles (red dots) present in the blood may enter the intima due to dis-functioning of the endothelial layer ((green) blocks). If the plaque region increases, the radius of the lumen is reduced and consequently the blood velocity and the wall shear stress are modified. The configuration is rotationally and translationally symmetric with respect to rotations about the z-axis and translations in the z-direction, respectively.*

growth of plaques in a positive way (Wang 2001, Malek et al. 1999, Gijsen et al. 2008), that is, higher shear stresses lead to reduced plaque formation in the artery. To elucidate the effects caused by shear stress on the plaque evolution, we take its influence on the remodeling of the artery explicitly into account. The equations governing the monocyte concentration (m), the macrophage concentration (M), the oxidized LDL (L_{ox}), and the fat-laden foam cells concentration (F) in the plaque residing in the intima are given by

$$\frac{dm}{dt} = (\Gamma(\sigma_w, L_{ox}) - d_m)m - \rho_1 m, \tag{2.1a}$$

$$\frac{dM}{dt} = \rho_1 m - \frac{\rho_{in} L_{ox}}{1 + L_{ox}/L_{th}} M, \tag{2.1b}$$

$$\frac{dL_{ox}}{dt} = \frac{qm}{1 + m/m_{th}} - \rho_L L_{ox} M - d_L L_{ox}, \tag{2.1c}$$

$$\frac{dF}{dt} = \frac{\rho_{in} L_{ox}}{1 + L_{ox}/L_{th}} M. \tag{2.1d}$$

These equations are new in the sense that we take wall shear stress into account, and have separate evolution of the monocytes and the macrophages, contrary to Ref. (Ougrinovskaia et al. 2010). The physical interpretation of these equations is as follows. The term $\Gamma(\sigma_w, L_{ox})m$ models the signaling reaction of the endothelium after LDL particles have entered the intima; it presumes a linear dependence on the monocyte concentration and a nonlinear (sigmoidal) dependence on the L_{ox} concentration. This term is furthermore assumed to be a decreasing function of the wall shear stress σ_w. The specific form of the term $\Gamma(\sigma_w, L_{ox})m$ is discussed below. The $-d_m m$-term models monocyte diffusion out of the plaque into the lumen and the

last term $-\rho_1 m$ designates the differentiation of monocytes into macrophages. These terms were also present in a model described in Ref. (Mckay et al. 2005), where the initiation process of atherosclerosis was studied in detail.

The macrophage evolution is described by Eq. (2.1b); the concentration of macrophages (M) increases as monocytes differentiate into macrophages. The macrophages can absorb several L_{ox} particles at their receptors after which they are turned into so-called foam cells (Kruth et al. 2002). The ingestion of L_{ox} by the macrophages will saturate for sufficiently high L_{ox} concentrations, which we implement by the sigmoidal term. We choose a sigmoidal dependence on L_{ox} for the sake of simplicity, but we checked that other functional forms to implement the saturation can be employed without any qualitative changes. Diffusion of macrophages is neglected, since they are typically larger than monocytes and therefore have a smaller diffusion coefficient.

Equation (2.1c) governs the evolution of L_{ox}, where we stress, that we consider only LDL particles that are immediately oxidized upon entering the intima. The three terms on the right-hand side of Eq. (2.1c) represent, LDL-uptake by the endothelial layer and oxidation by monocytes, the ingestion of oxidized-LDL by macrophages, and the diffusion of LDL out of the plaque region, respectively. The parameter q determines the rate of (unoxidized) LDL-uptake by the endothelial layer. However, not all LDL molecules that permeate the intima will get oxidized. The oxidization process requires the presence of monocytes/macrophages (Xing et al. 1998, Chisolm et al. 1999, Llodra et al. 2004). Since we only consider the oxidized-LDL in our model, we have combined the penetration of the LDL particles through the endothelial layer with the oxidation process in the single term $\frac{qm}{1+m/m_{th}}$ in Eq. (2.1c). For the reason that in order for the LDL to get oxidized the presence of monocytes is required, the first term on the right-hand side of Eq. (2.1c) has m in the numerator. Since the production of L_{ox} due to intake cannot grow indefinitely, there is a natural saturation incorporated by the $1+m/m_{th}$ in the denominator. The precise functional form of the saturation is not known; for concreteness we have taken the sigmoidal form.

The functional dependence of $\Gamma(\sigma_w, L_{ox})$ on σ_w and L_{ox} appearing in Eq. (2.1a) is taken as follows:

$$\Gamma(\sigma_w, L_{ox}) = \frac{\gamma_0}{1+\sigma_w/\sigma_0}\frac{L_{ox}}{1+L_{ox}/L_{th}}, \tag{2.2}$$

which is consistent with the fact that larger shear rates imply a smaller growth coefficient for the monocytes (Malek et al. 1999, Gijsen et al. 2008). The value of σ_0 designates the wall shear stress at which the growth rate of the monocyte concentration due to the signaling response by the endothelium is reduced with a factor of two compared to the zero wall shear rate response by the endothelium. From Eq. (2.2) it follows that for L_{ox} concentrations much smaller than L_{th}, the sigmoidal function increases linearly with L_{ox}, and for concentrations well beyond L_{th} the sigmoidal function saturates. We remark that Eq. (2.2) is a function that has the required biological characteristics; that is, it should decrease with increasing

σ_w, increase with L_{ox}, but be bounded when L_{ox} is very large. The functional dependence of Γ on L_{ox} was also studied in Ref. (Ougrinovskaia et al. 2010), where it was called a Michaelis-Menten function. It turned out that this functional form gave rise to dynamics that was much more stable and realistic than functional forms having more inflections. We have investigated the dynamics for different dependence of Γ on σ_w and L_{ox}, but this did not lead to any qualitative differences, and therefore we will only consider Γ given by Eq. (2.2) in this paper.

The factor γ_0 is a constant which determines the rate at which monocytes enter the intima for small wall shear stress and low L_{ox}. In this case the monocyte concentration increases linearly with L_{ox} at rate γ_0. The system of equations (2.1) is closed when σ is taken to be a parameter. The system (2.1) is the first model that we will explore in section 3.

2.2.2 Model B

The significance of the model of the previous subsection can be improved if we do not consider the wall shear stress as given, but calculate it in a self-consistent way. The wall shear stress σ_w can be computed if we assume that the flow is incompressible, which implies a constant throughput (Q) through the artery. Although healthy arteries can adjust in such a way that the wall shear stress is kept more or less constant, atherosclerosis affected arteries can no longer tune their diameter according to the shear stress value (Malek et al. 1999). If we solve the Navier-Stokes' equations for the cylindrical symmetric situation (Landau et al. 1987), commonly called Poiseuille flow, and prescribe no-slip boundary conditions at the artery walls, we obtain the quadratic velocity profile of the form $v(r,t) = v_{max}(t)\left(1-\left(\frac{r}{R}\right)^2\right)$. This implies that the throughput $Q = 2\pi\int_0^R rv(r,t)\,dr = \frac{\pi v_{max}(t)R^2(t)}{2}$, from which we infer that the central velocity $v_{max}(t) = 2Q/\pi R^2(t)$. The wall shear stress can now be calculated directly from the velocity profile and the expression for $v_{max}(t)$ and yields

$$\sigma_w = -\eta\frac{\partial v(r,t)}{\partial r}\Big|_{r=R(t)} = \frac{4Q\eta}{\pi R^3(t)}, \tag{2.3}$$

with η the viscosity of blood and $R(t)$ the radius of the artery.

The system is closed when we supplement Eqs. (2.1a-2.1c) with an equation describing the evolution of the radius of the artery. We will assume axial and translation symmetry with respect to the z-axis. The plaque volume $V(t)$ in the intima can then be calculated as $V(t) = -l_p\pi(R^2(t)-R_0^2)$, with R_0 the radius of the artery before the onset of atherosclerosis and l_p the length of the affected region in the artery.

During a time interval Δt the total plaque volume increases to the accumulation of plaque constituents. The volume of the plaque at $t+\Delta t$: $V(t+\Delta t)$ can therefore be expressed to first

order in Δt as

$$V(t+\Delta t) = V(t) + \left(\nu_M \frac{dM}{dt} + \nu_{Lox} \frac{dL_{ox}}{dt} + \nu_m \frac{dm}{dt} + \nu_F \frac{dF}{dt} \right) V(t) \Delta t, \tag{2.4}$$

where we simply summed over the increase in volume caused by the macrophages, oxidized-LDL, monocytes and foam cells and weighted each constituent with the volume of a single molecule of the respective substance. We remark that the units on both sides balance as all concentrations are measured in number of molecules per unit volume. From the literature we obtained the following values for the molecular volumes: $\nu_F = 10^{-13}\mathrm{m}^3$ (Gerrity 1981), $\nu_{L_{ox}} = 10^{-21}\mathrm{m}^3$ (Hulthe et al. 2000), $\nu_m = 10^{-17}\mathrm{m}^3$ (Gerrity 1981), $\nu_M = 10^{-14}\mathrm{m}^3$ (Krombach et al. 1997). We easily translate Eq. (2.4) in a differential equation for the plaque volume

$$\frac{dV}{dt} = \left(\nu_M \frac{dM}{dt} + \nu_{Lox} \frac{dL_{ox}}{dt} + \nu_m \frac{dm}{dt} + \nu_F \frac{dF}{dt} \right) V. \tag{2.5}$$

We will explicitly take all contributions to the volume change into account in our numerical simulations, but, of course, a good approximation would be to only consider the foam cell contribution as the foam cells act as a kind of storage place for the debris in the plaque; therefore they dominate the plaque volume for long times.

The equation for the radius of the artery is obtained by differentiating $V(t) = -l_p \pi (R^2(t) - R_0^2)$ and substituting Eq. (2.5) for $\frac{dV}{dt}$. If we next use Eqs. (2.1) to replace the $\frac{dM}{dt}$, $\frac{dL_{ox}}{dt}$, $\frac{dm}{dt}$, $\frac{dF}{dt}$ we arrive at

$$\begin{aligned} \frac{dR}{dt} = &\left(R - \frac{R_0^2}{R} \right) \frac{m \left(\rho_1 (\nu_M - \nu_m) - \nu_m d_m + \frac{\nu_m \gamma_0}{1+\sigma_w/\sigma_0} \left(\frac{L_{ox}}{1+L_{ox}/L_{th}} \right) + \frac{q \nu_{L_{ox}}}{1+m/m_{th}} \right)}{2} \\ &+ \left(R - \frac{R_0^2}{R} \right) \frac{M \left(-\rho_L \nu_{L_{ox}} L_{ox} + (\nu_F - \nu_M) \frac{\rho_{in} L_{ox}}{1+L_{ox}/L_{th}} \right) - \nu_{L_{ox}} d_L L_{ox}}{2}. \end{aligned} \tag{2.6}$$

Eqs. (2.1a-2.1c) and (2.6) together with Eqs. (2.3) and (2.2) constitute an autonomous system of four differential equations that can qualitatively describe the progression of atherosclerotic plaques.

In the following section we will investigate the behavior predicted by this system of differential equations. Here we remark that our approach differs in several respects from Ref. (Zohdi et al. 2004). Firstly, we concentrate on shear stresses instead of residence times of the monocytes near the intima. Secondly, we have explicit differential equations for the macrophages, monocytes, foam and LDL particles. At the end of this section, we briefly compare our results with those obtained in Ref. (Zohdi et al. 2004) to estimate the importance of the different effects.

η	σ_0	Q	d_L	ρ_1	d_m
0.004 Pas	1 Pa	$2.8\times10^{-6}\mathrm{m}^3/\mathrm{s}$	$2.4\times10^{-5}/\mathrm{s}$	$1.15\times10^{-6}/\mathrm{s}$	$5.75\times10^{-6}/\mathrm{s}$

Table 2.1: *The parameter values used in the numerical simulations. The value of η was raken from (Lipowsky 2005), σ_0 was taken inbetween the low wall shear stress and high wall shear stress values mentioned in (Malek et al. 1999), Q is taken from (Bonert et al. 2003), d_L from (Cobbold et al. 2002), ρ_1 from (Maoz et al. 1986), and d_m from (Mckay et al. 2005).*

2.3 Numerical implementation

Before investigating the dynamics contained in Eqs. (2.1a-2.1c), we rescale the equations using the following transformations:

$$\begin{aligned} \tilde{L} &= L_{ox}/L_{th}, & \tilde{m} &= m/L_{th}, & \tilde{M} &= M/L_{th}, & \tilde{F} &= F/L_{th}, & \tilde{\sigma} &= \sigma_w/\sigma_0, \\ \tilde{t} &= d_L t, & \varepsilon &= d_m/d_L, & a &= \gamma_0 L_{th}/d_L, & c &= \rho_1/d_L, & b &= \rho_{in} L_{th}/d_L, \\ d &= \frac{q m_{th}}{d_L L_{th}}, & e &= \rho_L L_{th}/d_L, & f &= m_{th}/L_{th}. \end{aligned} \tag{2.7}$$

These transformations yield the following set of reduced equations:

$$\dot{m} = \left(\frac{aL}{(1+\sigma)(1+L)} - \varepsilon - c\right) m, \tag{2.8a}$$

$$\dot{M} = cm - \frac{bML}{1+L}, \tag{2.8b}$$

$$\dot{L} = \frac{dm}{f+m} - eLM - L, \tag{2.8c}$$

$$\dot{F} = \frac{bLM}{1+L}, \tag{2.8d}$$

where the dot denotes differentiation with respect to $\tilde{t}$ and the tildes on m, M, L, and F are dropped for notational convenience. Notice that Eq. (2.8d) decouples from the other equations, which therefore determine the stability of the system (3.5).

We first consider the equations in absence of the closure relation which implies that we regard the shear stress σ as an adjustable parameter and do not consider the influence of remodeling of the artery on the flow profile, that is, we do not take into account Eq. (2.3).

2.3.1 Wall shear stress as a parameter

When the shear stress is simply considered a parameter, the system of differential equations given by Eqs. (3.5) is found to possess infinitely many equilibria, which are separated in two classes. The first class of equilibria, which we denote by I, are of the form

$(m,M,L) = (0,M_1,0)$, where M_1 can have any non-negative value. The second class of equilibria (*II*) corresponds to two points with $m \neq 0$, which we will denote $(m^{\pm},M^{\pm},L^*)$. These equilibria are born in a saddle-node bifurcation; the detailed expressions for $m^{\pm},M^{\pm},L^*$, are relegated to the appendix.

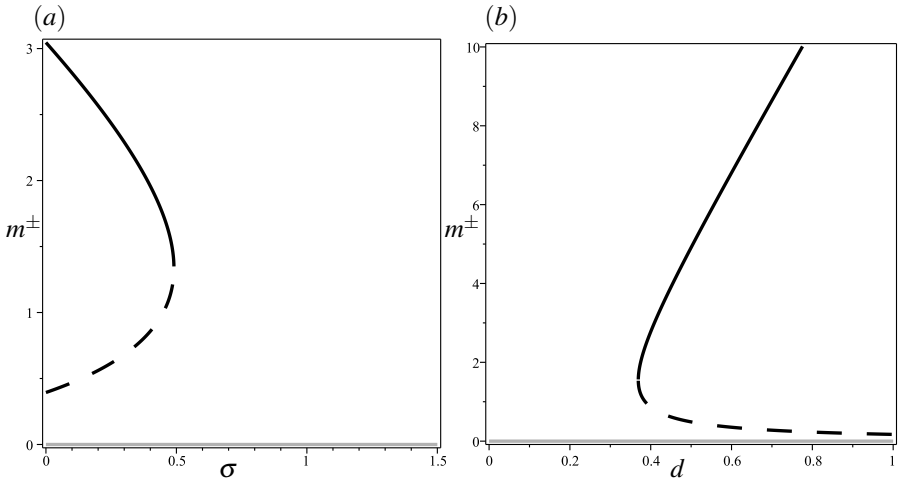

Figure 2.2: *(a) The (dimensionless) equilibrium monocyte concentration a a function of the wall shear stress σ. The (grey) solid-line $m = 0$ corresponds to the infinitely many marginally stable equilibria referred to as class A. The other curve consisting of two branches denotes the equilibrium m^+ (upper-branch solid) and m^- (lower branch dashed). The solid curves are linearly stable solutions, so we find that the system exhibits bi-stability. In (b) the same equilibria ($m^{\pm}$) are depicted, this time as a function of the LDL-intake d for fixed $\gamma = 1$. As soon as d exceeds the threshold value d_{thres}, the plaque-region can turn unstable and start to grow.*

In Fig. 2.2(a) we have plotted the equilibrium monocyte concentration, which was found by equating the left-hand side of Eqs. (2.8a)-(2.8c) to zero, for a typical choice of parameter values: $a = b = e = f = 1, \varepsilon = 0.01, c = 0.05, d = 0.30$; the values of ε and c follow directly from Table 2.1, the other parameters are unknown and simply set to 1 for computational convenience. We have checked our calculations for different values of e,b,f and found that the qualitative results do not change when varying these values with factors as high as 10, as long as the a and d parameters are changed accordingly. A precise bifurcation study which would in detail reveal the parameter dependence will be published elsewhere.

In Fig. 2.2(b) we took the same parameter values as in 2(a) except that we now set $\sigma = 1$, and varied d. The figures clearly show that for each value of d and σ, the $m = 0$ solution is (marginally) stable. However, for values of $d > d_{thres}$ or $0 \leq \sigma < \sigma_{thres}$, the system is bi-stable. Besides the class *I* equilibria one of the branches m^+ represents a stable

equilibrium, implying that depending on the initial conditions the solution curve either ends at the line $\{(m,M,L)|m=L=0\}$, or at $(m,M,L)=(m^+,M^+,L^*)$. A similar bi-stability was also observed in Ref. (Ougrinovskaia et al. 2010).

The physical interpretation of this bi-stability is as follows. The artery is initially in a state of class A, in which no monocytes are present in the plaque. When the average LDL-transport into the intima is then structurally increased which is modeled by an increased parameter value for d, beyond a certain threshold d_{thres}, or alternatively the wall shear stress is structurally decreased below a threshold value σ_{thres}, the plaque is highly susceptible to sudden changes in the L_{ox} or monocyte concentration. A sudden increase of the L_{ox} concentration may bring the system in the equilibrium state represented by m^+ in which the plaque region rapidly grows. An eventual decrease in d may stop this rapid growth of the plaque as a consequence of the accumulation of foam cells.

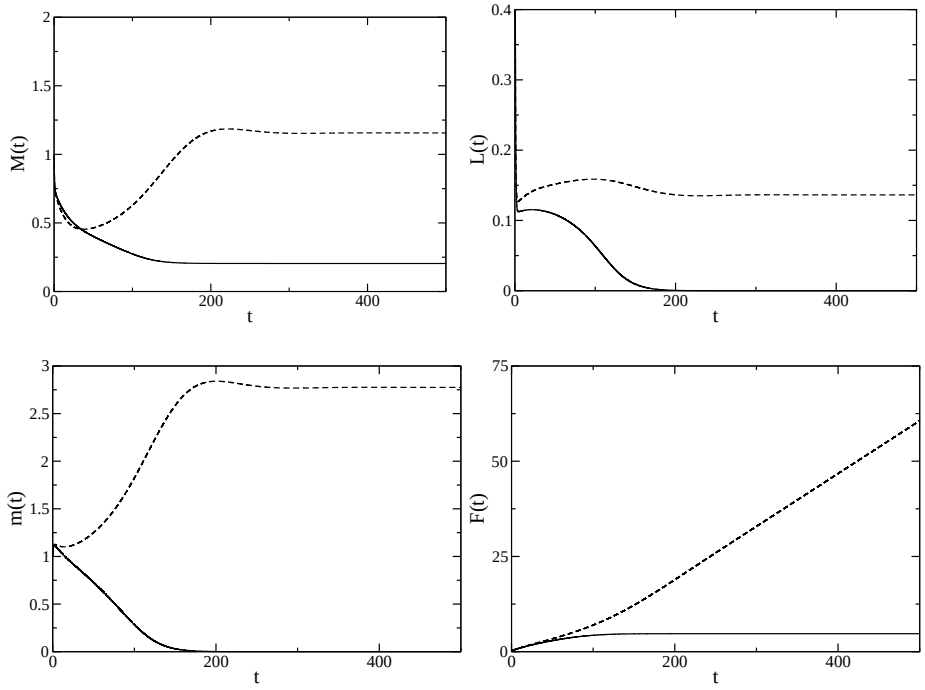

Figure 2.3: *Modeling the wall shear stress as a fixed parameter.The (dimensionless) concentration of the plaque constituents as a function of (dimensionless) time. The monocyte and macrophage concentration decay to 0, but the debris ending up in the fat-laden foam cells approaches a finite value. The L_{ox} concentration is determined by the intake parameter d. The solid curves correspond to $d=0.35$ and the dashed curves to $d=0.40$; all other parameters are kept constant at the values mentioned in the text and the shear stress $\sigma=1$.*

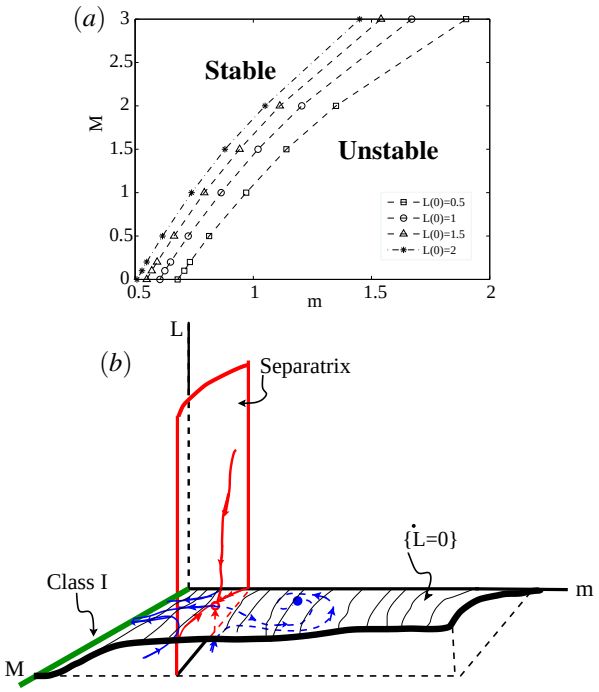

Figure 2.4: *Dependence of the stability of class I equilibria on initial conditions. In (a) curves in the (m,M)-plane for 4 different values of L_{ox} are plotted. The phase space above the curves (Stable) is attracted to the class I equilibria. The phase space in the lower right-hand corner is attracted to the attracting node (m^+,M^+,L^+) and gives rise to continuing plaque growth. In (b) a sketch of the three-dimensional phase space is shown. The separating surface (stable manifold of the saddle) is shown as well as the class I equilibria, the saddle point and the attracting node.*

Quantitatively this means that if the plaque resides in a state $(m,M,L_{ox}) = (0,M_0,0)$ at $t = t_0$, and the foam concentration F has a constant value F_0 , where $F_0 = \int_0^{t_0} \frac{bL(t)M(t)}{1+L(t)}\,dt$, the transition to the state (m^+,M^+,L^*) accomplishes a linear growth of the foam concentration in time $F(t) = F_0 + b(t-t_0)L^*M^+/(1+L^*)$.

The threshold values d_{thres} and σ_{thres} can easily be found from the eigenvalues. In the Appendix we derive the threshold values for d and σ, but we do not reproduce the lengthy expressions for the eigenvalues. For the parameter values we used in Fig. 2.2, the threshold value for d at $\sigma = 1$ is $d_{thres} = 0.369$. If we set $d = 0.30$, we find in accordance with Fig. 2.2 that $\sigma_{thresh} = 0.491$.

In Fig. 2.3 we show the results for a numerical solution of Eqs. (2.1a)-(2.1d), with parameter values $a = b = e = f = 1, \varepsilon = 0.01, c = 0.05$ and initial condition $(m(0),M(0),L(0)) = (1,1,1)$ for two values of d. The dashed curve corresponds to $d = 0.40$ and the solid one to

$d = 0.35$. The parameter values in Table 2.1, were obtained from experimental results reported in the literature; see the caption of Table 2.1. It can immediately be seen from Fig. 2.3 that the solid curves correspond to a cholesterol intake below the threshold value and the dashed curves have an intake value that exceeds the threshold value d_{thresh}.

From Fig. 2.3 one can see that for the case $d = 0.35$ the monocyte concentration drops rapidly, followed by the L_{ox} with some time delay. The macrophage and foam concentration approach a non-zero equilibrium value for dimensionless time $t \approx 200$, which translates into a time $200/d_L$, corresponding according to Table 2.1, to approximately 0.3 years, which is considerably shorter than the typical time span for the evolution of atherosclerosis of approximately 10-15 years.

In the case $d = 0.40$, corresponding to the dashed curves, the monocytes, macrophages and LDL concentrations approach a nonzero value, as the initial condition $(m(0), M(0), L(0)) = (1,1,1)$ drives the trajectory to the stable equilibrium (m^+, M^+, L^+). When the equilibrium is reached, the foam concentration increases linearly in time, in agreement with our asymptotic expression for F.

To investigate how the dynamics depend on the initial condition we used MATCONT (Dhooge et al. 2008) to vary the initial conditions. We plotted our results in Fig.2.4. From figure 2.4(a) it can be clearly seen that the curve separating the basin of attraction for class I equilibria and the attracting node, depends only moderately on the value of $L(0)$. The curves were obtained numerically by varying the initial conditions for 4 different values of $L(0)$. To summarize the dynamics we have constructed a three-dimensional sketch which displays the dynamics that occurs in the system in Fig.2.4(b). The dashed blue curves denote trajectories moving toward the stable node, the full lines connect to the M-axis, and the red curves to the saddle. The stable manifold of the saddle divides phase space in two regions, which either belong to basin of attraction of the the class I equilibria on the M-axis, or to the basin of attraction of stable node (m^+, M^+, L^+).

2.3.2 Self-consistent equations with remodeling

We next consider the coupled equations in which the wall shear stress is no longer a parameter, but is determined by Eq. (2.3). In this case we have 4 ordinary differential equations, whose equilibria are easily calculated. We consider the equations for $\tilde{m}$, $\tilde{M}$, $\tilde{L}_{ox}$ and $\tilde{R} = R/R_0$, where R_0 is the initial radius of the lumen. The equation for the monocytes is given, after substitution of the expression for the wall shear stress, by

$$\dot{\tilde{m}} = \lambda(\tilde{R}, \tilde{L})\tilde{m}, \tag{2.9}$$

where $\lambda(R, L)$ is defined by

$$\lambda(\tilde{R}, \tilde{L}) = \frac{a\tilde{R}^3}{\tilde{R}^3 + \alpha} \frac{\tilde{L}}{1 + \tilde{L}} - \varepsilon - c, \tag{2.10}$$

and we introduced a dimensionless parameter $\alpha \equiv \frac{4Q\eta}{\pi R_0^3 \sigma_0}$, and scaled the radius by R_0, hence $\tilde{R} = R/R_0$.

The equation for the (dimensionless) artery radius is governed by

$$\dot{\tilde{R}} = \frac{\xi}{2}\left(\tilde{R} - \frac{1}{\tilde{R}}\right)\left[\tilde{m}\left(\frac{a\tilde{R}^3\tilde{L}\tilde{\nu}_m}{(\alpha+\tilde{R}^3)(1+L)} + c\tilde{\nu}_M - \tilde{\nu}_m(\varepsilon+c)\right) + \frac{b\tilde{M}\tilde{L}}{1+\tilde{L}}(1-\tilde{\nu}_M) + \tilde{\nu}_L\left(\frac{d\tilde{m}}{f+\tilde{m}} - e\tilde{M}\tilde{L} - \tilde{L}\right)\right], \tag{2.11}$$

where we introduced $\xi = \nu_F L_{th}$. The specific volumes are all expressed relative to ν_F, that is, $\tilde{\nu}_m = \nu_m/\nu_F$, $\tilde{\nu}_M = \nu_M/\nu_F$, and $\tilde{\nu}_L = \nu_L/\nu_F$. The numerical values for these can be found from the values mentioned in subsection 2.1. This gives $\nu_L = 10^{-8}$, $\nu_m = 10^{-4}$, $\nu_M = 10^{-3}$. We now drop again the tildes and always refer to dimensionless system of differential equations given by Eq. (2.9), Eq. (2.11) and Eqs. (2.8b), (2.8c), as the self-consistent system (SCS) or model B.

The equilibria of the SCS equations are again easily calculated. We find that in this case there are infinitely many equilibria of class I, constituting a plane, which have the following form $(m,M,L,R) = (0,M^*,0,R^*)$, where M^* and R^* are values for the (dimensionless) macrophage concentration and artery radius that depend on the initial state. This class of equilibria is again found to be marginally stable. There is an additional equilibrium with $R = 1$, which is unstable, and we will ignore this state as we assume that some reduction in the lumen has already taken place, which implies that initially the radius $R < 1$. We will always choose $R(t=0) = 0.99$ in this paper. The extra coupling between the radius and the wall shear stress removes the bi-stable state that showed up when the wall shear stress was treated as parameter, and in this sense stabilizes the atherosclerosis process. This can be understood as follows. When the radius of the lumen decreases the shear stress increases and this drives the system to a state with $m = 0$ and $L = 0$ and the progression of atherosclerosis is halted, leading to a nonzero value of the lumen radius. The important question is what the final lumen radius will be and how fast the size of the lumen is reduced.

The calculation of how the artery radius decreases with time for sufficiently long times is similar to that of the parameter model. Almost all debris (except a small quantity of macrophages) will finally end up in the foam cells and we need therefore only take the foam contribution to the plaque volume into account. This means that for long timescales we only need to solve the separable differential equation

$$\dot{R} = \frac{\xi}{2}\left(R - \frac{1}{R}\right)\frac{bML}{1+L}. \tag{2.12}$$

When we integrate Eq. (2.12), we find that in the long time limit, the (dimensionless) radius of the lumen decreases with time as

$$R^2(t) = 1 - \left(1 - R^2(t=0)\right)e^{\xi I(t)}, \tag{2.13}$$

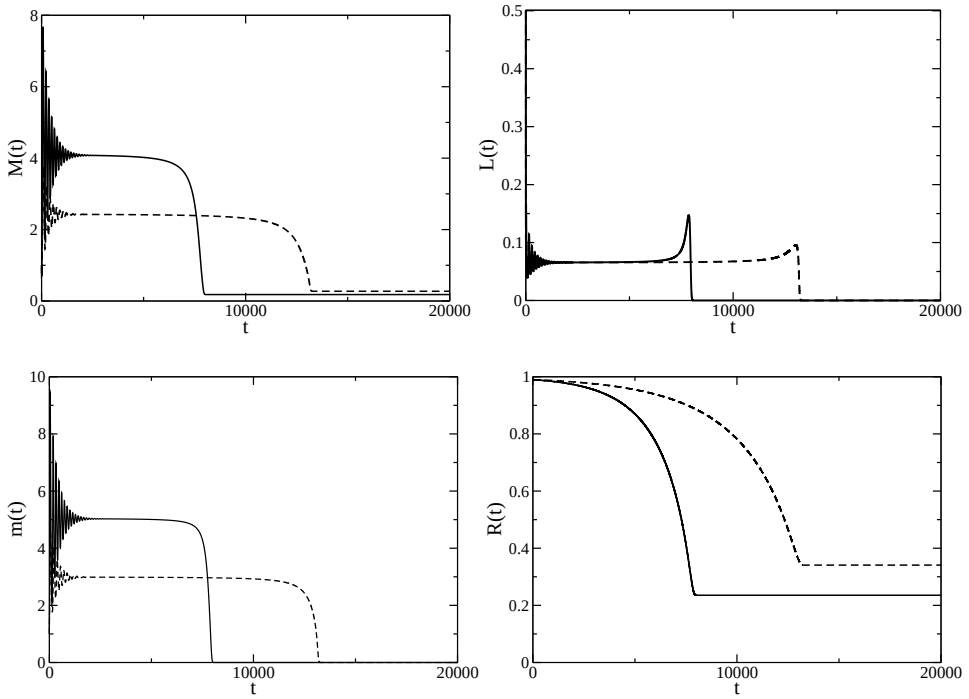

Figure 2.5: *Numerical solution of model B where the wall shear stress evolves with time. The (dimensionless) concentration of the plaque constituents and the lumen radius as a function of (dimensionless) time. The monocyte and oxidized LDL concentration decay to 0, but the debris ending up in the fat-laden foam cells approaches a finite value. The macrophage concentration is determined by the intake parameter d. The solid curves correspond to $d = 0.40$ and the dashed curves to $d = 0.30$; all other parameters are kept constant at the values mentioned in the text and we choose $\xi = 0.02$ and $\alpha = 0.05$, which corresponds to a realistic flow profile. The initial values were the same of in Fig. 2.3, that is, $(m(0), M(0), L(0)) = (1,1,1)$.*

where $I(t) = \int_0^t \frac{bL(t')M(t')}{1+L(t')}\,dt'$. This asymptotic expression implies that the lumen radius $R(t)$ will remain positive as long as $I(t) < -\frac{\ln\left(1-R^2(t=0)\right)}{\xi}$, which means for all times for our choice of parameters. We notice that to analyze the behavior of model B for small values of the lumen, the coordinate transformation $w(t) = 1/R(t)$ can be used, which was also employed in Ref. (Ougrinovskaia et al. 2010). In this way the equilibrium at $R = 0$ is transferred to $w = \infty$.

In Fig. 2.5 the concentrations of the plaque constituents and the lumen radius are depicted, where we kept all parameter values the same as in Fig. 2.3, except the values of d which were taken $d = 0.40$ and $d = 0.30$ for the solid and dashed curves, respectively. The

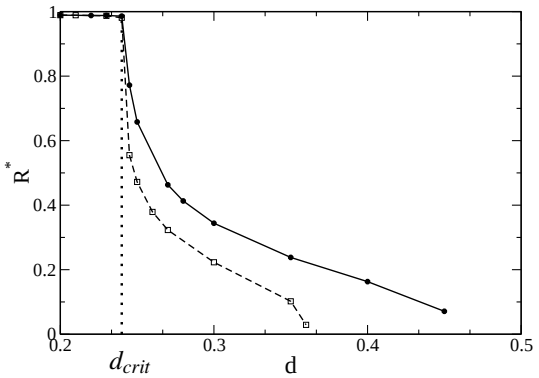

Figure 2.6: *Dependence of the stationary lumen radius R^* on the intake parameter d for two different values of α ($\alpha = 0.050$ solid and $\alpha = 0.025$ dashed) . One can clearly see that after a certain threshold value of $d = 0.24$ the radius greatly reduces with d. This reduction is largest when α is smaller.*

value of the parameter α was set to 0.05 and we checked that varying α did not lead to any qualitative differences in how the concentrations and lumen depend on time. For short times oscillations that die out rather soon are observed. These can be explained if one realizes that α has a small value and because R evolves on such a slow timescale it will be approximately constant on the time interval $[0, 1000]$, say. The dynamics observed will in this case mimic that of model A in which the system has an attracting node, besides the type I equilibria. The oscillations are around the values of m, M, L, that would correspond such a node. Only when R starts to decrease, the dynamics can no longer be approximated by that of model A, and strong deviations between the dynamics in the two models arise. The numerical results further show that for both values of d the evolution of R, L, m, M is comparable. The long time scale dynamics reveals that the macrophage concentration starts to drop slightly earlier than the monocyte concentration, which is caused by the parameter b being larger than c. This leads to the little bump in the L concentration at late times.

The most conspicuous differences between Fig. 2.3 and Fig. 2.5 besides the oscillations, is the fact that the lumen dynamics occurs on a much longer timescale, typically 10000-15000 units. A time span of 10000-15000 dimensionless time units corresponds to 11-16 years, which is in accord with clinical findings.

In Fig. 2.6 we show how the radius of the lumen evolves in time, as a function of the cholesterol intake parameter d for two different values of α, namely $\alpha = 0.025$, which corresponds to the values in Table 2.1, and $\alpha = 0.050$. The most conspicuous feature of Fig. 2.6 is the presence of a critical value for d, d_{crit}. Even though the system is no longer bi-stable, if the LDL-uptake exceeds this critical value d_{crit}, the equilibrium value for the lumen radius is extremely reduced (approximately 50%) compared to the value of the radius with

LDL-uptake slightly below d_{crit}.

From Fig. 2.6 it can also be inferred that the lumen radius reduction depends rather sensitively on the value of α. For small α values the lumen radius is greatly diminished. Even though we do not pretend the model to be quantitative, monitoring the evolution of the radius of the lumen in time, provides information about the value of α and ξ. Comparing the evolution of the lumen radius seen during a clinical test with theoretically obtained curves for different values of α and ξ, might lead to better estimates for α and L_{th}, from which in turn values for L_{th} and σ_0 could be determined, and possibly order of magnitude estimates for the remaining parameters.

To summarize, we developed a qualitative model and studied two different cases of the model. One case in which the wall shear stress was treated as a parameter and another case (model B) in which the flow was coupled to the dynamical processes that are pertinent in atherosclerosis. For model A, we report that the system is bi-stable and that the foam concentration may grow indefinitely in time, depending on d and σ.

We find that coupling to the flow, as implemented in model B, leads to a class of marginally stable equilibrium states. The bi-stability present in the parameter model A has disappeared.

Finally, we compare our results with the model of Zohdi *et al.* (Zohdi et al. 2004). In this work which describes remodeling of the artery as a consequence of absorption of LDL particles, depending on the velocity of the LDL particles than the wall shear stress. This results in a linear dependence of the lumen radius on time in contrast to our findings. We expect that the differences between the results can be attributed to the differences in the uptake mechanisms of LDL particles.

2.4 Conclusion

We constructed two models A and B for long time evolution of plaques in arteries, combining both chemical reactions in the intima and remodeling of the plaque region. Our models illustrate that both LDL-uptake and wall shear stress play important roles in the evolution of atherosclerotic plaques.

Comparison of the two models shows that the major differences between a model which treats the wall shear rate as given (A) and one which incorporates the evolution of the wall shear stress in a self consistent manner (B), is that the bi-stability between two classes (I and II) of equilibrium states in model A, is no longer present in model B. In this sense coupling to the flow stabilizes the dynamics. Nevertheless, although the threshold value of the cholesterol intake disappeared in model B, we demonstrated numerically that there is still a critical value of the LDL-uptake d_{crit}, which is independent of the shear rate parameter α, beyond which the lumen radius will drastically decrease. The occlusion of the lumen does depend on the shear rate parameter α once the LDL-uptake has passed the critical value. This seems to suggest that it is indeed beneficial to maximize the value of α and most

importantly, minimize the consumption of LDL cholesterol. When the artery is affected by atherosclerosis, the lumen reduction might be diminished by sufficient physical exercises, leading to a larger Q and consequently a greater value of α.

The models presented here have a qualitative character. To make quantitative comparison with experiments possible in the near future a number of crucial modifications to the model that we presented here are required.

The most pertinent subjects for future investigation to facilitate comparison with clinical and experimental results are the following. First of all, three dimensional computation of the blood flow is necessary in order to calculate the wall shear stress. Secondly, the entering of monocytes and LDL particles into the intima is known to be a complicated processes in which both residence times and shear stresses play a role. It would be interesting to know the relative importance of shear stress effects compared to direct absorption. Future research by the authors address such questions. Thirdly, the reactions taking place in the intima and specifically the role played by cytokines needs to be incorporated. Recent findings (Hansson and Libby 2006) confirmed their importance in destabilizing the cap that covers the plaque, by inhibiting the collagen production. Finally, we neglected here the elasto-mechanical properties of the vulnerable cap. It is known that smooth muscle cells, but also collagen plays a key role in the formation and remodeling thereof (Holzapfel and Gasser 2000). One could think of future models in which these processes are incorporated in a mesoscopic fashion, or instead of models which combine macroscopic elasticity with fluid flow.

We think that the present analysis may help in providing a basis for such more sophisticated models.

Acknowledgment

JLAD thanks Dr J. Wentzel for stimulating discussions and providing assistance with understanding the biological process. The anonymous referees' comments were very much appreciated and have considerably improved this paper.

Appendix

To calculate the stability of the equilibria, the Jacobian J of system (3.5) is calculated. We find that J is given by

$$J = \begin{pmatrix} \frac{aL}{(1+\sigma)(1+L)} - \varepsilon - c & 0 & \frac{am}{(1+\sigma)(1+L)^2} \\ c & \frac{-bL}{1+L} & \frac{-bM}{(1+L)^2} \\ \frac{df}{(f+m)^2} & -eL & -eM-1 \end{pmatrix}. \tag{2.14}$$

For the equilibrium (m,M,L)=$(0,M_1,0)$, where M_1 can have any positive value, this implies that the eigenvalues are respectively

$$\lambda_1 = -(\varepsilon + c), \qquad \lambda_2 = -(eM_1 + 1), \qquad \lambda_3 = 0. \tag{2.15}$$

As $\lambda_1, \lambda_2 < 0$ for all parameter values and $\lambda_3 = 0$, these equilibria are always marginally stable. This implies that a small perturbation shifts the system from the equilibrium $(0,M_1,0)$ in phase space to a new one with $(0,M_2,0)$. There are two more equilibria (m^*,M^*,L^*), which have $m^* \neq 0$. These can easily be found to obey

$$\begin{aligned} L^* &= \frac{(\varepsilon + c)(1+\sigma)}{a - (1+\sigma)(\varepsilon + c)}, \\ M^* &= \frac{cm^*(1+L^*)}{bL^*}, \\ (m^*)^2 + m^* &\left[f - \frac{db}{ec} + \frac{(1+\sigma)(1+d)b(\varepsilon+c)}{eac} \right] + \frac{fb(1+\sigma)(\varepsilon+c)}{eac} = 0. \end{aligned} \tag{2.16}$$

From the expression for L^* is transpires that in order for the equilibrium to exist $a > (1+\sigma)(\varepsilon + c)$. Solving the quadratic equation for m^* gives rise to two branches m^+ and m^-, which satisfy

$$m^{\pm} = -\frac{f - \frac{db}{ec} + \frac{(1+\sigma)(1+d)b(\varepsilon+c)}{eac}}{2} \pm \frac{\sqrt{H}}{2}, \tag{2.17}$$

where $H = \left[f - \frac{db}{ec} + \frac{(1+\sigma)(1+d)b(\varepsilon+c)}{eac} \right]^2 - 4\frac{bf(1+\sigma)(\varepsilon+c)}{eac}$; H should be positive in order for the equilibria to exist. For the parameter values considered the m^+ solution is stable and the m^- unstable. To determine the threshold values for σ and d, we should calculate when J has an eigenvalue zero for one of the equilibria of class B. As this implies that the $\det J = 0$, we immediately find that this implies that $m^* = \left[\frac{db - efc}{2ec} - \frac{(1+\sigma)(1+d)b(\varepsilon+c)}{2eac} \right]$. The value of σ, coined σ_{thres}, for which this value of m^* is attained is easily seen to be

$$\sigma_{thres} = \frac{-bcd^2 - ceadf + eacf - 2bdc - bc + bd^2a - 2bd\varepsilon + bda - b\varepsilon d^2 - b\varepsilon + 2a\sqrt{efcbd + cefd^2b - c^2f^2e^2d}}{(1+d)^2 b(\varepsilon + c)}, \tag{2.18}$$

or expressed in terms of the intake parameter d, this threshold reads

$$d_{thresh} = \frac{eafc + b\sigma c + bc + b\varepsilon + b\sigma\varepsilon + 2\sqrt{eacfb\varepsilon + eafc^2b + eacbf\sigma\varepsilon + eafc^2b\sigma}}{b(a - (\varepsilon + c)(1+\sigma))} \tag{2.19}$$

For model B the calculations are analogous, except that we now have to deal with a four-dimensional system as the equations for the radius R is coupled to evolution of the monocytes. but now we only find the class A equilibria which are marginally stable and

the trivial equilibrium $(m,M,L,R) = (0,0,0,1)$. The class A equilibria are of the form (m,M,L,R)=$(0,M_1,0,R_1)$, where M_1 is the equilibrium value of M and R_1 the equilibrium value of the lumen. Which equilibrium value is obtained depends on the initial conditions; the equilibria of class A are all marginally stable since they have two zero eigenvalues, one arises from the calculation in the same way as in model A, the other zero eigenvalue comes from the equation of the lumen radius R.

Submitted as: M.A.K. Bulelzai, J.L.A. Dubbeldam, H.G.E Meijer – *" Bifurcation analysis of a model for atherosclerotic plaque evolution, Submitted to Physica D."*

Chapter 3

Bifurcation analysis for the evolution of atherosclerotic plaques

A man should look for what is, and not for what he thinks should be.

Albert Einstein

Abstract

We analyze two ordinary differential equation (ODE) models for atherosclerosis. The ODE models describe long time evolution of plaques in arteries. We show how the dynamics of the first atherosclerosis model (model A) can be understood using codimension-two bifurcation analysis. The LDL intake parameter is the first control parameter and the second control parameter was either taken to be the conversion rate of macrophages or the wall shear stress. Our analysis reveals that in both cases a Bogdanov-Takens (BT) point acts as an organizing center. The bifurcation diagrams are calculated partly analytically and to a large extent numerically using AUTO07 and MATCONT. The bifurcation curves show that the concentration of LDL in the plaque as well as the monocyte and the macrophage concentration exhibit oscillations for a certain range of values of the control parameters. Moreover, we find that there are threshold values for both the cholesterol intake rate and the conversion rate of the macrophages. It was found that larger conversion rates of macrophages lower the threshold value of cholesterol intake and vice versa. We further argue that the dynamics for model A can still be discerned in the second model (model B) in which the slow evolution of the radius of the artery is coupled self-consistently to changes in the plaque volume. The very slow evolution of the radius of the artery compared to the other processes makes it possible to use a slow manifold approximation to study the dynamics in this case. We find that in this case the model predicts that the concentrations of the plaque constituents may go through a period of oscillations before the radius of the artery will start to decrease. These oscillations hence act as a precursor for the reduction of the artery radius by plaque growth.

3.1 Introduction

Atherosclerosis is a chronic inflammation of the layers of the artery wall, which gives rise to plaque formation that may ultimately lead to a blockage of the blood supply to vital parts

of the human body. The subject of how atherosclerotic plaques grow and how they may eventually rupture has been investigated since a long time. One mechanism that is responsible for the onset of atherosclerosis is endothelial injury after which subsequent biochemical phenomena take place that trigger the formation of plaques in arteries. The evolution of atherosclerotic plaques is characterized by accumulation of so-called lipid-laden foam cells over time (Crowther 2005) in a part of the arterial wall that is called the intima. The evolution of plaques involves a number of different substances of which some are carried with the blood flow and others reside in the layers of the artery. Important constituents include LDL-cholesterol, monocytes, macrophages, cytokines and smooth muscle cells. Besides the biochemical reactions that occur within the plaque mechanical stimuli were shown to play an important role in the development of atherosclerosis (Gijsen et al. 2008, Slager et al. 2005). Especially the shear stress that is exerted by the blood on the endothelial layer is crucial. It was found that high wall shear stress leads to a reduced plaque growth. The growth of a plaque region is therefore anisotropic: the plaque grows predominantly in the downstream direction where the shear stress is much lower than upstream (Yang and Vafai 2006, Ross 1993). Also during later stages in which smooth muscle cells proliferate and a fibrous cap covering the plaque is constructed, biomechanical factors become important for the stability and elasticity of the cap (Holzapfel and Gasser 2000).

Although beneficial effects of high wall shear stress on plaque evolution have been demonstrated in experiments (Slager et al. 2005, Gijsen et al. 2008), hardly any mathematical model has been developed that takes biomechanical effects into account. In a recent paper (Bulelzai and Dubbeldam 2012), we put forward an ODE model for the progression of atherosclerosis which includes wall shear stress effects. This model was inspired by a model of (Zohdi et al. 2004), who introduced a phenomenological model to describe plaque evolution by focusing on particle adhesion rather than wall shear stress. Another ODE model was developed by (Ougrinovskaia et al. 2010) for the initiation of the disease. Even though ODE models can never capture all aspects that are relevant for atherosclerosis, ODE models can give qualitative results that can serve as guidelines for clinical experiments. Moreover, ODEs are relevant limiting cases for partial differential equation (PDE) models (Bulelzai et al. 2013). These PDE-models usually contain parameters whose values are not always known from experiments. Bifurcation analysis can provide clues for the parameter values and the correctness of the model.

In this paper we analyse the dynamics associated with the progression of atherosclerosis by performing a codimension-two bifurcation analysis of the two models proposed in (Bulelzai and Dubbeldam 2012). These models referred to as model A and B, respectively, consider the evolution of the plaque in two cases. In model A the dynamics of plaque constituents is modeled without taking into account biomechanical effects. In model B, these effects were included by presuming a wall shear stress dependent recruitment of monocytes. The assumption of a constant throughput of the blood through the artery leads then to a self-

consistent model, in the sense that a smaller radius gives rise to larger flow velocity which implies on its turn an increased wall shear stress in a consistent way. The importance of such coupling of the blood flow to the plaque is essential in predicting how the radius of the artery behaves and how the total volume of the plaque evolves.

We organize this paper as follows: In Section 2 we present the models A and B. In Section 3 we focus on the codimension-two bifurcation diagram with two different sets of control parameters. We first consider the dynamics in the case that the LDL-intake rate and the ingestion rate of (oxidized) LDL are the control parameters and later we replace the ingestion rate by the wall shear stress. In both cases, we obtain similar bifurcation diagrams which have a Bogdanov-Takens (BT) point as an organizing center. This allows us to unfold the dynamics for a wide range of parameters. For model B which has a trivial bifurcation diagram, we perform a slow-fast analysis in Section 4 as the radius of the artery evolves on a much longer time scale than the typical time scale associated with the biochemical responses of the plaque constituents. We calculate the slow-manifold and determine the evolution of the artery radius. In Section 5, we discuss the physical interpretation of our bifurcation studies and finally in Section 6 we present the conclusions.

3.2 Introduction of models A and B

3.2.1 Model A

The evolution equations for model A are given as:

$$\dot{m} = \left(\frac{aL}{(1+\sigma)(1+L)} - \varepsilon - c \right) m, \tag{3.1a}$$

$$\dot{M} = cm - \frac{bML}{1+L}, \tag{3.1b}$$

$$\dot{L} = \frac{dm}{f+m} - eLM - L, \tag{3.1c}$$

$$\dot{F} = \frac{bLM}{1+L}. \tag{3.1d}$$

The physical interpretation of this coupled system is described in (Bulelzai and Dubbeldam 2012) and we will only give a brief explanation of the terms and parameters here. All parameters and variables in the model are dimensionless and nonnegative. The dot denotes the time derivative and since the equation for F (3.1d) decouples from the system, we only consider the three equations for m, M and L. In this model, which is called model A, in accordance with (Bulelzai and Dubbeldam 2012), the shear stress σ is simply considered a parameter. In contrast to model B where σ is calculated self-consistently using the relation between the radius of the artery and the flow velocity of the blood. The first equation

Eq. (3.1a) determines the evolution of the monocytes (m). The monocyte concentration increases due to the presence of oxidized LDL molecules in the plaque, which is represented by the first term on the righthand-side of Eq. (3.1a). The parameter a determining the rate at which monocytes are recruited from the blood is not experimentally known. The second and third term describe diffusion out of the plaque region and the process in which monocytes are converted into macrophages (M). Eq. (3.1b) describes the conversion of moncocytes into macrophages and the conversion of macrophages into foam cells with rate b. The ox-LDL cholesterol concentration (L) evolves according to Eq. (3.1c), which accounts for oxdidation by monocytes of unoxidized LDL entering the plaque from the blood. The intake rate of LDL cholesterol is denoted by d and is a control variable. The ingestion of ox-LDL by the macrophages and diffusion out of the plaque are accounted for by the second and third terms. Finally, the macrophages end up as foam cells with a conversion rate b, which is modeled in Eq. (3.1d).

3.2.2 Model B

The previously defined model A is made self-consistent by requiring that the wall shear stress σ is not a control parameter, but rather a dynamic quantity whose evolution is governed by an ordinary differential equation. Assuming a Poiseuille profile of the flow and demanding incompressibility, the wall shear stress $\sigma(t)$ and the artery radius $R(t)$ are seen to be related by

$$\sigma(t) = \frac{\alpha}{R^3(t)}, \tag{3.2}$$

where α is a constant proportional to the viscosity and the throughput through the artery. For details about the model we refer to (Bulelzai and Dubbeldam 2012).

Model B consists of the evolution equations of m, M, L, which are given by Eqs. 3.1(a-c) as in model A, and the evolution of the artery radius, or equivalently, the wall shear stress $\sigma(t)$. The evolution equation for σ is derived in (Bulelzai and Dubbeldam 2012) and reads

$$\dot{\sigma} = -\frac{3}{2}\xi\sigma(1-(\frac{\sigma}{\alpha})^{\frac{2}{3}})[m(\frac{aL\nu_m}{(1+\sigma)(1+L)} + c\nu_M - \nu_m(\varepsilon+c))$$

$$+\frac{bML}{1+L}(1-\nu_M) + \nu_L(\frac{dm}{f+m} - eM - L)]. \tag{3.3}$$

In Eq. (3.3) ξ is a small parameter and therefore model B constitutes a so-called slow-fast system with m, M, L the fast variables and σ the slow variable. We further remark that the parameters ν_i denote the volumes of the different constituents with respect to the foam cells and therefore $\nu_i \ll 1$. Hence a good approximation of Eq. (3.3) is

$$\dot{\sigma} = -\frac{3}{2}\xi\sigma\left(1-\left(\frac{\sigma}{\alpha}\right)^{\frac{2}{3}}\right)\frac{bML}{1+L}. \tag{3.4}$$

We can summarize model B by the following four evolution equations:

$$\dot{m} = \left(\frac{aL}{(1+\sigma(t))(1+L)} - \varepsilon - c \right) m, \tag{3.5a}$$

$$\dot{M} = cm - \frac{bML}{1+L}, \tag{3.5b}$$

$$\dot{L} = \frac{dm}{f+m} - eLM - L, \tag{3.5c}$$

$$\dot{\sigma} = -\frac{3}{2}\xi\sigma \left(1 - \left(\frac{\sigma}{\alpha} \right)^{\frac{2}{3}} \right) \frac{bML}{1+L}. \tag{3.5d}$$

3.3 Bifurcation analysis

In this section we will study the dynamics of model A, by first constructing a codimension-two bifurcation diagram for model A. The bifurcation diagram obtained for model A will serve as a starting point for our slow-fast analysis of model B. We proceed to discuss the general features of the dynamics and the bifurcation diagram in the next subsection, while the detailed computations are relegated to appendix A.

3.3.1 Codimension-two bifurcation diagram of model A

The system of differential equations given by Eqs. (3.1) is found to possesses infinitely many equilibria, which are separated in two classes. The first class of equilibria (infinitely many), which we denote by type *I*, are of the form $(m,M,L) = (0,M_0,0)$, where M_0 can have any non-negative value; we will denote this line with l in this paper. The second class of equilibria (type *II*) corresponds to two points with $m \neq 0$, which we will denote by $(m^{\pm},M^{\pm},L^{*})$.

We study the existence and stability of the equilibria by varying two parameters. First, we consider the bifurcation diagram in the (b,d)-plane in which both the ingestion of oxidized cholesterol by macrophages and the intake rate of LDL particles are control parameters. The reason for choosing d is that it is the natural parameter of the model as it determines the total number of LDL cholesterol entering into the plaque region and b because it determines the effect of macrophage secretory products such as, Interleukin-6 which determines how fast LDL-particles are eliminated from the plaque region (Frisdal et al. 2011).

Moreover, the two-dimensional bifurcation diagram allows a Bogdanov-Takens (BT) point to be identified which acts as an organizing center. As general references to the bifurcations we encounter see for example (Guckenheimer and Holmes 1983, Kuznetsov 1996).

There is a critical value of e such that the Bogdanov-Takens bifurcation is degenerate, i.e. there is a codimension-three bifurcation. Hence, we find qualitatively different bifurcation diagrams depending on the value of e. We therefore discuss both cases separately. The parameters a, f, ε, c are kept fixed throughout the paper and their values are set to $a = f = 1$,

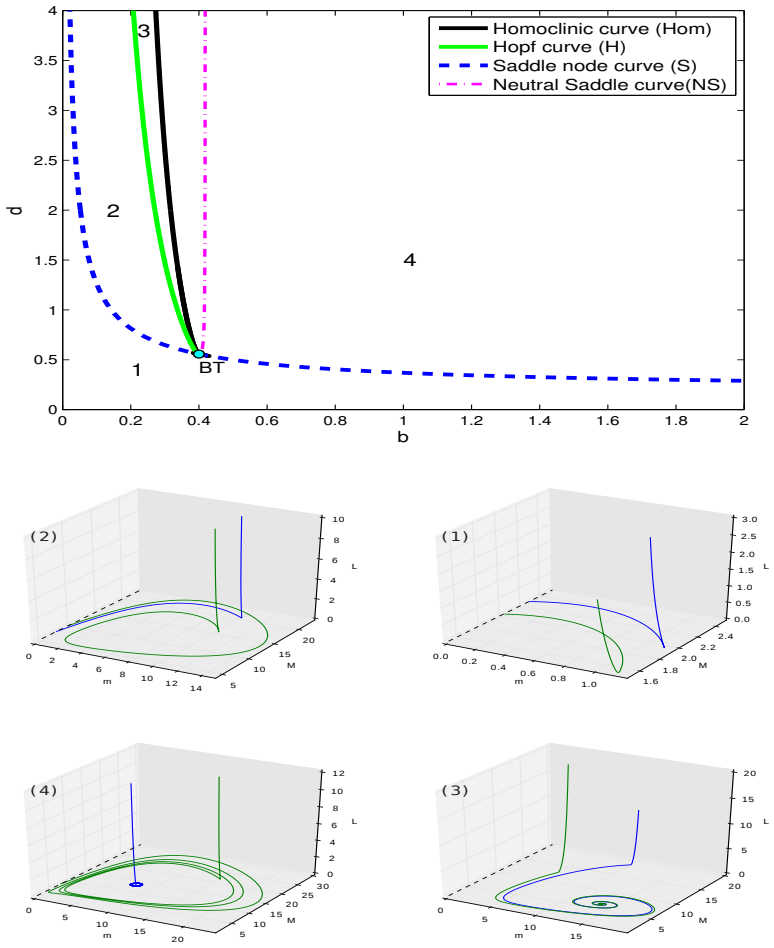

Figure 3.1: *The two-dimensional bifurcation diagram for $e = 1$. A Bogdanov-Takens point (BT) acts as an organizing center. The Hopf curve (H), the homoclinic curve (Hom) and the saddle node curve (S) intersect at BT. Simulations corresponding to regions (1-4) are also shown. The line of marginal equilibria l is shown with dashed black lines in the portraits and colors green and blue, show the two orbits starting from different initial conditions. The normal form coefficient for BT point, $s = sign(a_1/b_1)$, is positive here and is relegated in the appendix A.*

$\varepsilon = 0.01$ and $c = 0.05$. For the (b,d)-diagram, σ is fixed and set to 1.0; for the (σ,d)-diagram, the value of b is fixed and set to 0.7 in this paper.

Bifurcation diagram for $e = 1$

For the values of the parameters mentioned above, we find the two-dimensional bifurcation diagram displayed in Fig. 3.1, using the numerical continuation package AUTO07 (Doedel and Oldman 2012). The phase portraits that correspond to regions (1-4) in Fig. 3.1, are depicted at the borders of Fig. 3.1.

The dynamics in the respective regions (1-4) is as follows. In region (1) there are no equilibria beside the ones on the invariant manifold l, so all trajectories will end there, independent of the initial condition. For the atherosclerosis this implies that in this regime any perturbation in m, M, L, will lead to a small increment in the total plaque volume, which is reflected by a small increase in the foam concentration F (Equation 3.1d), which acts as a reservoir for the plaque components.

When d is increased so that the curve S is crossed, a saddle node bifurcation occurs in which two new equilibria are generated, both of which are repelling. This implies that in region (2) the phase portrait is very similar to that of region (1). Only when d is further increased, and hence the Hopf-curve (H) is crossed and region (3) is entered, the dynamics is very different. One of the equilibria born in the saddle node bifurcation turns stable and an unstable limit cycle emerges through a subcritical Hopf bifurcation. The unstable limit cycle separates the basin of attraction of the invariant line l and the attracting equilibrium (m^+, M^+, L^*), and therefore the system is bistable. An even further increase in d leads to a homoclinic bifurcation Hom in which the stable and unstable manifolds of the equilibrium (m^-, M^-, L^*), connect after which the unstable limit cycle vanishes. When we enter region (4), we are left with an attracting focus and a saddle besides the invariant line l. In this region (4) bistability therefore remains, but the basin of attraction of the attracting equilibrium (m^+, M^+, L^*) has expanded as can be seen from the phase portrait.

Bifurcation diagram for $e = 5$

When we change the value of the parameter $e = 1$ to $e = 5$, we have a diagram in which the positions of Hom and H curve are interchanged. In this case, it is known that there will be a point GH on the Hopf curve (H) where the first Lyapunov coefficient vanishes (Dumortier et al. 1991). At this point the Hopf bifurcation changes from subcritical to supercritical. Moreover, there will be a curve (saddle node of limit cycles curve) which connects the point GH to NS, the point where the neutral saddle curve and the homoclinic curve meet. This gives rise to four new regions (5) and (6), (7) and (8) where regions (6), (7) and (8) are so close to the homoclinic and Hopf curves that they cannot be discerned in Fig. 3.2(a), but in the qualitative sketch 3.2(b) their size has been exaggerated to clarify their presence.

The phase portraits corresponding to region (1-8) are shown in Fig. 3(a) and (b), again quantitatively and qualitatively, respectively. We remark that we can draw two-dimensional phase portraits as the saddle point has a two-dimensional stable manifold for the parameter

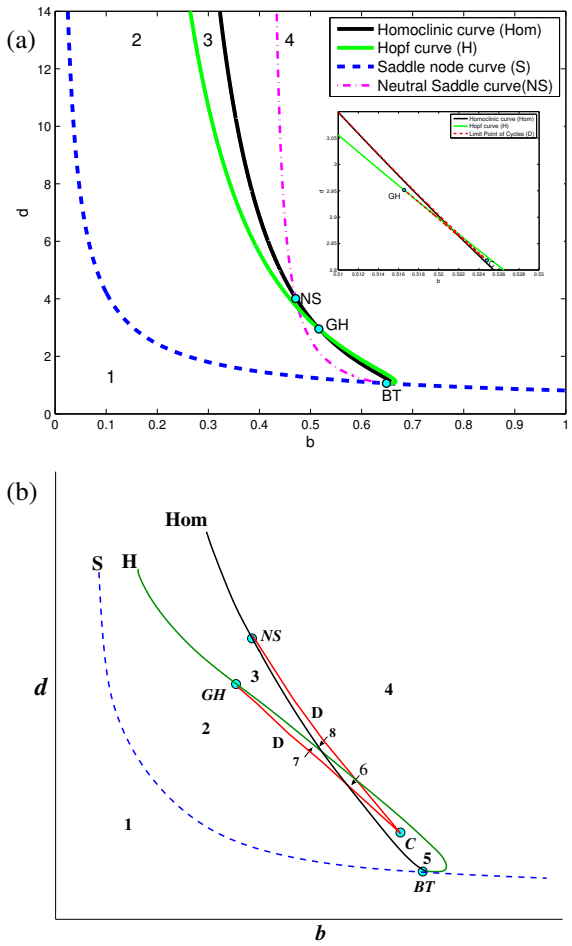

Figure 3.2: *Two-dimensional bifurcation diagram for $e = 5$, (a) and a qualitative sketch of bifurcation diagram (b). A Bogdanov-Takens point (BT) acts as an organizing center. The Hopf curve (H), the homoclinic curve (Hom) and the saddle node curve (S) intersect at BT. The inset and (b) show small parameter regions (5)-(8) that are bounded by a curve of limit point cycle bifurcations (denoted by D), which originates in a cusp point (C), connecting the degenerate Hopf point (GH) with the neutral saddle point (NS). The sign of the critical normal form coefficients for the BT point, $s = sign(a_1/b_1)$ is negative in this case (See Appendix A).*

values that we consider. In Fig. 3(b) the vertical direction corresponds to L and the horizontal axis is in the m-direction. The line l of equilibria is denoted by a solid filled circle, the saddle

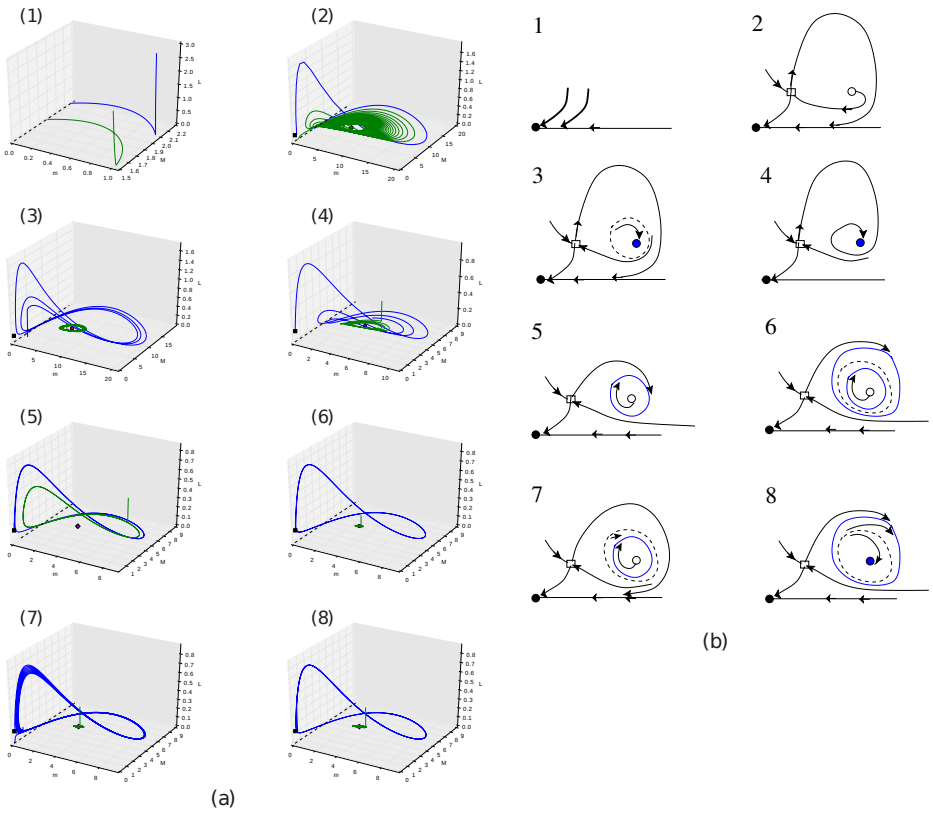

Figure 3.3: *Both three-dimensional(a) and two-dimensional(b) phase portraits for different regions for model A. (a) Green and blue lines stand for two different initial conditions to obtain the portraits. The line of marginal equilibria l is shown with dashed black lines in the portraits and colors green and blue, show the two orbits at different initial conditions. (b) The line l of equilibria is denoted by a solid filled circle, the saddle point by an open square and stable (unstable) focus by a filled (open) circle. Stable limit cycles are designated by solid closed curves and unstable ones by dashed curves.*

point by an open square and stable (unstable) focus by a filled (open) circle. Stable limit cycles are designated by solid closed curves and unstable ones by dashed curves.

Regions (1-4), which were also present for the case $e = 1$, are accessed when d is sufficiently large. This implies that for sufficiently large cholesterol intake no qualitative difference between the $e = 1$ and $e = 5$ scenario is observed. This can be understood by realizing that e determines how fast the LDL disappears in the presence of macrophages. A larger cholesterol intake counteracts an enhanced value of e and therefore the phase portraits (1)-(4) are still present for d large enough. When we cross the curve D of limit point cycle

bifurcations from region (2) to (7), we see from Fig. 3(b) that two limit cycles are created, one stable and one unstable. The equilibria remain of saddle and unstable focus type. There is bistability as there is one stable limit cycle as well as the line of equilibria l. We remark that in Fig. 3(a) we can distinguish a stable limit cycle near the unstable focus (diamond) and the orbit starting near the saddle that eventually arrives in l. When crossing the homoclinic curve (Hom) from region (7) one enters region (6), where two stable limit cycles are present and the two type II equilibria remain of the same type as in (6); the system again exhibits multistability. Region (5) can be accessed by crossing the curve D of limit point cycle bifurcations in which a stable and an unstable limit cycle collide, leaving the system with a single stable limit cycle and the stability of equilibria unaltered.

The dynamics in the remaining region (8) can be explored if one crosses the curve D of limit point cycle bifurcations from region (4). In this case the stability of the equilibria remain unaltered and a pair of limit cycles, one stable and one unstable, is created. Again multistability is found. This time between the stable focus, equilibria of class I and the stable limit cycle. In Fig. 3(a)(8) the stable equilibrium and limit cycle are shown.

3.3.2 Bifurcation diagram in the (σ, d)-plane

Instead of considering the bifurcations of system (3.1), we can also study the bifurcations in the (σ, d)-plane, where σ determines the wall shear stress which is an important quantity as it determines the biomechanical effects. Moreover, the parameter d sets the timescale in the model and σ is slowly varying in the self-consistent model B. The diagram obtained for this set of parameters will therefore also be useful in analyzing the dynamics of model B, which is the subject of the next section. We first briefly discuss Fig. 3.4 which shows the bifurcation curves for varying σ and d. As can be seen by comparing Fig. 3.4(a) and (b) with Figs. 3.1 and 3.2 the diagrams are very similar. The labels (1)-(4) correspond to the portraits that were shown in Fig. 3.1. The marginal fixed point $(0, M_0, 0)$ exists for all parameter values and is a global attractor below the saddle node-curve (S). Above the S-curve there are the two nontrivial fixed points of type II. One is a saddle whose stable manifold is a separatrix for the basin of attraction between the marginal fixed point and another steady state. This second steady state is stable for sufficiently high values of σ. For decreasing values of σ we encounter a subcritical Hopf bifurcation and the only attractor is the invariant line l of marginally stable equilibria. The Hopf curve meets the S-curve at a Bogdanov-Takens bifurcation from where also a homoclinic bifurcation curve emerges. There exists an unstable periodic solution for parameter values between the Hopf and the homoclinic curve. Note that the Hopf curve crosses the d-axis at $d \approx 0.8$. This intersection point moves to very high values of d when decreasing b. Increasing b, on the other hand, shifts the Hopf curve and BT-point to negative values of σ. Next we set $e = 2$ and keep d and σ as bifurcation parameters. The main qualitative change in the bifurcation diagram is that the Hopf curve close to

the BT-point is now supercritical. This is accompanied by the appearance of a generalized Hopf (GH) and a neutral saddle (NS) point on the Hopf and homoclinic curves, respectively. These codimension-two bifurcation points are connected by a short curve corresponding to a curve of limit point cycles (D) bifurcations. This implies that there is a region with stable oscillations delimited by the Hopf (H), homoclinic (Hom) and (D) curve. We note that for higher values of e the (D) curve exhibits a cusp bifurcation.

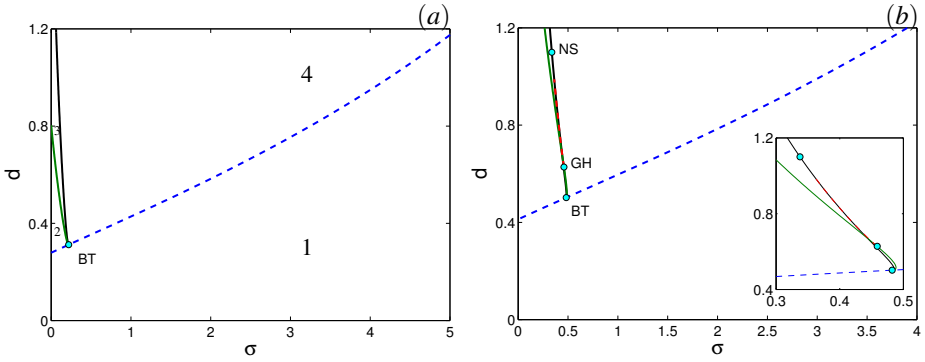

Figure 3.4: *Bifurcation diagrams for $e = 1$ (a) and $e = 2$ (b). The significance of the curves is as follows: saddle node curve (dashed blue), Hopf curve (solid green), homoclinic curve (solid black) and the curve of double limit cycles (dashed red). Codimension-two bifurcation points are Bogdanov-Takens (BT), Generalized Hopf (GH), neutral homoclinic loop (NS) indicated by light blue markers. The sign for second Lyapunov coefficient for GH point is negative. The sign for critical normal form coefficients, $s = sign(a_1/b_1)$ is positive for $e = 1$ and negative for $e = 2$ (See Appendix A).*

3.4 Slow-fast analysis of model B

The system (3.5) constitutes a slow-fast system with a small parameter ξ. Slow-fast systems have attracted much interest lately. The complicated geometry of slow manifolds near a folded node was numericaly studied in (Desroches et al. 2008). The applications of slow-fast dynamics, and the immediately related ramped-bifurcation theory, to climate models has recently lead to the surprising prediction of a so-called compost bomb instability by (Wieczorek et al. 2011). We apply a similar analysis here. The equations (3.5)(a-c) constitute the fast system. The slow system (d) is analyzed by scaling time $\tau = \xi t$, where τ is the slow time scale. The new system of differential algebraic equations can be summarized as

$$\xi \dot{x} = f(x,\sigma), \qquad \dot{\sigma} = g(x,\sigma), \tag{3.6}$$

where $x = (m,M,L)$ are the fast variables and $f(x,\sigma)$ and $g(x,\sigma)$ are smooth and continuously differentiable functions given by the system (3.5). According to Fenichel's first theo-

rem, the reduced slow system in the limit of $\xi \to 0$ is given as:

$$0 = f(x,\sigma), \qquad \dot{\sigma} = g(x,\sigma). \tag{3.7}$$

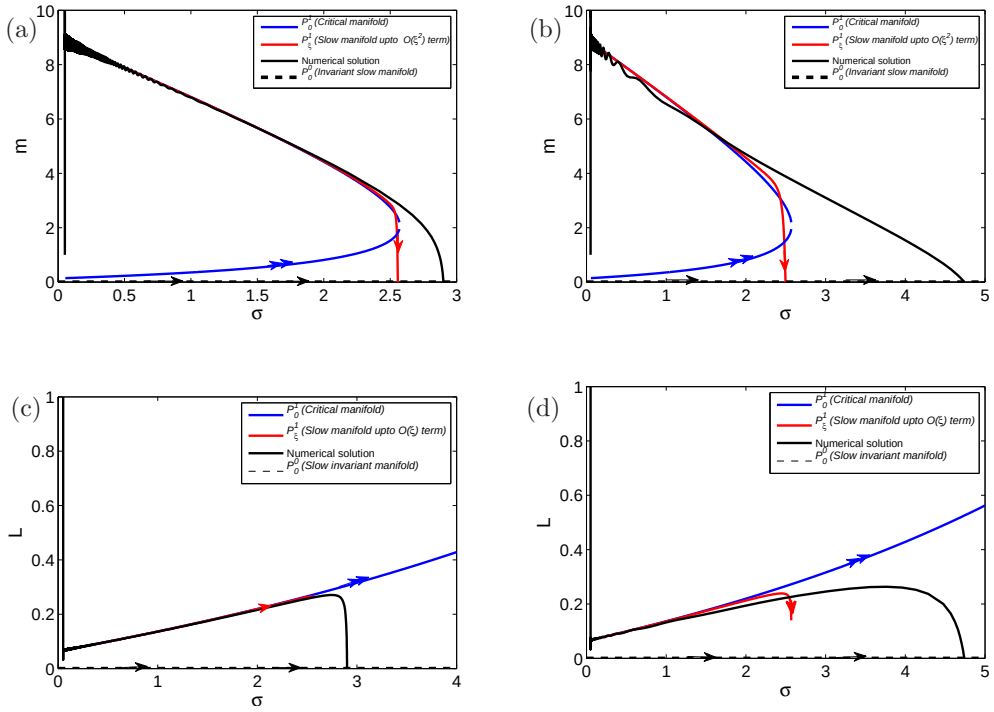

Figure 3.5: *(a,c) with $\xi = 0.0002$ and (b,d) with $\xi = 0.002$; Slow manifold calculated for two different values of ξ using fixed values for parameters, which are already mentioned in this paper. The numerical solution (black), approximation of slow manifold (red) are shown along with the critical manifold (blue). The line $m = 0$ and $L = 0$ (dashed) are also shown, which constitute the invariant slow manifold.*

The critical manifolds are obtained by solving the equations $f(x,\sigma) = 0$ and read

$$P_0^0 = \{(m,M,L) \mid m = 0, M = M_0, L = 0\}$$

$$\text{and } P_0^1 = \{(m,M,L) \mid m = m_0^+(\sigma), M = M_0^+(\sigma), L = L_0^*(\sigma)\}.$$

The time evolution of the reduced (one-dimensional) system, is obtained by evaluating $g(x,\sigma)$ on the slow manifold P_0^1, which yields

$$\dot{\sigma} = -\frac{3bM_0^+(\sigma)L_0^*(\sigma)\sigma}{2}\left(1 - \left(\frac{\sigma}{\alpha}\right)^{\frac{2}{3}}\right). \tag{3.8}$$

The slow manifolds $P_{\cdot}^{(0,1)}$ exist by the virtue of geometric singular perturbation theory, e.g. see (Arnold and Jones 1994). The superscripts in the manifold $P_{\cdot}^{(0,1)}$ stand for the two different classes of equilibria that we mentioned earlier. For the type I equilibria, this manifold is invariant implying $P_{\cdot}^{(0,1)} = P_0^0$ (dashed black line in Fig. 3.5). For the nontrivial equilibria we find the first and second order perturbations in ξ by the substitution $P_{\cdot}^1(\sigma) = P_0^1(\sigma) + \xi P_1^1(\sigma) + \xi^2 P_2^1(\alpha)$ (Kaper and Kaper 2002, Gear et al. 2005, Wieczorek et al. 2011, Guckenheimer et al. 2012) and find:

$$\begin{aligned} \mathcal{O}(\xi): &\quad (D_x f)P_1^1 = (DP_0^1)g, \\ O(\xi^2): &\quad (D_x f)P_2^1 = (DP_1^1)g + (DP_0^1)((D_x g)P_1^1) - \frac{1}{2}(D_x^2 f)(P_1^1, P_1^1), \end{aligned} \tag{3.9}$$

where $D_x f$ is 3×3 matrix of partial derivatives $\partial f_i / \partial x_j$, (DP_0^1) is 3×1 matrix of partial derivatives $\partial P_0^1 / \partial x_i$, $(D_x g)$ is 1×3 matrix of partial derivatives $\partial g / \partial x_i$. When we solve Eqs. (3.9) we obtain:

$$P_1^1 = \{(m,M,L) \mid m = m_1^+(\sigma), M = M_1^+(\sigma), L = L_1^*(\sigma)\} \quad \text{and}$$

$$P_2^1 = \{(m,M,L) \mid m = m_2^+(\sigma), M = M_2^+(\sigma), L = L_2^*(\sigma)\},$$

where $M_i^+(\sigma), m_i^+(\sigma)$ denote the i-th order approximation of the stable equilibrium. For details of the calculations we refer the reader to Appendix B.

3.4.1 Dynamics with shear stress

In the full system we show several characteristic simulations starting with $(m,M,L,R) = (1,1,1,0.99)$ for various values of d. These initial values are chosen such that the orbit does not always jump immediately to the marginal fixed point. The first case is with low d. For any positive σ there is no nontrivial steady state and the orbit quickly returns to the marginal fixed point, see Fig. 3.6(a). The net change of R is small and the artery stays open. The second case is for medium values of d, i.e. above the curve S, but below the Hopf curve H. Then it depends on the choice for α which scenario occurs as it determines the initial σ value. For $d = 0.6$ and $\alpha = 0.05$ the nontrivial steady states are both unstable and the trajectory shows a transient outburst of monocytes but then the orbit approaches the marginal fixed point, see Fig. 3.6(b). Here too, the artery radius remains large. Changing $\alpha = 0.13$, we observe oscillations whose amplitude slowly diminishes until σ is too large and nontrivial dynamics is no longer supported, see Fig. 3.6(c). For higher values of d, there is a stable nontrivial steady state. The orbit displays damped oscillations while converging to it. Then R decreases and σ increases so that the steady state moves and the orbit tries to follow it until σ comes close to a critical value determined by the (S) curve, see Fig. 3.6(d). In the latter two cases the final radius R is considerably smaller. In Fig. 3.7, we have presented two

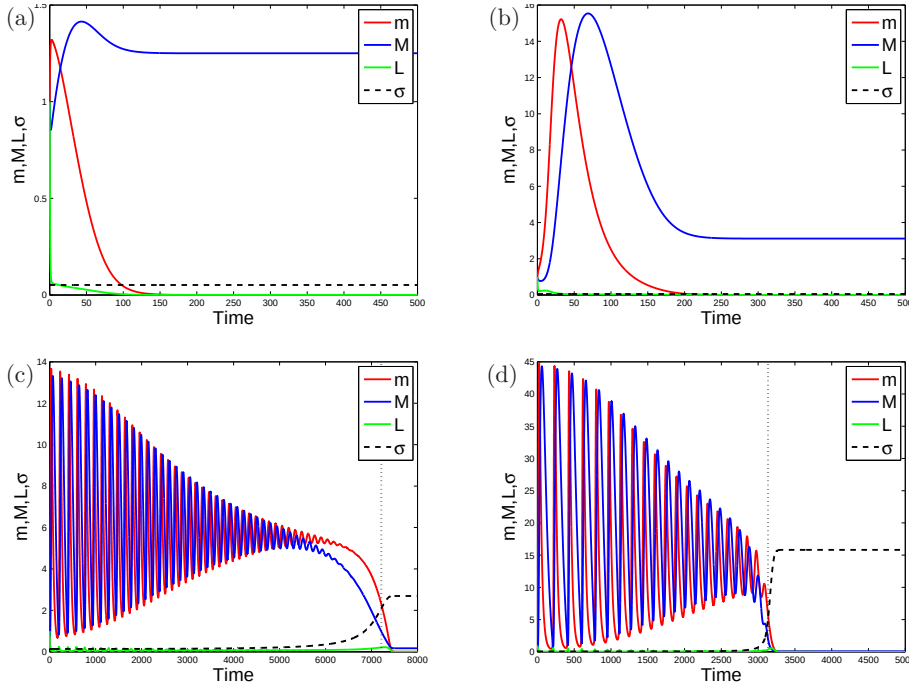

Figure 3.6: *Time-evolution σ, the monocytes, ox-LDL macrophage and concentrations for (a) $d = 0.2$; (b,c) $d = 0.6$; (d) $d = 1.2$. We choose $\xi = 0.002$ and $\alpha = 0.05$ and all other parameters are mentioned in the text except $\alpha = 0.13$ in (c). The vertical dashed line indicates that σ crossed the critical value. Note the different time-scales of the various simulations.*

graphs obtained with two different initial conditions with $e = 2$. In Fig. 3.7(a), the initial value for radius is 0.99 and in Fig. 3.7(b) we set $R(0) = 0.999$ and changed the value of α accordingly.

3.5 Physical interpretation

In this section we discuss the physical interpretation of the phase portraits in regions (1-4) and bifurcation diagrams. The small regions are not discussed as they will be very hard to find experimentally. In both models A and B, a high value of cholesterol intake (d) increases the oxidized-LDL particle concentration, which in turn increases the volume of the plaque. The two parametric bifurcation diagrams in this paper, shed more light on the ingestion rate of macrophages and effects of endothelial shear stress. We employed the functional form of $\frac{1}{(1+\sigma_w/\sigma_0)}$ in the evolution of the monocytes to model the effect that low shear stress at the endothelium causes more plaque accumulation. It is well established that low or oscillatory

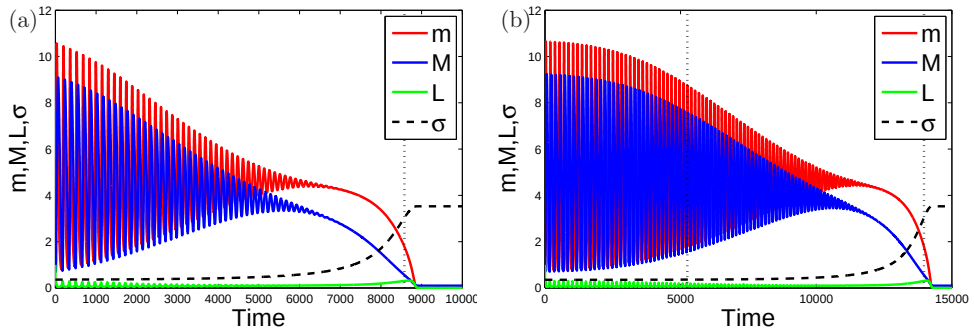

Figure 3.7: (a) *with* $R(0) = 0.99$, (b) *with* $R(0) = 0.999$*; Time-evolution of shear stress, monocytes, ox-LDL and macrophages concentrations for* $d = 1.0$,$e = 2$,$\alpha = 0.35$ *and with two different initial conditions. The vertical dashed line indicates that* $\sigma(t)$ *crosses a critical values. In (b), since* σ *is initially very low, first the Hopf curve is crossed (shown dotted) while in* (a)*, due to a larger initial perturbation, only crossing of the S-curve can be detected.*

wall shear stress is a plaque promoting condition (Gijsen et al. 2008, Slager et al. 2005). Regions of high shear stresses do not experience plaque growth while regions of low and oscillatory wall shear stress do.

We first comment on the bifurcation diagrams corresponding to model A and next discuss the consequences for model B. It is evident from Figs. 3.1, 3.2 and 3.4 that region 1 is the healthy region in model A. The critical value of d increases (following the saddle-node curve) with wall shear stress (see Fig. 3.4) and decreases with b, whose value determines how fast macrophages are transformed into foam cells. The dependence of the critical value of d on σ is as expected, as high shear stress is in general favorable to diminish plaque growth and the dependence of d_{crit} on b is also no surprise as faster ingestion of LDL by macrophages will result in enhanced plaque formation. The marginally attracting manifold l corresponds to both monocytes and ox-LDL concentrations zero. Perturbing the system in this state will only alter the macrophage concentration to a new constant value.

In region 2 model A has an unstable node. In the (b,d) diagram this region corresponds to conversion rates of macrophages that are sufficiently large to deplete the cholesterol in the plaque and therefore the plaque will only experience growth during a small period of time, after which the plaque turns stationary again. In the (σ,d)-diagram, region 2 correponds to wall shear stress values that are sufficiently low not to have any other stable states except the invariant line l. This region marks a parameter range in which plaques do not grow indefinitely, but behave similarly to region 1 in which a perturbation in LDL can lead to a limited decrease of the artery radius.

In region 3 model A has an unstable limit cycle and a stable focus. The presence of a stable focus indicates that the plaque may start to grow indefinitely, depending on the initial

conditions. If the intial values of the monocytes, macrophages and LDL are such that they are in the region of attraction of the focus, the plaque will grow indefinitely with oscillations in the concentrations of the plaque constituents that gradually die out. When the initial conditions are outside the attraction zone of the focus, a limited plaque growth is established, which is in general preceeded by transient oscillations in the concentration of plaque constituents. The same reasoning is true for region 3 in the (σ, d)-plane, which is surprising since a large σ value is considered to lead to less plaque growth. In our model, σ is also responsible for the recruitment of monocytes from the blood in the plaque. Increased values of σ imply an impeded recruitment of monocytes and hence only a moderate population of macrophages. These macrophages ingest LDL, but due to the small value of $b = 0.7$, the LDL survives long enough to enhance the LDL concentration and subsequently this leads to an increased monocyte concentration. The oscillations that are created will in general die out to zero, but for particular initial values they can approach a constant nonzero value and the plaque will grow indefinitely. We should stress here that the bifurcation diagram Fig. 3.4 was made for $b = 0.7$. When $b > 1$ the BT-point will disappear and the dependence of the dynamics on σ is in accordance with expectations. This would suggest that for real arteries $b > 1$.

If the system is in region 4, the plaque will in general grow indefinitely, although for certain initial conditions the plaque growth ends in finite time. Region 4 can be accessed for high values of σ or high values of the ingestion rate b. The fact that large values b are detrimental can easily be comprehended. The larger the value of b the more macrophages are converted into foam cells and consequently a large plaque growth results. The dependence on σ is explained similarly to the behavior in region 3. In region 4 the wall shear stress is large enough to sustain a certain amount of monocytes that induces a small population of macrophages. Therefore the LDL particles can survive long enough to attract more monocytes and LDL molecules into the plaque, which leads to a growing plaque volume for $b = 0.7$. Again we remark that this dependence on σ disappears for $b > 1$.

In model B all solutions will finally reach the invariant manifold l. So we discuss the transients that arise when the system is perturbed from its initial state, that we take to be on l. Small perturbations to the system in this state will again die out, but the artery radius will decrease a little. Still, several consecutive perturbations can lead to sigificant reduction in artery radius.

For model B the dynamics in region 2 stabilizes after transient oscillations in the constituents of the plaque. The wall shear stress first increases as depicted in Fig. 3.6(b), and then stabilizes to a constant value. This means that here the radius of the artery has decreased and subsequent perturbations in the plaque constituents may cause further reductions in the artery size. For short times, the unstable limit cycle implies a continuous periodic growth of plaque constituents, but eventualy the radius reduction of the artery, or equivalently, the growth of σ, will come to a halt, when $\sigma(t)$ crosses the S-curve. Starting from region 3 or

4 in model B corresponds to assuming higher values of α and hence a higher volume flux through the artery. Depending on the value of b we find that the radius reduction increases with α, as was the case for the results presented here for $b = 0.7$, or decreases with α, which was the case for $b = 1$ which was presented in (Bulelzai and Dubbeldam 2012).

3.6 Conclusions

The evolution of atherosclerotic plaque is explored by varying different parameters which affect its growth in arteries. We explored codimension-two bifurcation diagrams for a model of atherosclerosis in which the wall shear stress was assumed to be a parameter. We showed that the dynamics is governed by a Bogdanov-Takens point that acts as an organizing center. Depending on the value of e, a parameter that controls at what rate oxidized LDL disappears from the plaque, the order of homoclinic and the Hopf curve emanating from the BT-point changes. Crossing of homoclinic and Hopf curves gives rise to a few extra regions in the bifurcation diagram which are so tiny, however, that observing these in experiments will be extremely difficult.

The bifurcation analysis was next used to analyze a self-consistent model in which the shear stress was no longer a parameter, but evolved dynamically. By using techniques from slow-fast systems, we explored the growth of plaques for this more realistic model. Depending on the values of the conversion rate b of the macrophages we find that larger plaques results from higher blood velocities ($b < 1$), or larger plaques correspond to smaller blood velocities ($b \geq 1$), suggesting that $b > 1$ is the relevant parameter regime.

Our analysis reveals that before plaques start to grow they will generally go through a period where the concentrations of the plaque constituents oscillate, before the plaque starts to grow significantly. If this behavior is robust and remains even in more complicated models, this precursor of the onset of artery occlusion could be an indicator that might eventually be used in a clinical environment. Of course, one should realize that the model we investigated in this paper lacks a lot of components that will modify, at least quantitatively but possibly also qualitatively, the behavior of the system. For example, the shape of the plaque is entirely neglected and this will lead to changes in the flow profile and the wall shear stress is therefore no longer constant along the artery. Moreover, cytokines and HDL particles have not been taken into account, which have been shown to influence plaque growth (Ougrinovskaia et al. 2010). The bifurcation study we performed here illustrates its relevance to identiying parameter regions that are clinically sensible and makes predictions about the dynamical behavior of plaques that may be put to a clinical test.

3.7 Acknowledgment

MAKB and JLAD would like to thank Wim van Horssen for scientific discussions. JLAD is grateful to Sebastian Wieczoreck and Bernd Krauskopf for their help with AUTO and for stimulating discussions about the dynamics in the investigated models.

3.8 Appendix A

To calculate the stability of the equilibria of class I, we shift the equilibria $(0, M_0, 0)$ to the origin O, by introducing $\bar{M} = M - M_0$. We may then cast equations (3.1) in the following form

$$\begin{pmatrix} \dot{m} \\ \dot{\bar{M}} \\ \dot{L} \end{pmatrix} = A \begin{pmatrix} m \\ \bar{M} \\ L \end{pmatrix} + \begin{pmatrix} \frac{a}{1+\sigma} mL + \mathcal{O}(||m, \bar{M}, L||^3) \\ -b\bar{M}L + bM_0L^2 + \mathcal{O}(||m, \bar{M}, L||^3) \\ -\frac{d}{f^2} m^2 - e\bar{M}L + \mathcal{O}(||m, \bar{M}, L||^3), \end{pmatrix}, \tag{3.10}$$

where we defined the matrix A by

$$A = \begin{pmatrix} -c-\varepsilon & 0 & 0 \\ c & 0 & -bM_0 \\ \frac{d}{f} & 0 & -eM_0 - 1 \end{pmatrix}. \tag{3.11}$$

The eigenvalues of A are easily found to be $\lambda_1 = -(\varepsilon + c)$, $\lambda_2 = -(eM_0 + 1)$, $\lambda_3 = 0$. The corresponding eigenvectors are given by $\mathbf{v}_1 = (-\frac{f(-eM_0 - 1 + \varepsilon + c)}{d}, \frac{f(-eM_0 - 1 + \varepsilon + c)c + dbM_0}{d(\varepsilon + c)}, 1)^T$, $\mathbf{v}_2 = (0, bM_0/(eM_0 + 1), 1)^T$, and $\mathbf{v}_3 = (0, 1, 0)^T$.

3.8.1 Equilibria of Type II

Equilibria II are given as:

$$\begin{aligned} L^* &= \frac{(\varepsilon + c)(1 + \sigma)}{a - (1 + \sigma)(\varepsilon + c)}, \\ M^{\pm} &= \frac{cm^*(1 + L^*)}{bL^*}, \\ (m^*)^2 + m^* &\left[f - \frac{db}{ec} + \frac{(1 + \sigma)(1 + d)b(\varepsilon + c)}{eac} \right] + \frac{fb(1 + \sigma)(\varepsilon + c)}{eac} = 0. \end{aligned} \tag{3.12}$$

Solving the quadratic equation for m^* gives two values m^+ and m^-, which satisfy:

$$m^{\pm} = -\frac{f - \frac{db}{ec} + \frac{(1+\sigma)(1+d)b(\varepsilon+c)}{eac}}{2} \pm \frac{\sqrt{\Delta}}{2},$$

$$\text{where } \Delta = \left[f - \frac{db}{ec} + \frac{(1+\sigma)(1+d)b(\varepsilon+c)}{eac} \right]^2 - 4\frac{bf(1+\sigma)(\varepsilon+c)}{eac}.$$

Since the equation is quadratic in m^*, the two roots have either both positive or both negative. In order for equilibria (II) to exist and being both positive, the following conditions must hold:

$$\text{C1:} \quad a > (1+\sigma)(\varepsilon+c) \quad \text{C2:} \quad f - \tfrac{db}{ec} + \tfrac{(1+\sigma)(1+d)b(\varepsilon+c)}{eac} < 0 \quad \text{C3:} \quad \Delta > 0.$$

The conditions C2 and C3 can be summarized in a condition imposed on d

$$d \geq d_{crit} := \frac{feca + (1+\sigma)(c+\varepsilon)b + 2\sqrt{b(1+\sigma)(c+\varepsilon)feca}}{b(a-(1+\sigma)(c+\varepsilon))}.$$

These equilibria are born from a saddle-node bifurcation as shown in (Bulelzai and Dubbeldam 2012). Here we describe a generic bifurcation of codimension-two to unfold the dynamics these equilibria govern.

3.8.2 Bogdanov-Takens singularity calculations

The system (3.1) at equilibria type II passes through Bogdanov-Takens singularity. We would like to obtain the normal form by center manifold reduction. On the center manifold, the dynamics is described by the reduced equations $x' = y, y' = a_1x^2 + b_1xy$. We will compute the critical normal form coefficients a_1 and b_1 and show that a_1 is never zero, while b_1 can vanish. For the computation, we know that the double zero eigenvalues are located where the parameters (d,e) pass through the values $d_{crit} = \frac{faec+b(c+\varepsilon)(1+\sigma)\pm 2\sqrt{faecb(c+\varepsilon)(1+\sigma)}}{b(a-(c+\varepsilon)(1+\sigma))}$ and $e_{crit} = \frac{ab^3(c+\varepsilon)(1+\sigma)^3}{fc(a^2-(c+\varepsilon)(1+\sigma)(a+b(1+\sigma)))^2}$. We chose e_{crit} value for the calculation of normal form and not b_{crit} as the equation is linear in e. The value for d_{crit} implies a sharp turn (collision of equilibria type II). The value for $m^{\pm}$ at this point is $\frac{\sqrt{faecb(1+\sigma)(\varepsilon+c)}}{aec}$. To calculate the critical coefficients, involved in the degeneracy conditions in Bogdanov-Takens bifurcation analysis, we follow (Kuznetsov 1999). The Jacobian matrix at these critical values, is given by:

$$J_{crit} = \begin{bmatrix} 0 & 0 & \frac{f((-\varepsilon-c)\sigma-c+a-\varepsilon)^2A}{b(1+\sigma)^2a^2} \\ c & -\frac{b(\varepsilon+c)(1+\sigma)}{a} & -\frac{cf((-1-\sigma)c+(-1-\sigma)\varepsilon+a)^2A}{a^2b(1+\sigma)^2(\varepsilon+c)} \\ d_{crit}f\left(f+\frac{fA}{ab(1+\sigma)}\right)^{-2} & -\frac{e_{crit}(\varepsilon+c)(1+\sigma)}{a-(1+\sigma)(\varepsilon+c)} & \frac{-e_{crit}cfA-b^2(1+\sigma)^2(\varepsilon+c)}{b^2(1+\sigma)^2(\varepsilon+c)} \end{bmatrix}, \quad (3.13)$$

where $A = a^2 - (\varepsilon+c)(1+\sigma)(a+(1+\sigma)b)$. At this bifurcation point, two eigenvalues are zero, and there exist two linearly independent (generalized) eigenvectors $q_{0,1} \in \mathbb{R}^3$ for J_{crit},

and two eigenvectors $p_{0,1} \in \mathbb{R}^3$ for its transpose such that

$$J_{crit} q_0 = 0, \quad J_{crit} q_1 = q_0, \quad J_{crit}^T p_1 = 0, \quad J_{crit}^T p_0 = p_1.$$

The eigenvectors are given by:

$$q_0 = \begin{bmatrix} \frac{(\varepsilon+\sigma\varepsilon+c+\sigma c)b}{ac} \\ 1 \\ 0 \end{bmatrix},$$

$$p_1 = \begin{bmatrix} \frac{(a-(1+\sigma)(\varepsilon+c))ca^2}{-(1+\sigma)^3(\varepsilon+c)^2b^2+(1+c+\varepsilon)(a-(1+\sigma)(\varepsilon+c))a(1+\sigma)b+(a-(1+\sigma)(\varepsilon+c))a^2} \\ -\frac{(1+\sigma)(\varepsilon+c)((-\varepsilon-c)\sigma-c+a-\varepsilon)ba}{-(1+\sigma)^3(\varepsilon+c)^2b^2+(1+c+\varepsilon)(a-(1+\sigma)(\varepsilon+c))a(1+\sigma)b+(a-(1+\sigma)(\varepsilon+c))a^2} \\ \frac{\left(-b(1+\sigma)^2(\varepsilon+c)+((-\varepsilon-c)\sigma-c+a-\varepsilon)a\right)^2((-\varepsilon-c)\sigma-c+a-\varepsilon)^2fc}{\left(-(1+\sigma)^3(\varepsilon+c)^2b^2+(1+c+\varepsilon)((-\varepsilon-c)\sigma-c+a-\varepsilon)(1+\sigma)ab+((-\varepsilon-c)\sigma-c+a-\varepsilon)a^2\right)(1+\sigma)^2ba} \end{bmatrix},$$

and the generalized eigenvectors are given by:

$$p_0 = \begin{bmatrix} 1 \\ \frac{-(1+\sigma)(\varepsilon+c)b+ac}{ac} \\ g_0 \end{bmatrix},$$

$$q_1 = \begin{bmatrix} g_1 \\ g_2 \\ \frac{b^2a(1+\sigma)^3(\varepsilon+c)}{f\left(-b(\varepsilon+c)\sigma^2-(\varepsilon+c)(a+2b)\sigma+(-a-b)\varepsilon+(-a-b)c+a^2\right)((-\varepsilon-c)\sigma-c+a-\varepsilon)^2c} \end{bmatrix}.$$

where the lengthy expressions g_0, g_1, g_2 are given by:

$$\begin{aligned} g_0 \quad = \quad & \frac{-\left(a^2-(1+\sigma)(\varepsilon+c)a-b(1+\sigma)^2(\varepsilon+c)\right)^2(a-(1+\sigma)(\varepsilon+c))f}{\left(a^3+((1+c+\varepsilon)b-\varepsilon-c)(1+\sigma)a^2-b(1+\sigma)^2(1+c+\varepsilon)(\varepsilon+c)a-(1+\sigma)^3(\varepsilon+c)^2b^2\right)(\varepsilon+c)(1+\sigma)^2ba^3} \times \\ & \left[\left((-1+c)\varepsilon+c^2\right)a^3-(\varepsilon+c)(1+\sigma)\left((1+c+\varepsilon)b+(-1+c)\varepsilon+c^2\right)a^2\right. \\ & \left.+b(1+\sigma)^2(1+\varepsilon)(\varepsilon+c)^2a+b^2(1+\sigma)^3(\varepsilon+c)^3\right], \end{aligned}$$

$$
\begin{aligned}
g_1 \quad = \quad & \frac{1}{\left(-(1+\sigma)^3(\varepsilon+c)^2b^2+(1+c+\varepsilon)(a-(1+\sigma)(\varepsilon+c))a(1+\sigma)b+(a-(1+\sigma)(\varepsilon+c))a^2\right)((-1-\sigma)c-\sigma\varepsilon+a-\varepsilon)c^2a^3}\times \\
& \Big[-(1+\sigma)^7(\varepsilon+c)^5b^5+2\left((1+c+\varepsilon)a-\tfrac{1}{2}(c+2\varepsilon+2)(\varepsilon+c)(1+\sigma)\right)(\varepsilon+c)^3(1+\sigma)^5ab^4 \\
& -\left((1+c+\varepsilon)^2a+(\varepsilon+c)\left(c^2-2c-\varepsilon^2-4\varepsilon-1\right)(1+\sigma)\right)(\varepsilon+c)(a-(1+\sigma)(\varepsilon+c))(1+\sigma)^3a^2b^3 \\
& +\left((1+c+\varepsilon)\left(c^2+(-1+\varepsilon)c-2\varepsilon\right)a-(\varepsilon+c)\left(c^3+(1+2\varepsilon)c^2+\left(-1+\varepsilon^2-\varepsilon\right)c-2\varepsilon-2\varepsilon^2\right)(1+\sigma)\right) \\
& (a-(1+\sigma)(\varepsilon+c))(1+\sigma)^2a^3b^2+\left(c^2+(1+\varepsilon)c-\varepsilon\right)(a-(1+\sigma)(\varepsilon+c))^2(1+\sigma)a^4b+ \\
& (a-(1+\sigma)(\varepsilon+c))^2ca^5\Big],
\end{aligned}
$$

and

$$
\begin{aligned}
g_2 \quad = \quad & \frac{1}{\left(-(1+\sigma)^3(\varepsilon+c)^2b^2+(1+c+\varepsilon)(a-(1+\sigma)(\varepsilon+c))a(1+\sigma)b+(a-(1+\sigma)(\varepsilon+c))a^2\right)((-\varepsilon-c)\sigma-c+a-\varepsilon)ca^2}\times \\
& \Big[-(1+\sigma)^6(\varepsilon+c)^4b^4+2\left((1+c+\varepsilon)a-\tfrac{1}{2}(c+2\varepsilon+2)(\varepsilon+c)(1+\sigma)\right)(\varepsilon+c)^2(1+\sigma)^4ab^3 \\
& -(a-(1+\sigma)(\varepsilon+c))\left((1+c+\varepsilon)^2a+(\varepsilon+c)\left(c^2-3c-\varepsilon^2-4\varepsilon-1\right)(1+\sigma)\right)(1+\sigma)^2a^2b^2 \\
& +(1+c+\varepsilon)(c-2)(a-(1+\sigma)(\varepsilon+c))^2a^3(1+\sigma)b-(a-(1+\sigma)(\varepsilon+c))^2a^4\Big].
\end{aligned}
$$

The coefficients a_1 and b_1 involved in the degeneracy conditions, are given as:

$$
a_1 = \langle p_1, B(q_0,q_0)\rangle \quad \text{and} \quad b_1 = \langle p_0, B(q_0,q_0)\rangle + \langle p_1, B(q_0,q_1)\rangle,
$$

where $B(.,.)$ is the multilinear form of the Hessian of (3.1), and for two vectors u and v is calculated as :

$$
B(u,v) \quad = \quad \left[\frac{a(u_1v_3+u_3v_1)}{(1+L^*)^2(1+\sigma)}-\frac{2am^+u_3v_3}{(1+\sigma)(1+L^*)^3},-\frac{b(u_2v_3+u_3v_2)}{(1+L^*)^2}+\frac{2bM^+u_3v_3}{(1+L^*)^3},-\frac{2dfu_1v_1}{(f+m^+)^3}-e\left(u_2v_3+u_3v_2\right)\right].
$$

Calculating the coefficients at the critical values of parameters, we obtain:

$$
a_1 \quad = \quad -\frac{(1+\sigma)^4(\varepsilon+c)^3b^4}{(a+(1+\sigma)b)\left(-(1+\sigma)^3(\varepsilon+c)^2b^2+(1+\sigma)a((-\varepsilon-c)\sigma-c-\varepsilon+a)(1+c+\varepsilon)b+a^2((-\varepsilon-c)\sigma-c-\varepsilon+a)\right)fc},
$$

For all positive parameters, it is evident that the critical normal form coefficient a_1 is nonzero. The condition $BT.1$ is thus satisfied. The other parameter is calculated as:

$$
b_1 \quad = \quad -\frac{\left((1+\sigma)^3(\varepsilon+c)^2b^2-(1+\sigma)a(a-(1+\sigma)(\varepsilon+c))(1+c+\varepsilon)b+a^2(a-(1+\sigma)(\varepsilon+c))\right)(\varepsilon+c)^2b^3(1+\sigma)^3}{fc\left(-(1+\sigma)^3(\varepsilon+c)^2b^2+(1+\sigma)a(a-(1+\sigma)(\varepsilon+c))(1+c+\varepsilon)b+a^2(a-(1+\sigma)(\varepsilon+c))\right)^2}.
$$

This parameter may change sign, resulting in a (simple) degenerate BT bifurcation. The condition $BT.2$ is satisfied only except when $b_1 \neq 0$. So, on this point, there is a codimension-three bifurcation point. This point is a value of b such that:

$$
c \quad = \quad \frac{-2b^2\sigma^2\varepsilon-ab\sigma-2ab\sigma\varepsilon-4b^2\sigma\varepsilon-2b^2\varepsilon-2ab\varepsilon+a^2+ba^2-ab\pm\sqrt{g_4}}{2b(1+\sigma)(a+b+b\sigma)},
$$

where,

$$
g_4 \quad = \quad a^4-2a^3b\sigma-2a^3b-2a^4b+b^2a^4+\sigma^2b^2a^2-2a^3b^2\sigma+4b^3\sigma^2a^2+8a^2b^3\sigma+2a^2b^2\sigma+4b^3a^2+b^2a^2-2a^3b^2.
$$

One of these values is positive. Since, we considered e_{crit} instead of b_{crit} for normal form computation, we can easily change them to understand the results in this paper. For

the parameters, we chose in the first part of this paper, where b was varied along with d, the value of e at which a codimension-three bifurcation occurs is found to be approximately $e = 1.7$. Similarly, in the later part of this paper, when we varied σ and d, the value of e at which a codimension-three bifurcation occurs is $e = 1.45$. This value following the above calculations agrees with our Matcont computations (**?**).

3.9 Appendix B

We calculated the first order approximation for slow manifold using Eq. (3.9) by solving the following set of equations simultaneously:

$$P_1^1 = \begin{bmatrix} 0 & 0 & \frac{am_0^{\pm}(\sigma)}{(1+\sigma)\left(1+L_0^*(\sigma)\right)^2} \\ c & -\frac{bL_0^*(\sigma)}{1+L_0^*(\sigma)} & -\frac{cm_0^{\pm}(\sigma)}{L_0^*(\sigma)\left(1+L_0^*(\sigma)\right)} \\ \frac{df}{\left(f+m_0^{\pm}(\sigma)\right)^2} & -eL_0^*(\sigma) & -\frac{ecm_0^{\pm}(\sigma)(1+L)}{bL_0^*(\sigma)} - 1 \end{bmatrix} \begin{bmatrix} m_1^{\pm}(\sigma) \\ M_1^{\pm}(\sigma) \\ L_1^*(\sigma) \end{bmatrix} = g \begin{bmatrix} \frac{d}{d\sigma}m_0^{\pm}(\sigma) \\ \frac{d}{d\sigma}M_0^{\pm}(\sigma) \\ \frac{d}{d\sigma}L_0^*(\sigma) \end{bmatrix}$$

For the second order approximation for slow manifold, the following system was solved simultaneously (coming from Equation (3.9)):

$$P_2^1 = \begin{bmatrix} 0 & 0 & \frac{am_0^{\pm}(\sigma)}{(1+\sigma)\left(1+L_0^*(\sigma)\right)^2} \\ c & -\frac{bL_0^*(\sigma)}{1+L_0^*(\sigma)} & -\frac{cm_0^{\pm}(\sigma)}{L_0^*(\sigma)\left(1+L_0^*(\sigma)\right)} \\ \frac{df}{\left(f+m_0^{\pm}(\sigma)\right)^2} & -eL_0^*(\sigma) & -\frac{ecm_0^{\pm}(\sigma)(1+L)}{bL_0^*(\sigma)} - 1 \end{bmatrix} \begin{bmatrix} m_2^{\pm}(\sigma) \\ M_2^{\pm}(\sigma) \\ L_2^*(\sigma) \end{bmatrix} = g \begin{bmatrix} \frac{d}{d\sigma}m_1^{\pm}(\sigma) \\ \frac{d}{d\sigma}M_1^{\pm}(\sigma) \\ \frac{d}{d\sigma}L_1^*(\sigma) \end{bmatrix}$$

$$+ \left(\begin{bmatrix} \frac{d}{d\sigma}m_0^{\pm}(\sigma) \\ \frac{d}{d\sigma}M_0^{\pm}(\sigma) \\ \frac{d}{d\sigma}L_0^*(\sigma) \end{bmatrix} \right) \left(\begin{bmatrix} 0 & \frac{\partial g}{\partial M}|_{P_0^1} & \frac{\partial g}{\partial L}|_{P_0^1} \end{bmatrix} \begin{bmatrix} m_1^{\pm}(\sigma) \\ M_1^{\pm}(\sigma) \\ L_1^*(\sigma) \end{bmatrix} \right)$$

$$-\frac{1}{2} \begin{bmatrix} 0 & 0 & \frac{a}{(1+\sigma)\left(1+L_0^*\right)^2} \\ 0 & 0 & 0 \\ 0 & -e & \frac{ecm_0^{\pm}}{bL_0^{*2}} \end{bmatrix} \begin{bmatrix} m_1^{\pm 2}(\sigma) \\ M_1^{\pm 2}(\sigma) \\ L_1^{*2}(\sigma) \end{bmatrix}.$$

Submitted as: M.A.K. Bulelzai, J.L.A. Dubbeldam, D.J.P. Lahaye – *"Atherosclerotic plaque growth by shear stress dependent low-density lipoprotein transfer: the effect of recirculation, Submitted to Cardiovascular Engineering and Technology."*

Chapter 4

Atherosclerotic plaque growth by shear stress dependent low-density lipoprotein transfer: the effect of recirculation

We can't solve problems by using the same kind of thinking we used when we created them.

Albert Einstein

Abstract

In atherosclerosis low-density lipoproteins accumulate in a plaque that is formed in the wall of an artery. To prevent atherosclerosis or to slow down its progression, a better understanding of all parameters influencing its time evolution is essential.

In this paper we develop a finite element model that predicts the time evolution of atherosclerosis in medium and large sized arteries by treating the plaque growth as a moving boundary problem. The permeability of the endothelium layer is taken to be shear stress dependent in agreement with clinical findings. The blood flow is governed by the incompressible Navier-Stokes equations and the low density lipoproteins are convected with the blood while diffusing. In the plaque the LDL particles are assumed to be instantaneously oxidized and subject to diffusion only. The computed blood velocity profiles are shown to be in good agreement with published work on pulsating flows for short times and with results on non-pulsating flows for fixed stenosis.

It is found that flow reversal downstream of the stenosis reduces the wall shear stress in the zone of recirculation. This leads to a rise in the concentration of low-density lipoproteins in this zone and consequently to a reduction of the low-density lipoproteins flux from the artery to the intima. The lumen radius reduction was found to increase linearly in time for the first few years with a growth rate depending on the recirculation. The lumen area reduction for first few years of growth is found to match the experimental studies. For longer times the high shear stresses impede plaque remodeling in the radial direction, the plaque will broaden and experience diminished growth. Our results confirm that Poiseuille flow is a good first approximation to model atherosclerotic plaque growth in the presence of blood flow.

4.1 Introduction

The transport of molecules across the vascular interface is a vital physiological process in the micro-circulation of blood in large and medium-sized arteries. The interface between the blood flowing region of the artery, often referred to as the lumen, and the wall of the artery is called the endothelium. The endothelium is a thin layer of endothelial cells which control the permeability of the arterial wall. Once the endothelium is damaged or malfunctioned, the low-density lipoproteins (LDL) which are carried with the flowing blood, may permeate into the outer layer of the arterial wall, known as the intima (Nielsen 1996, Ross 1993). Oxygen radicals, which are present in the blood can, due to their small size, easily enter the intima, where they can oxidize the LDL which are then converted to oxidized low-density lipoproteins (ox-LDL). This is the onset of atherosclerotic disease. There is a whole series of biochemical events that take place once oxidized LDL has initiated plaque formation. The immune system acts to suppress the inflammation caused by oxidized LDL in the intima, which in fact enhances the plaque evolution. First the artery tries to accommodate the plaque by remodeling outward (away from the lumen), but eventually also inward remodeling takes place which in its turn affects the blood flow. The constriction formed by the plaque leads to a recirculation region behind the plaque, which was found to increase plaque growth. During the later stages of plaque growth a thin fibrous cap is formed. Rupture of this cap leads to stroke and myocardial infarction (Ross 1993, Ethier 2002, Pedley and Luo 1995), which is one of most common causes of death in the Western world. In order to understand the evolution of plaques, and in particular the remodeling of the artery and its relation with the blood flow, mathematical models are imperative. In this paper we present a qualitative mathematical model that focuses on the remodelling of the plaque region and studies the effect of blood recirculation on plaque growth.

We employ clinical investigations of the accumulation of ox-LDL in the intima (Nielsen 1996, Ross 1993) and generalize previous numerical work concerned with the fluid phase momentum and mass transport (Rappitsch and Perktold 1996a, Rappitsch et al. 1997) in which the artery wall was stationary to a *moving boundary problem*. In a recent work of (Fok 2012), intimal thickening was treated as a free boundary problem in which a radial cross section was considered and a semi-analytical model for the lumen radius was derived. Our aproach differs from this in that we study the interaction of blood flow on the evolution of plaques and we are particularly interested in *axial* direction and assume a radially symmetric situation. PDE models for early lesion growth were considered in (Calvez et al. 2009, Khatib et al. 2012). In (Calvez et al. 2009), the effect of the presence of a stenosis has been studied for short times and (Khatib et al. 2012) concentrated on reaction-diffusion processes and proves the existence of traveling concentration waves.

Since arterial wall permeability has been found to be influenced by wall shear stress (Caro et al. 1971, Ogunrinade et al. 2002), a number of studies have investigated wall shear stress

dependent transport properties (Rappitsch and Perktold 1996a, Rappitsch et al. 1997, Sun et al. 2006). In these studies the transport of LDL particles and oxygen was modelled and it was found that low wall shear stress can indeed significantly increase (ox)-LDL accumulation in the arterial wall. In this paper we also take wall shear stress dependence into account. In (Bulelzai and Dubbeldam 2012, Ougrinovskaia et al. 2010)), simple heuristic ODE models were developed, out of which (Bulelzai and Dubbeldam 2012) predict the remodelling and occlusion of the artery.

In this paper we improve on those simplified models by numerically solving the Navier-Stokes equations in an axisymmetric domain that is changing with time. We validate our model by comparing our numerical results with other results from the literature for fixed stenosis. This comparision shows excellent agreement. The main result of our investigation of the moving boundary problem is that although the growth of the plaque region shows only mild dependence on the flow recirculation, significant enhancement can be found in the flux of LDL from the lumen into the plaque and the ox-LDL concentration downstream of the stenosis. This effect is attributed to the lower wall shear stress in the recirculation zone, which leads to higher influx in the region affected by atherosclerosis. So although global differences are minor, the local composition of the plaque can differ significantly as a result of coupling between blood flow and plaque growth.

We organize this paper as follows. In Section 2 we introduce the mathematical model, which consists of incompressible Navier-Stokes equations, the LDL transport equation and a diffusion equation for ox-LDL particles. We also present the equation for the movement of the endothelial wall in the lumen, the geometry and initial and boundary conditions.

In Section 3, we present our numerical findings for fixed Reynolds (Re) and Peclet (Pe) numbers. Results include the calculation of velocities, shear stresses, fluxes and concentrations of LDL and ox-LDL over the time. We obtained these results using the Finite Element based package COMSOL 3.5. In order to quantify the effects of the recirculation zone, we compare results of the full model with those in which a Poiseuille velocity profile is imposed. We summarize our numerical findings in Section 4.

4.2 The model

We first introduce the mathematical model that accounts for fluid dynamics in the arterial lumen and arterial wall movement. In Fig. 4.1 we schematically show the geometry considered. The lumen is denoted by $\Omega_1 = \{(r,z,\theta)|0 < r < R(z,t), z \in [-l_u, l_p + l_d], \theta \in [0,2\pi]\}$, where l_u is the length of the artery upstream of the plaque; the length of the artery in the downstream direction is denoted by l_d and l_p is the fixed width of the plaque region. The function $R(z,t)$ describes the moving boundary that separates the region occupied by the blood flowing through the artery, called the lumen, from the region inside the artery wall, called the intima. The initima is defined as:

$\Omega_2 = \big\{(r,z,\theta)|R(z,t) < r < R_0, z \in [-l_u, l_p + l_d], \theta \in [0,2\pi]\big\}$.
We assume axial symmetry and therefore θ-dependence will be ignored. The assumption of *axial* symmetry for biological flows is justified as long as the Reynolds number is less than a critical Reynolds number calculated by Jamison *et al.*(Sheard et al. 2009). The function $R(z,t)$ that constitutes the boundary between Ω_1 and Ω_2 is easily seen to give rise to the boundary $\partial\Omega_w = \{(r,z,\theta)|r = R(z,t), z \in [-l_u, l_p + l_d], \theta \in [0,2\pi]\}$.

Length is made dimensionless by applying nondimensionalization with respect to the radius of the lumen (at $z = -l_u$) R_0. Velocities (denoting the radial velocity with u and axial velocity with v) are expressed with respect to U_0, which is the average velocity of the blood through the artery at $z = -l_u$, and a reference time t_{ref} is given by R_0/U_0. The pressure p can be expressed relative to $\rho_b {U_0}^2$ with ρ_b the blood density; the definition of the Reynolds number $\text{Re} = \frac{\rho_b U_0 R_0}{\mu}$ then completes a nondimensionalized description. In summary the relation between dimensionful quantities (without a tilde) and dimensionless quantities (with tilde) is as follows

$$\tilde{r} = \frac{r}{R_0}, \quad \tilde{z} = \frac{z}{R_0}, \quad \tilde{u} = \frac{u}{U_0}, \quad \tilde{v} = \frac{v}{U_0}, \quad \tilde{t} = \frac{tU_0}{R_0}, \quad \tilde{p} = \frac{p}{\rho_b {U_0}^2}, \quad \text{Re} = \frac{\rho_b U_0 R_0}{\mu},$$

where the parameter μ is the dynamic viscosity.

We next turn to the dynamical properties of our system. The bulk blood flow is governed by the incompressible Navier-Stokes equations; the LDL particles are modeled by a convection-diffusion equation and the oxidized-LDL concentration, which is only present in the plaque, is modeled by a diffusion equation. The LDL is convected with the velocity of the blood which is calculated from the Navier-Stokes equations in Ω_1 and is further also subject to diffusion. We assume that as soon as the LDL is transfered through the endothelial layer and enters the intima, it immediately gets oxidized and evolves according to a diffusion equation. The blood flow is assumed to be incompressible, isothermal, laminar and Newtonian, in a two-dimensional axisymmetric blood vessel. From now on we will drop the tilde symbol on the dimensionless quantities and any reference made to the velocities (u,v), coordinates (r,z), pressure and time will always imply the dimensionless quantity.

In cylindrical (dimensionless) coordinates, the model equations are:

$$\frac{1}{r}\frac{\partial}{\partial r}(ru) + \frac{\partial v}{\partial z} = 0, \tag{4.1a}$$

$$\frac{\partial u}{\partial t} + u\frac{\partial u}{\partial r} + v\frac{\partial u}{\partial z} = -\frac{\partial p}{\partial r} + \frac{1}{\text{Re}}\Big(\frac{1}{r}\frac{\partial}{\partial r}\left(r\frac{\partial u}{\partial r}\right) + \frac{\partial^2 u}{\partial z^2} - \frac{u}{r^2}\Big), \tag{4.1b}$$

$$\frac{\partial v}{\partial t} + u\frac{\partial v}{\partial r} + v\frac{\partial v}{\partial z} = -\frac{\partial p}{\partial z} + \frac{1}{\text{Re}}\Big(\frac{1}{r}\frac{\partial}{\partial r}\left(r\frac{\partial v}{\partial r}\right) + \frac{\partial^2 v}{\partial z^2}\Big). \tag{4.1c}$$

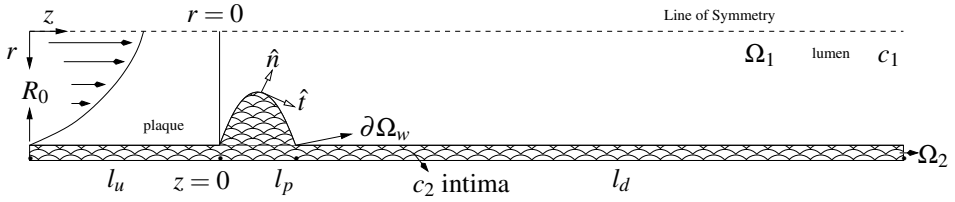

Figure 4.1: *A schematic representation of the idealized artery that we consider. The endothelium layer corresponds to the boundary* $\partial\Omega_w$.

Equation 4.1(a) is the continuity equation, and Equations 4.1(b,c) are the Navier-Stokes equations that describe the flow in the presence of axial symmetry in the blood domain Ω_1. The radial component of the velocity is denoted by u and the axial component (in the z-direction) by v;

The evolution of the concentration of LDL particles in the lumen (Ω_1), which we designate by c_1, is governed by a convection-diffusion equation

$$\frac{\partial c_1}{\partial t} + u\frac{\partial c_1}{\partial r} + v\frac{\partial c_1}{\partial z} = \frac{1}{\mathrm{Pe}}\Big(\frac{1}{r}\frac{\partial}{\partial r}\Big(r\frac{\partial c_1}{\partial r}\Big) + \frac{\partial^2 c_1}{\partial z^2}\Big). \tag{4.2}$$

Equation (4.2) is nondimensionalized by a expressing the LDL concentration with respect to a reference concentration C_0. The dimensionless Peclet number Pe, which controls the relative importance of convection with respect to diffusion, is defined as $\mathrm{Pe} = \frac{U_0 R_0}{D_1}$. Here the parameter D_1 is the diffusion constant for the LDL in the lumen. As LDL is assumed to be oxidized instantaneously on entering Ω_2 there will only be ox-LDL in the intima. The ox-LDL concentration is denoted by c_2. Since there is no blood flow in the intima, c_2 will only diffuse in region Ω_2. In dimensionless form the diffusion equation in Ω_2 reads

$$\frac{\partial c_2}{\partial t} = d_f\Big(\frac{1}{r}\frac{\partial}{\partial r}\Big(r\frac{\partial c_2}{\partial r}\Big) + \frac{\partial^2 c_2}{\partial z^2}\Big). \tag{4.3}$$

Equation (4.3) was made dimensionless by again expressing the concentration with respect to C_0. The parameter d_f is the dimensionless diffusion coefficient $d_f = \frac{D_2}{U_0 R_0}$, with D_2 the diffusion coefficient of c_2 in the intima. The system of differential equations (4.1-4.3) will be coupled through a common *time-dependent boundary* constituted by the endothelial layer $\partial\Omega_w(t)$.

4.2.1 Initial and Boundary conditions

In this subsection we first supply inital and boundary conditions on the stationary boundaries. Next the boundary conditions at the moving boundary $\partial\Omega_w$ are discussed. We take the

following initial conditions:

$$u(0,r,z) = 0, \qquad v(0,r,z) = 2(1-r^2),$$
$$c_2(0,r,z) = 0, \qquad c_1(0,r,z) = 1.$$

At the inlet, the blood flow profile is assumed to be fully developed laminar flow and the concentration c_1 is a given constant, whereas c_2 obeys a Neumann boundary condition:

$$v(r) = 2(1-r^2), \qquad c_1 = 1, \qquad \frac{\partial c_2}{\partial z} = 0, \qquad \text{at } z = -l_u/R_0. \tag{4.4}$$

At the outlet boundary, zero surface traction force is assumed and a vanishing concentration gradient:

$$-p\mathbf{n^o} + \mu \frac{\partial \mathbf{u}}{\partial \mathbf{n^o}} = 0, \qquad \frac{\partial c_1}{\partial z} = \frac{\partial c_2}{\partial z} = 0 \qquad \text{at } \ z = L/R_0, \tag{4.5}$$

where $\mathbf{n^o}$ is the outward pointing unit normal to the outlet boundary. At the wall $\partial\Omega_w$, a no-slip condition is prescribed. The axi-symmetric setting implies that at $r = 0$ a Neumann condition is satisfied both by (u,v) and by c_1, which yields

$$u = 0, \qquad \frac{\partial v}{\partial r} = 0, \qquad \frac{\partial c_1}{\partial r} = 0 \qquad \text{at } r = 0.$$

At the moving wall $\partial\Omega_w$, the (dimensionless) wall flux J_{c_1} of LDL from the lumen into the intima is taken as:

$$J_{c_1} = \frac{\hat{J}_{c_1}}{J_0} = -\frac{\partial c_1}{\partial \mathbf{n}}\bigg|_{\partial\Omega_w} = k_1 \xi(|\tau_w|) c_1, \tag{4.6}$$

where $\hat{J}_{c_1}$ is the dimensionful flux and $J_0 = \frac{D_1 C_0}{R_0}$ is a reference flux; the dimensionless diffusive permeability k_1 is defined as $k_1 = \frac{C_0 \hat{k}_1}{J_0}$, with $\hat{k}_1$ the dimensionfull permeability constant. The quantity k_1 is also known in the literature as the *Sherwood-number* and commonly abbreviated as Sh, a notation that we will also adopt in this paper. We further notice that the flux J_{c_1} does not depend on the flow velocity due to the no slip conditions.

The boundary condition (Equation 4.6) is in accordance with clinical observations by (Niehaus et al. 1977) that the LDL influx is proportional to the LDL concentration in the blood. Clinical observations further suggest that low wall shear stress enhances atherosclerosis (Slager et al. 2005, Sakllarios et al. 2010, Rappitsch and Perktold 1996b). We include the function $\xi(|\tau_w|)$ in Equation (4.6) to model the dependence of the permeability on wall shear stress. Its functional form was taken as

$$\xi(|\tau_w|) = \frac{1}{1 + |\tau_w|/\tau_0}. \tag{4.7}$$

in correspondence with (Bulelzai and Dubbeldam 2012). The parameter τ_0 in Equation (4.7) is the value of the wall shear stress at which the value of ξ, and therefore the LDL flux from the lumen to the intima, is reduced to half its value without wall shear stress. We note that a flux condition depending on the wall shear stress is not new and was, for example, also applied in (Rappitsch and Perktold 1996a) and (Quarteroni et al. 2002). However, in that case oxygen transport was modelled and therefore a different functional dependence on τ_w was chosen in which the permeability increases with wall shear stress. Moreover, in (Rappitsch and Perktold 1996a) and (Quarteroni et al. 2002) simulations were only performed for boundaries fixed in time.

In region Ω_2 the ox-LDL only diffuses. At the moving wall $\partial\Omega_w$, c_2 satisfies the following boundary condition:

$$J_{c_2} = \frac{\hat{J}_{c_2}}{J_0} = -\frac{D_2}{D_1}\frac{\partial c_2}{\partial \mathbf{n}}\bigg|_{\partial\Omega_w} = -k_1\xi(|\tau_w|)c_1 + k_2 c_2. \tag{4.8}$$

This flux boundary condition implies that we assume the LDL which diffuses through the wall, is immediately converted into ox-LDL in addition there is some leakage of ox-LDL into the lumen. This leakage of will be very small, since due to processes taking place in the plaque it will be much more difficult for ox-LDL to escape from the plaque region than it is for LDL to enter Ω_2. The permeability k_2 will therefore in general be much smaller than k_1 and hence we neglect the $k_2 c_2$ term in our numerical computations.

4.2.2 Moving Geometry

In order to facilitate comparison with the literature with fixed stenosis, we introduce the function $h(z) = R_0 - R(z, t=0)$ that defines $\partial\Omega_w(t)$ at time $t = 0$,

$$h(z) = \begin{cases} ze^{-a_0 z^2} & \text{for} \quad 0 \le z \le l_p/R_0, \\ 0 & \text{otherwise.} \end{cases} \tag{4.9}$$

Here a_0 is a parameter determining the initial shape of the plaque region. We derive the evolution of the boundary $\partial\Omega_w(t)$, by finding an evolution equation for $R(z,t)$. To proceed we make the crucial assumption that the evolution of R only occurs on a very long time scale. This allows to impose no slip boundary conditions for u and v

$$u = 0, \qquad v = 0, \qquad \text{on } \partial\Omega_w(t). \tag{4.10}$$

To derive the evolution equation for $R(z,t)$ we define the function $f(r,z,t) \equiv r - R(z,t)$ as in (Crank 1984). The level curve $f(r,z,t) = 0$ implicitly defines the boundary $\partial\Omega_w(t)$. The evolution of f is governed by

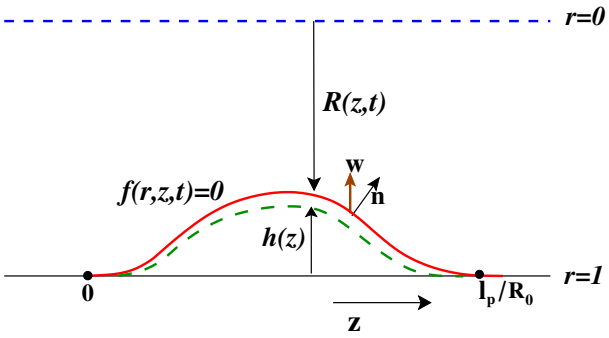

Figure 4.2: *A schematic representation of the plaque bounded by the implicit relation $f(r,z,t) = 0$, which defines $R(z,t)$ implicitly. This representation of the boundary can be used to derive an evolution equation for $R(z,t)$. In our model we assume that the interface only moves in the radial direction.*

$$\frac{\partial f}{\partial t} + \nabla f \cdot \mathbf{w} = 0, \tag{4.11}$$

where $\mathbf{w}$ is the velocity of the boundary. Equation (4.11) is used generally for moving boundary problems, such as the confined Muskat problem. In that problem, which can be applied to model tumor growth (Pozrikidis 2010), the velocity of the wall is always in the direction of the normal $\mathbf{n}$. Here we follow a different route, however. Since the plaque will be covered by a fibrous cap whose elastic characteristics are unknown and also evolve in time, we make the simplifying assumption that the wall only moves in the radial direction; see also Fig. 4.2. Moreover, the plaque growth is supposed to be proportional to the initial shape of the plaque $h(z)$. The major advantage of this assumption is that it removes instabilities such as so-called "fingering regions" that are commonly present in the muskat problem (Gazolaz et al. 2013), but not observed for plaques (Pherson et al. 1992). Since our model is only qualitative as we ignore many processes such as cap formation and smooth muscle cell proliferation, taking place in the intima, this assumption will only quantitatively modify our results. Our model indeed incorporates the sugestion already put forward by (Sandler and Bourne 1963) that the rate of accumulation of atherosclerotic tissue is proportional to the accumulated amount of (oxidized) LDL in the plaque.

We can now recast Equation (4.11) in the form

$$(\nabla f \cdot \hat{\mathbf{r}}) w_r = -\frac{\partial f}{\partial t} = \frac{\partial R}{\partial t}, \tag{4.12}$$

where w_r is the velocity of the boundary in the radial direction and $\hat{\mathbf{r}}$ is the unit vector in the radial direction. We use that the velocity w_r is proportional to the total incoming flux times $h(z)$, that is, $w_r = \gamma(k_1 \xi(|\tau_w|)c_1 - k_2 c_2)\, h(z)$, with the dimensionless constant γ proportional

to the volume of a mole of oxidized LDL-particles relative to the standard volume R_0^3. The value of the proportionality constant will be determined later by the requirement that the plaque evolves on a time scale of about 10 years. If we substitute the expression for w_r in Equation (4.12) and use that $f(z,r,t) = r - R(z,t)$, we find

$$\frac{\partial R}{\partial t} = -\gamma h(z)\left[k_1 \xi(|\tau_w|)c_1 - k_2 c_2\right]. \tag{4.13}$$

Equation (4.13) determines the evolution of the plaque boundary $R(z,t)$. It is supplemented with the initial condition $R(z,0) = R_0 - h(z)$, and automatically satisfies $R(z,t) = R_0$ at $z = 0$ and $z = l_p/R_0$.

We notice that in the limiting case for which z-dependence of c_1, c_2 and ξ is absent, Equation (4.13) predicts a linear decrease in time of $R(z,t)$. This result differs from the time dependence found in (Bulelzai and Dubbeldam 2012), where the plaque volume was found to grow linearly with time and consequently the arterial radius to decrease as a square root of time. The reason for this is that although there was no z-dependence in (Bulelzai and Dubbeldam 2012), the inward flux was supposed to be independent of the radius of the artery, whereas here we consider the inward flux to be proportional to $R(z,t)$.

4.3 Methods

4.3.1 Numerical Details

We implemented our model in Comsol Multiphysics 3.5 which is a finite element package for the solution of PDEs. We coupled the Navier-Stokes equations for the blood flow in the artery to a convection-diffusion equation for the LDL concentration in the lumen and a diffusion equation for oxidized LDL in the intima. The movement of the endothelium is taken into account by a applying a moving mesh implementation which is based on an Arbitrary Euler-Lagrangian formulation (with a Winslow smoothing method). The model is discretized in space using default setting second order Lagrangian elements for the velocity and linear order elements for the pressure and the concentrations c_1 and c_2 on an unstructured triangular mesh. To suppress spurious oscillations in regions with high mesh Peclet numbers, crosswind diffusion was added to the convection-diffusion equation with its parameter $\delta_{cd} = 0.35$ for linear elements as described in (Krakauer 2007).

The resulting spatially discrete model, which consists of 10^5 elements with a refined mesh near the moving boundary, is integrated in time using a BDF scheme from DASPK (Brenan et al. 1996) with an adaptively chosen time stepping scheme. The accuracy of this procedure is governed by specifying absolute and relative tolerances whose values we choose 10^{-7} and 10^{-3}, respectively.

4.3.2 Validation and comparison with published work

To validate the numerical results before solving the model, we compare our numerical results with those of (Ismail et al. 2008) and (Rappitsch and Perktold 1996a). We use these two references to validate two different aspects of our model. First, the flow and the moving geometry are validated and next the convection-diffusion of the LDL into the plaque.

Validation of velocity profile in the presence of a moving wall

In (Ismail et al. 2008), pulsatile blood flow in a slightly tapered geometry with a tapering angle $\phi \ll 1$ is studied. The stenosis is assumed to be overlapping, that is, a stenosis is prescribed at a certain interval of z values, just as in our model. For all other values of z a slightly tapered channel is assumed, whose radius $R(z,t) = (mz+b)a_1(t)$ varies both with time and with z. Initially $a_1(t) = 0$ and the geometry of the channel outside the stenotic area is simply $R(z,0) = mz+b$, where b is the radius of the artery at $z = 0$ and m is related to the tapering angle ϕ, via $tan(\phi) = m$.

In (Abdullah and Amin 2010), (Chakravarti and Mandal 2000) and (Ismail et al. 2008), the Navier-Stokes equations were approximately solved for a pressure that was changing periodically in time, but with the extra assumption that for very small arteries the pressure does not depend on radius. This assumption was justified in (Pedley and Luo 1995). We have simulated the same tapered geometry (small sized artery) as in (Ismail et al. 2008) with the same boundary conditions and time dependence of the pressure, but in contrast to (Ismail et al. 2008) we do not use the assumption that the pressure is independent of radius. Rather we solve the complete Navier-Stokes equations (including the $\frac{\partial p}{\partial r}$ term) for different tapering angles ϕ for the two-dimensional axi-symmetric case. A comparison is presented in Fig. 4.3, which depicts both the radial and axial velocity as a function of the normalized radius $x = \frac{r}{R(z,t)}$ at two different times. We find excellent agreement between our results and those of (Ismail et al. 2008). This validates our numerical results for short times.

Validation of convection-diffusion equation

For the validation of the solution of the convection-diffusion equation especially near the wall, stationary computations for the case of a fixed stenosis were carried out and compared with the results of (Rappitsch and Perktold 1996a). In this paper, two models for oxygen diffusion through the endothelium have been studied. In one model the wall permeability was a constant, whereas in the other model a shear-dependent wall permeability was supposed. We implemented our convection-diffusion model in COMSOL for the special case of a non-moving geometry and for both a constant permeability and a permeability with the same functional form as in (Rappitsch and Perktold 1996a). All parameters were chosen in agreement with (Rappitsch and Perktold 1996a). Our computations were performed us-

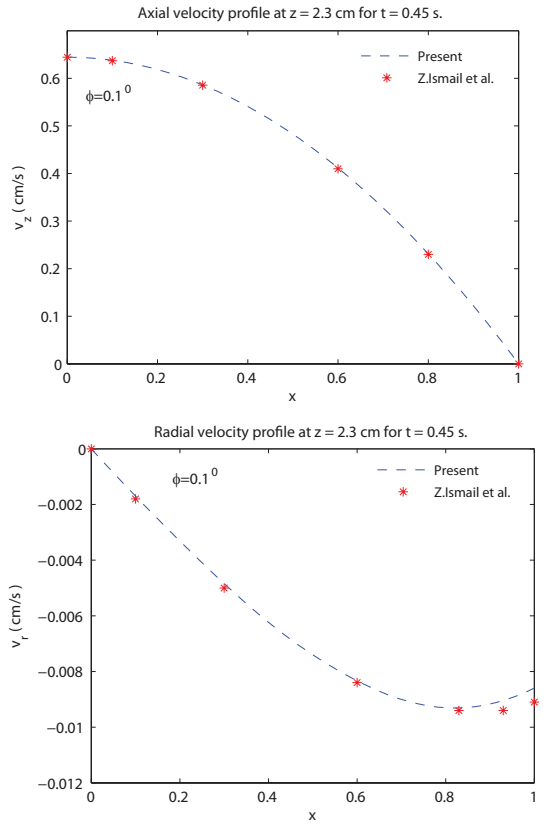

Figure 4.3: *Velocity profiles obtained at different locations in a tapered channel with tapering angle ϕ and pulsatile blood flow. At the horizontal axis $x = \frac{r}{R(z,t)}$ is plotted to facilitate comparison with (Ismail et al. 2008).*

ing quadratic elements for the velocity and cubic elements for convection-diffusion equation combined with the SUPG method[1]. The results and the comparison are shown in Fig. 4.4(a) for a fixed permeability and in (b) for a permeability that increases linearly with wall shear stress. Our results corroborate Rappitsch's results and further validate our model. Notice that the minimum concentration is at the peak of the constriction, which is located at $z = 3.36$ for both cases. There is an additional broad maximum in Fig. 4.4(b) that is caused by the re-circulation behind the constriction causing a low wall shear stress and consequently a small flux into the intima resulting in a larger oxygen concentration near the wall.

[1]The local constriction for this simulation we used the second degree Bezier curve as the stenotic curve was not mentioned in (Rappitsch and Perktold 1996a)

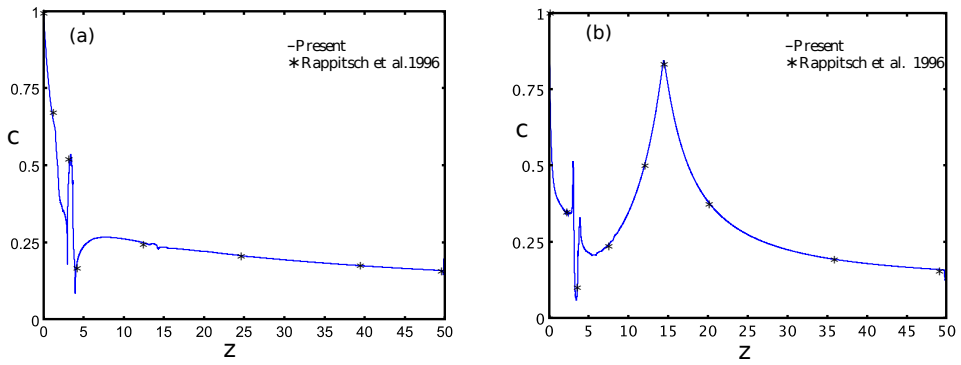

Figure 4.4: *Normalized wall concentration for oxygen. In (a) the permeability is constant and in (b) it varies linearly with wall shear stress.*

Table 4.1: **Numerical Values used in the simulations (this paper) with their units**

Parameter	Description	Value	Units
$\hat{k_1}$	LDL permeability	3×10^{-8} (Nielsen 1996)	cm/s
$\hat{k}_2$	ox-LDL permeability	0	cm/s
l_p	Length of stenosis	1.42 (Rappitsch and Perktold 1996a)	cm
l_d	Downstream length	72.14 (Rappitsch and Perktold 1996a)	cm
l_u	Upstream length	4.62 (Rappitsch and Perktold 1996a)	cm
L	End point of artery	73.56 (Rappitsch and Perktold 1996a)	cm
R_0	Reference radius	0.71 (Rappitsch and Perktold 1996a)	cm
C_0	Reference LDL concentration	2.6×10^{-6} (Goldstein and Brown 1977)	mole/cm^3
$\hat{\gamma}=\gamma R_0^3$	Volume coefficient	7.0×10^3	cm^3/mole
U_0	Reference velocity	4.52	cm/s
ρ_b	Blood density	1.05 (Rappitsch and Perktold 1996a)	g/cm^3
μ	Dynamic viscosity (Blood)	0.035 (Rappitsch and Perktold 1996a)	Poise
D_1	Diffusion coefficient (Blood)	1×10^{-6} (Dabagh et al. 2009)	cm^2/s
D_2	Diffusion coefficient (Intima)	1×10^{-6}	cm^2/s
τ_0	Shear stress parameter	500	dyne/cm^2
a_0	Plaque shape parameter	2.02	
Re	Reynolds number	100	
Pe	Peclet number	3.2×10^6	
Sh	Sherwood number	0.0213	

4.4 Results and Discussions

The model (4.1-4.3) was simulated in combination with a moving mesh to investigate the influence of time dependent constriction on a compliant artery, generalizing the study of (Rappitsch and Perktold 1996a) to the case of a progressing plaque. The main parameters in the problem are the Reynolds number, Peclet number, the Sherwood number Sh and the parameter γ, which determines the volume taken by oxidized LDL particles in the plaque. The values of most of the parameters are available in the literature and are presented in Table 4.1. The value of $\hat{\gamma} = \gamma R_0^3$ depends besides the volume of oxidized-LDL particles on the elasticity of the arterial wall. Since we do not have a consistent theory how to calculate γ from first principles we will simply set γ to the value in Table 4.1, as this leads to the correct timescale for the evolution of the plaque in the artery. In (Bulelzai and Dubbeldam 2012), a similar parameter was introduced to fix the time scale of the plaque evolution.

In all our simulations we use the parameter values given in Table 4.1, unless mentioned otherwise. We first present the full model results and next discuss the dependence on Re, the flow profile and the Peclet number. All numerical results were verified for several choices of mesh spacing and values of the absolute and relative accuracy. The results presented were obtained using a relative accuracy of 10^{-3} and an absolute accuracy of 10^{-7}. Triangular linear elements were used for the concentrations, quadratic for velocity and linear elements for the pressure. The percentage of stenosis is calculated as $(1 - \frac{A_1}{A_2}) \times 100$, where A_1 is lesion diameter or area and A_2 is diameter or area at the reference site (Ota et al. 2005). We will mean stenosis percentages in terms of diameter if not stated otherwise in this paper. We follow (Rappitsch and Perktold 1996a) for stenosis percentage convention.

In Fig. 4.5 we display results of the numerical simulation of the model (4.1-4.3). The axial velocity as well as the stream lines are shown for 3 different (dimensionless) times t_1, t_2, t_3, which correspond to a diameter reduction of the lumen of 30% ($t_1 = 1.21 \times 10^8$) , 50% ($t_2 = 2.04 \times 10^9$) , 70% ($t_3 = 3.13 \times 10^9$). It can be seen from Fig. 4.5(a) and (d), which refer to 30% stenosis, that there is hardly any recirculation in this case and consequently only a very narrow boundary layer. In fact from the streamlines shown in (d) it appears that there is no recirculation region at all. However, this is a consequence of the fact that only limited number of streamlines is shown as Fig. 4.5(a) shows that the curve for $z = 2$ attains slightly negative values near $r = 1$, evidencing the presence of a small recirculation zone. The time t_1 for which 30% stenosis is reached is equivalent to 6.2 years, which is qualitative agreement with numerical calculations by (Liu and Tang 2010). For larger times and hence for greater stenosis presented in (b) and (e) for the 50% case and in (c) and (f) for 70% lumen reduction, the constriction is large enough to produce a significant recirculation zone behind the plaque. This can easily be seen from the stream profiles (e) and (f) and can also be inferred from (b) and (c) as v takes negative values for r close to 1. Because the stenosis grows in time, the recirculation is enhanced as well and negative values of v can be found for rather large values of z in Fig. 4.5(c).

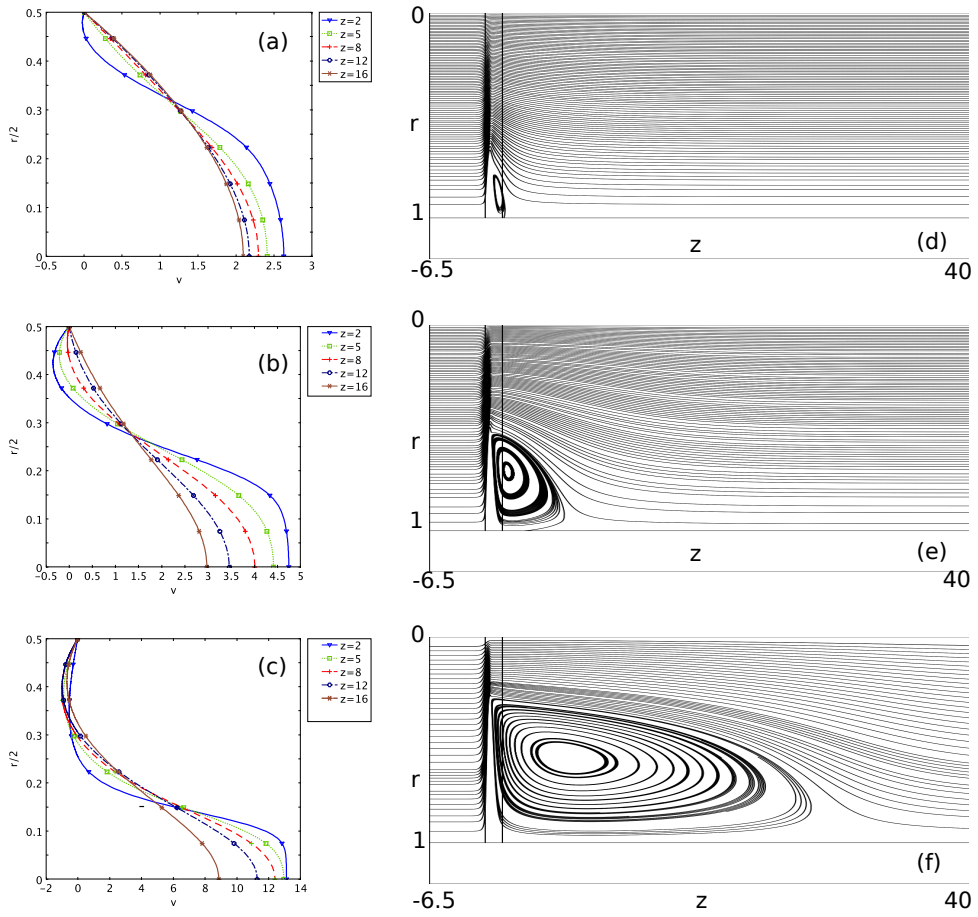

Figure 4.5: *The axial velocity as a function of r for three different degrees of stenosis (a-c) and the corresponding streamlines (d-f). The picture is not to scale, the vertical axis is blown up by a factor of 25 for presentation purposes. The plaque is confined to interval $[0,2]$. In (a) the stenosis is 30% and the velocity is slightly negative near $z = 2$ and $r = 1$, although this cannot be discerned from the corresponding stream function (d). For 50% stenosis ((b) and (e)) v is negative near the end of the plaque region at $z = 2$. For 70% stenosis ((c) and (f)) the larger recirculation zone is evident and negative velocities are present in a boundary layer near $r = 1$ and a large number of z values.*

To examine the validity of our results for large Re, we compare the calculated velocity profiles of our model at $\mathrm{Re} = 100$ with computations carried out by (Ahmed and Giddens 1983) and (Varghese et al. 2007) for different constrictions at $\mathrm{Re} = 500$ (not shown here). Surprisingly, we find perfect agreement for $z = 2$ and 50% stenosis; see Fig. 4.5(b). For

other values of z the agreement is still rather good. This suggests that our results remain valid beyond the Reynolds number $\mathrm{Re} = 100$ for which we carried out our computations.

We next turn to the plaque itself, which resides in the interval $[0,2]$. The function $R(z,t)$ defines the plaque boundary and is shown in Fig. 4.6. The shape approximately remains the same as the boundary movement was assumed to be proportional to the initial shape of the plaque, as defined in Equation (4.9). Only for very high degrees of stenosis the plaque starts to deform. The modeling assumption that the plaque can not extend beyond $z = 2$, prevents the plaque from growing further in the axial direction, although we allow the LDL-flux to be nonzero everywhere in order to facilitate comparison with other numerical works.

To investigate the details of plaque growth and the effect of wall shear stress on the progression of plaque we calculated the wall shear stress and the flux of LDL into the intima. Our results our depicted in Fig. 4.7 for three different degrees of stenosis.

From Fig. 4.7(a,c,e) and the insets of the figures it can be seen that for small negative z the wall shear stress decreases, this is due to the plaque that is already felt by the flow via the boundary layer before actually reaching the constriction. Due to the presence of the plaque starting at $z = 0$ the wall shear stress increases for small positive z until it reaches a maximum near the peak of the occlusion. Then the wall shear stress rapidly drops attaining a minimum for the value of z corresponding to the separation point. Since this happens in Fig. 4.7(a), (c) and (e) it demonstrates the presence of a recirculation zone for all three cases including the 30% stenosis. Just after the separation point τ_w increases reaching a maximum after which τ_w decreases again reaching 0 at end of the recirculation zone. It then gradually increases till it reaches the same constant value it had at the entrance of the artery at $z = -6.5$. When comparing Fig. 4.7(a), (c) and (e), the most conspicuous difference is the shift of the second minimum $\tau_w = 0$ to larger z values for increasing times, and hence increasing degrees of stenosis. The maximum of the curves is, of course, also increasing for increasing stenosis. The corresponding flux curves all reach a maximum at the separation points where $\tau_w = 0$ and have a minimum at the maximum constriction where τ_w is maximal. The flux into the intima was calculated in (Rappitsch and Perktold 1996a) for oxygen. Our results are in qualitative agreement with their findings.

In Fig. 4.8, the evolution of the LDL concentration is presented for the 3 different times t_1, t_2, t_3 as was done for the velocity in Fig. 4.5. Fig. 4.8(a) shows non-monotonic behavior of the LDL concentration as a function of the axial coordinate z; the corresponding density profiles are depicted in Fig. 4.8(e-g). From (a) and the enlargement in (b) it can be seen that the z dependence of the LDL concentration at the wall is very similar to that of Fig. 4.4(a). The LDL concentration rises from $z = 0$, the location where the plaque starts, till it reaches a maximum at the peak of the stenosis. The maximum is followed by a relatively sharp decline in the LDL concentration due to a separation point in the flow that is close to the point of maximal stenosis. The concentration then gradually increases again in the recirculation zone as here the flow is in the negative z-direction. When the recirculation zone ends, the

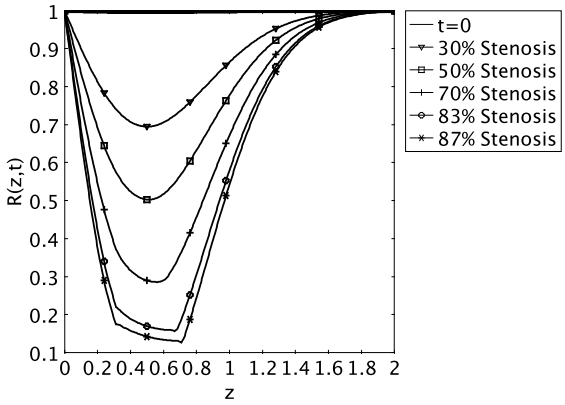

Figure 4.6: *The plaque shape for different degrees of stenosis. The function $R(z,t)$ remains regular up to very high degrees of stenosis.*

concentration attains another local maximum after which it decreases again with z. Since the permeability decreases with $|\tau_w|$ in our model, it is not surprising that the broad maximum that appeared for large z in the model of oxygen transport of (Rappitsch and Perktold 1996a) in which the permeability was assumed to increase with τ_w, is absent here; see for comparison also Fig. 4.4. Near the local maximum of the concentration some fluctuations can be seen which were also observed in (Quarteroni et al. 2002); see also Fig. 4.8(b). The continuous growth of the plaque leads to an expanding recirculation zone that is reflected in the second maximum in c_1 moving to the right with increasing time. In the corresponding concentration density profile Fig. 4.8(e) the region with a very low LDL concentration can be discerned as a dark region. The increasing size of the dark region in Fig. 4.8(f-g) is evidence for the growing recirculation zone. In Fig. 4.8(c) we show the LDL concentration for a fixed value of $z = 14$ as a function of the radial coordinate. Nonmonotonicity appears for the case of 70% stenosis, which reflects again the presence of recirculation at $z = 14$. For shorter times and hence smaller stenosis, there is no recirculation and at $z = 14$ as the recirculation zone so much smaller.

We stress that although the plaque cannot grow beyond $z = 2$ in our model as we assume the artery to be healthy apart from [0,2], the recirculation could constitute a risk for spreading of the plaque in the axial direction. For completeness we also show the concentration c_2 of ox-LDL in the intima in (d), which is rather smooth. The insets show, however, that the although c_2 is maximal at the top of the constriction for 30% stenosis, this maximum shifts to larger z values, which is caused by the wall shear stress evolution as was presented in Fig. 4.7.

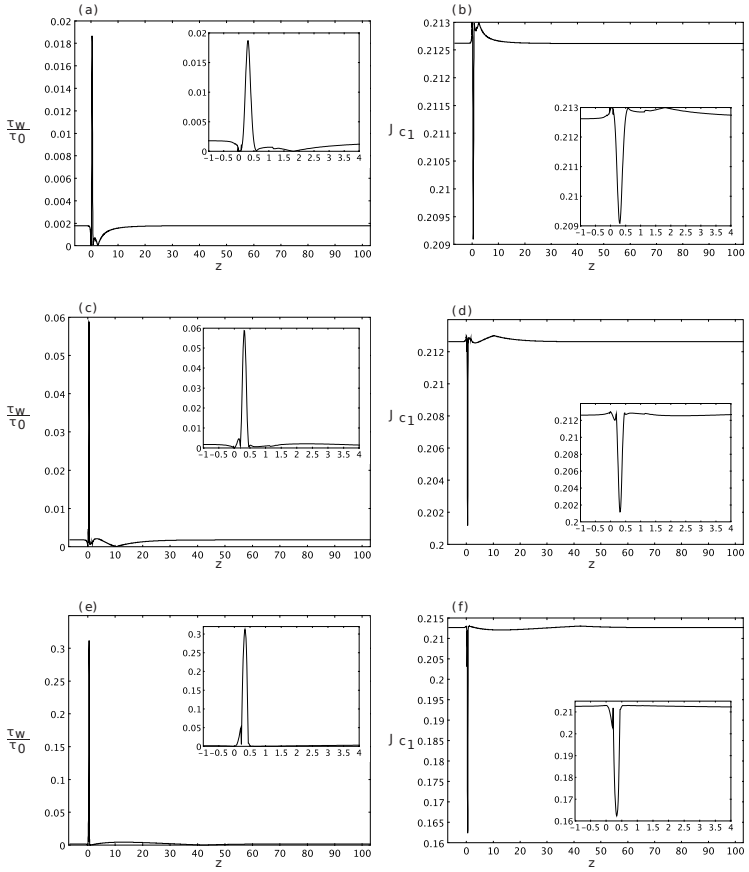

Figure 4.7: *The normalized wall shear stress τ_w/τ_0 as a function of z for 30% (a), 50% (c) and 70% (e) stenosis. In (b), (d), (f), the corresponding fluxes are shown. It is clear that the wall flux is large determines by the wall shear stress, as the curves follow each other: vanishing wall shear stress corresponds to a maximum in the flux and a maximum in the wall shear stress leads to a minimum in the flux.*

Finally, we emphasize that there is only a very small difference between the maximum and minimum values of the concentration, as compared to the average LDL concentration in the lumen. This is due to the small value of the Sherwood number $\mathrm{Sh} = 0.0231$, or equivalently, the small permeability ($\hat{k}_1$) of the endothelial layer. In Fig. 4.13, it is shown that the concentrations may have a high value if the sherwood number is large.

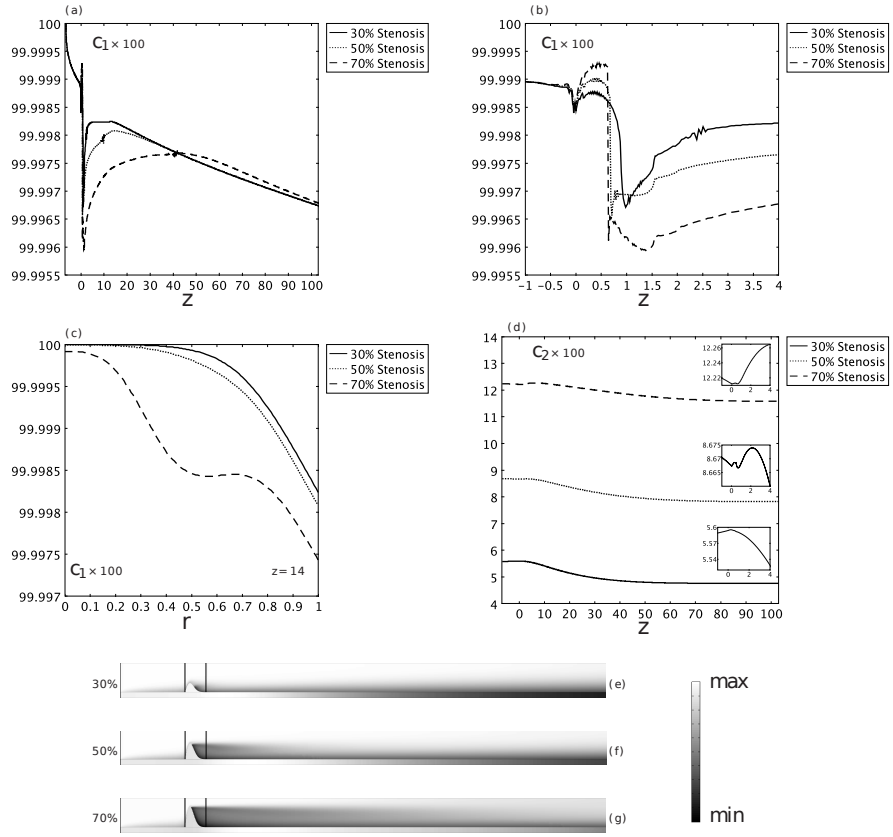

Figure 4.8: *(Dimensionless) LDL concentration as a function of the axial length (a) and a zoomed-in picture (b). The concentration c_1 as a function of the radial coordinate (c) displays nonmonotonic behavior for large times. The concentration c_2 varies only gently as a function of z (d). In (e-g) the accompanying concentration profiles for LDL (c_1) in the lumen and for ox-LDL (c_2) in the intima are displayed. For a convenient presentation we have scaled the radial direction in (e-g) with a factor of 12.*

4.4.1 Comparison with experiments

In (Stadius et al. 1992), different measurements on the time evolution of plaques in rabbits were performed. By sacrificing rabbits with a 2% cholesterol diet, the intimal area of iliac arteries were monitored over 40 days. (Fok 2012) presented a mathematical model for the reduction in intimal area by the evolution of smooth muscle cells and was compared with (Stadius et al. 1992). As clinical data on human evolution of plaques is scarce, we compared

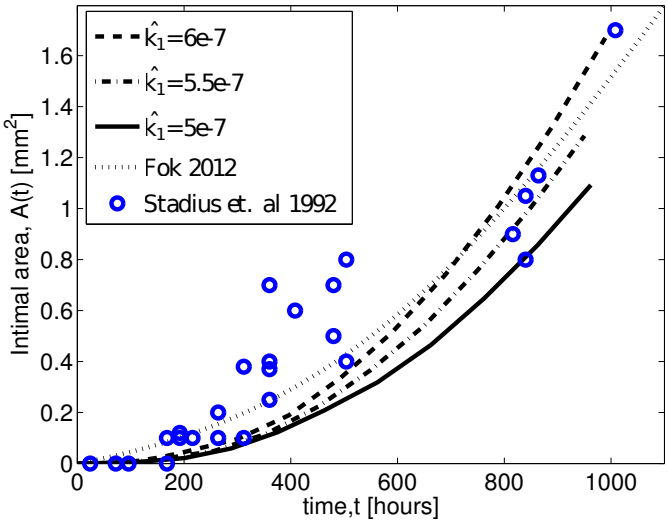

Figure 4.9: *Comparison of model with animal studies (Stadius et al. 1992) and a model of intimal reduction through smooth muscle cell death (Fok 2012). The calculated graphs for different values of endothelial permeability ($\hat{k}_1$) are obtained at peak of stenosis (at $z = 0.4$). The dotted curve is from (Fok 2012) with parameter values $\theta_0(0) = \pi/8$, $\alpha = 0.02$ and $\beta = 24$.*

our time dependent results with both (Stadius et al. 1992) and (Fok 2012). It is worthwhile to note that our model has a z-dependent component while in the model of (Fok 2012), the intimal cross sectional area was considered. We calculate the cross sectional area of the idealized artery at the peak of stenosis (at $z = 0.4$) for comparison. In the model of (Fok 2012), three parameters were adjusted to acheive the agreement with clinical study from (Stadius et al. 1992). In our model, there is only one parameter $\hat{k}_1$ which may be varied to fit the experiments. For human arteries, we choose the parameter $\hat{k}_1$ to be 3×10^{-8}cm/s from (**?**). But for rabbit studies, the curves fit best when values of $\hat{k}_1$ are of the order of 10^{-7}cm/s. (Ogunrinade et al. 2002) have mentioned that in rabbits aorta, values for low permeability lie in the range of $1 - 2 \times 10^{-8}$cm/s and increases to as much as 5×10^{-7}cm/s for high permeability regions. In Fig. 4.9, we present the comparison for three different values of $\hat{k}_1$: 6×10^{-7}, 5.5×10^{-7} and 5×10^{-7}cm/s.

To gain more insight in the exact influence of the recirculation zone, the permeability dependence on τ_w and the high value of Pe on the progression of atherosclerosis, we developed two approximate models that we discuss in the following subsection.

4.4.2 Two simplified models: the zero-convection model and the Poiseuille model

When we consider the limit Pe $\to 0$ of the model governed by (4.1-4.3), Equation (4.2) reduces to a simple diffusion equation and the blood velocity consequently vanishes in Ω_1. The reduced model will be called the *zero-convection model*. This model allows us to quantify the effects resulting from a shear stress dependent permeability, since the wall shear stress is identically zero throughout the domain. A second simplified model is obtained if we simplify the blood flow by imposing the blood flow to be Poiseuille in Ω_1 and to obey mass conservation. The permeability is taken to depend on wall shear stress through ξ as defined in Equation (4.7) just as for the full model. As the Poiseuille model has by definition no recirculation zone it allows us to study the effect of flow recirculation on plaque progression.

We implemented the zero-convection (ZC) model and the Poiseuille model and kept all parameters the same as for the full model Equations (4.1-4.3) except Pe . For the Poiseuille model we also keep the same boundary conditions as for the full model, but for the ZC-model we need to modify the boundary conditions at the non-moving part of the lower boundary, that is, for $r = 1$ and $z \in [-l_u/R_0, 0] \cup [l_p/R_0, L_0/R_0]$ we took homogeneous Neumann boundary conditions as otherwise all LDL will have diffused through the endothelium before reaching the constriction. This complication does not arise in the convective models, in which the fast convection process leads to a constant supply of LDL throughout Ω_1.

The results are displayed in Fig. 4.10, where we plotted in (a) the concentration c_1 as a function of z for three different degrees of stenosis for the ZC-model and in (b) for the Poiseuille model. For the ZC-model time was made dimenionless by expressing time with respect to the reference time $t_{\text{ref}} = 0.157\,\text{s}$, whose value was taken the same as for the full model and the Poiseuille model. In (a) the LDL concentration is seen to be a monotonically decreasing function of z for all times, whereas for the Poiseuille model (b) c_1 exhibits non-monotonic behavior. This difference arises from the fact that the movement of the wall is completely determined by c_1 in the ZC-model, and hence there is no relation between movement of the wall and the permeability. In the Poiseuille model there is interaction between the fluid velocity and the influx of LDL into the intima: at positions where the wall shear stress is high the influx is low and vice versa. But comparing Fig. 4.10(b) with Fig. 4.8(a) shows that the (local) maximum in the concentration at $z = 20$ for the Poiseuille model is independent of the rate of stenosis, whereas it shifts to larger z values for the full model. Of course, in the ZC-model c_1 is depleted for large z as there is no supply of LDL into this region by convection in contrast to the Poiseuille model. Finally, we remark that the plaque progresses more slowly in the ZC-model than in the Poiseuille model.

We next compare the Poiseuille model with the full model in Fig. 4.11. Panel (a) displays the concentration profiles as a function of t for three different values of z for the Poiseuille model and in (b) the full model results are shown. In Fig. 4.11(a) the concentration curves

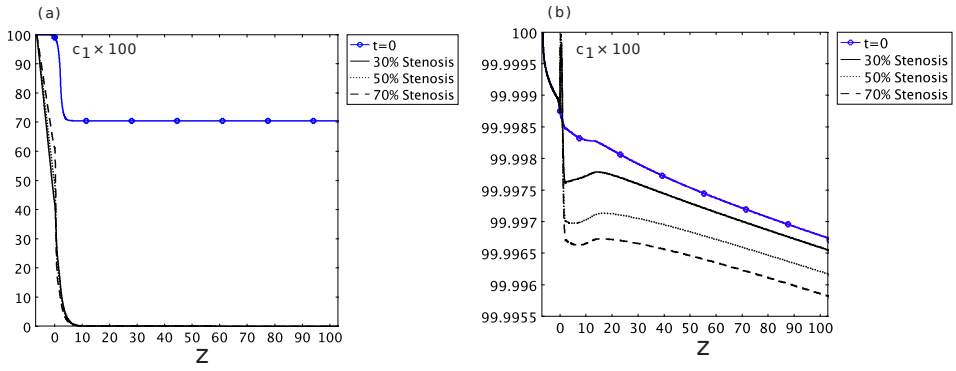

Figure 4.10: *Dimensionless concentration of LDL-particles at different degrees of stenosis at the moving boundary $\partial\Omega_w$ for the zero-convection model (a) and the Poiseuille model (b). The 30% stenosis degree is reached after 3.76×10^9, 1.21×10^9 time-units in ZC and Poiseuille model, respectively. The 50% stenosis degree is reached after 6.18×10^9, 2.04×10^9 time-units in ZC and Poiseuille model, respectively.*

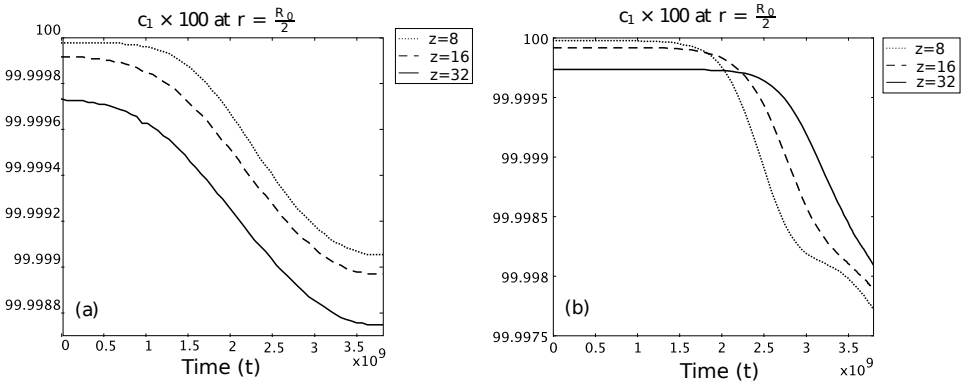

Figure 4.11: *Dimensionless concentration versus dimensionless time at three different locations downstream of the stenosis for the Poiseuille model (a) and the full model (b). Recirculation in (b) leads to crossings of the concentration curves corresponding to different values of z.*

are more or less parallel, whereas in (b) crossings of concentration curves corresponding to different z occur. This is again evidence for presence of a recirculation zone that extends at least to $r = 0.5$.

It is very interesting to see how recirculation affects the growth of the plaque region. To

this end we investigate the growth of the plaque volume, $V_p(t)$, defined by

$$V_p(t) = 2\pi \int_0^2 \int_{R(z,t)}^1 r dr dz, \tag{4.14}$$

in time.

In Fig. 4.12(a), the reduction in the minimal radius of the lumen is shown against time for the two different models discussed above. It can be seen from Fig. 4.12(a) that the full model leads to the largest reduction, closely followed by the Poiseuille model. The small differences between the Poiseuille and the full model are due to the fact that the value of $R_{\min}$ is largely determined by the wall shear stress at the top of the constriction. This value was seen to be only slightly larger in the full model as compared to the Poiseuille model and therefore the time dependence is very similar in both cases.

In Fig. 4.12(b), the plaque volume is depicted for the different models. Here we see again the same phenomenon as in (a), but the difference between Poiseuille model and the full model result is more pronounced. The volume increase of the plaque is, however, not limited to the increase of the plaque height, but includes growing of the width of the plaque. Due to presence of a recirculation zone in the full model, the plaque grows much faster in this region in the full model than in the Poiseuille model. This illustrates that the effect of recirculation is mainly to extend the plaque in the axial region rather than leading to an increased plaque height.

In this study, we are only concerned with the evolution in such a way that for longer times, the flow remains laminar and the evolution of plaques is not influenced by turbulence. In large sized arteries, realistically the flow Reynolds number becomes higher than what we have considered here. The impact of a high Reynolds number on the fixed stenosis is studied by various authors (See(Varghese et al. 2007, Mittal et al. 2001)). We repeated the simulations for different Reynolds numbers of laminar limit (100-500) but the temporal changes in LDL transfer remained similar in nature. The obvious change was in the length of recirculation zone which caused an enhanced growth of the constriction in time. The length of recirculation zone for high Reynolds numbers' flow involves simulations which are called Large Eddy Simulation (LES) ((Varghese et al. 2007, Mittal et al. 2001, Lantz and Karlsson 2012)). The computational costs increase with increasing Reynolds number due to the growing length of recirculation zone, which requires larger meshes.

4.5 Conclusions

We have developed a partial differential equations model describing the evolution of atherosclerosis for medium and large sized arteries. In our model the movement of the endothelium is

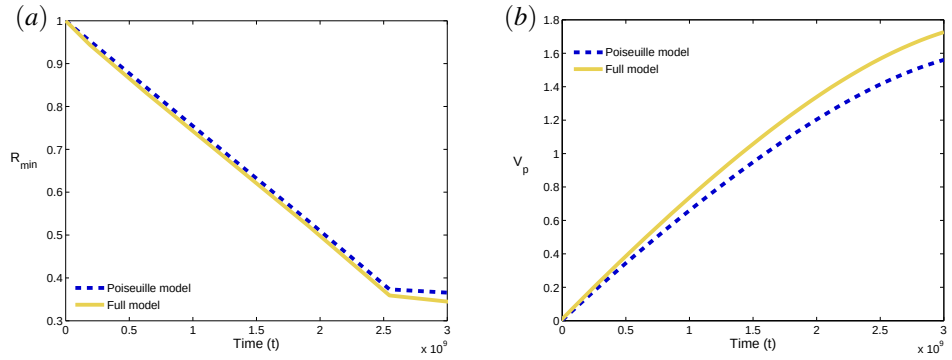

Figure 4.12: *The minimal value of $R(z,t)$ (a) and the plaque volume V_p (b) as a function of time for the Poiseuille model and the full model. Both models start at $R_{\min} = 1$ which corresponds to stenosis-free artery, which then decreases linearly with time. In the Poiseuille model the maximal constriction evolves slightly faster than for the full model. At $t \approx 2.5 \times 10^9$ time steps the minimal radius no longer grows as the shear stress becomes very large. The plaque then starts to remodel mostly in the axial direction. The plaque volume (b) first increases quadratically in time, but the growth levels off for larger times, when the t^2 term starts to play a role.*

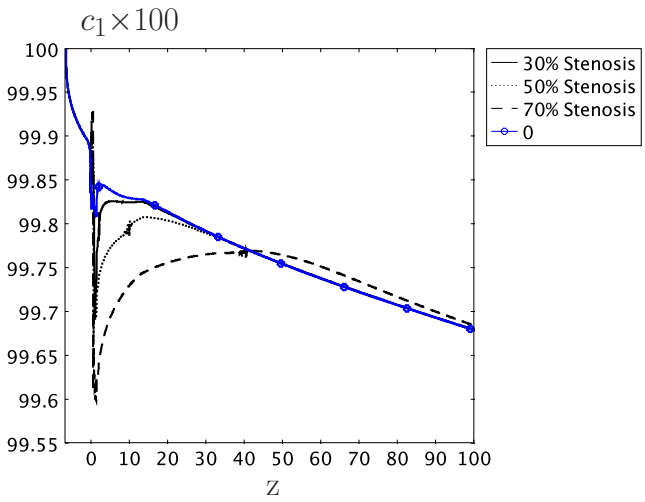

Figure 4.13: *The dimensionless concentration at four different times by varying the parameter $\tilde{k}_1$ from 3×10^{-8} to 3×10^{-6} while all other parameters were same as in the main model.*

governed by the shear-dependent low-density lipoprotein flux balance. The plaque growth is studied as a moving boundary problem. Although the model is only qualitative in nature it illustrates the effects of wall shear stress dependent permeability on plaque growth, by numerical computation of the movement of the plaque and the transfer of LDL particles.

The model was discretized in space by a finite element method and advanced in time by a time-stepping scheme. Numerical results were validated with published work on pulsating flows for short time scales and non-pulsating flow for fixed stenosis.

The flux of low-density lipoproteins across the endothelium was shown to depend rather strongly on wall shear stress. For the limiting case of Poiseulle flow additional numerical simulations were performed. LDL concentrations and plaque volume were compared with the full model results. It was shown that recirculation leads to larger plaque volumes and is hence detrimental to plaque evolution. Our computations suggest that recirculation leads predominantly to a broader plaque. Comparison with Poiseuille flows also revealed that assuming a Poisseuile flow renders results that compare well with solutions of the full Navier-Stokes model. This implies that a good estimate of plaque progression can be obtained at less expense. It also validates results previously obtained in (Bulelzai and Dubbeldam 2012) with ODE models in which Poiseuille flow was implicitly assumed.

To our knowledge there exist no experimental or clinical data in which systematic measurements of plaque shapes and occlusion areas are recorded in time. Clinical data of plaque shapes have revealed, however, that atherosclerotic plaques widely vary in shape (Cheng et al. 2006). The model that we investigated offers opportunities to improve models for atherosclerosis by taking the plaque geometry into account and can be seen as a step forward to bridge to enormous gap that exists between clinical observations and mathematical modeling.

Predicting the shape of the plaque could also be a possible way to determine parameters in the model. This would require data from clinical experiments and extension of the present model to include processes that have been neglected in this analysis. Extension of the model to include cap formation, elastic behavior, and biochemical processes such as macrophage recruitment, proliferation and diffusion is a daunting computational and modelling task in which close collaboration between the biomedical and the modeling society is demanded. Important steps on incorporating elasticity have been made by Holzapfel in e.g. (Holzapfel and Gasser 2000) and more recently by (van der Broek et al. 2011). This gives opportunities to create more advanced models in the near future.

4.6 Acknowledgment

We thank Duncan van der Heul and Rizwan Qaiser for their professional support. We are grateful to F. Gijssen for his comments and discussing clinical results. The Quaid-e-Awam University and TUD are acknowledged for financial support.

Chapter 5

Conclusions

In mathematics the art of proposing a question must be held of higher value than solving it.

Georg Cantor

This thesis presents models for the evolution of Atherosclerosis. In this study, we presented time dependent analysis of this disease and discussed criticall parameters, by which disease evolves rapidly. In the first Chapter, we gave a review of biomechanical and biochemical processes, which are involved in its progression. We also discussed how flow of blood has an impact on this disease. In Chapter 2, we introduced the model A and model B with a detailed analysis on how and why this model was chosen. We distinguish between the two models by incorporating shear stress as a parameter in model A and shear stress as a dynamic quantity in model B. Furthermore, it was also assumed that all the LDL that enters into the intima, are oxidized immidiately. It is pertinent to mention here, that we took two different equations for the evolution of monocytes and macrophages. The LDL supply to the walls of artery was taken as a parameter. We did not consider diffusion of macrophages out of the diseased area. The degradation of macrophages was directly added to the foam cells evolution. Comparing the two models, model A and model B, we find that the bistability of model A between two different states of equilibria type I and equilibria type II was no longer present in model B. This means that coupling the blood flow with evolution equations stabilizes the dynamics of the whole system. Nevertheless, although the threshold value of the cholesterol intake disappeared in model B, we demonstrated numerically that there is still a critical value of the LDL-uptake d_{crit}, which is independent of the shear rate parameter α, beyond which the lumen radius will drastically decrease. For high values of α, we see that plaques take much higher time to reduce the radius of arteries.

In chapter 3, we presented the complete bifurcation picture of codimension two of models A and model B. We found another critical value (Hopf curve), below which plaques are subjected to higher amounts of infiltration of monocytes recruitment. This thus, contributes to higher concentrations of plaques in arteries in areas of low endothelial shear stress. Though we did not cover codim 3 analysis in this thesis, we still found another parameter, that can influence the phase space and influences the growth of plaques.

In addition to a one-dimensional time dependent nonlinear system, and Poiseuille flow velocity, we also implemented the incompressible Navier-Stokes equations along with the convection-diffusion equation for LDL in chapter 4. We implemented a time-dependent moving boundary analysis for atherosclerosis. In this chapter, we explored different flow conditions and their impact on the evolution of plaques. The movement of wall of artery was governed by the flux of LDL. The flux of LDL across the endothelium was shown to depend strongly on wall shear stress. LDL concentrations and plaque volume were compared with the full model results. It was shown that recirculation leads to larger plaque volumes and is hence detrimental to plaque evolution. Our computations suggest that recirculation leads predominantly to a broader plaque and suggests importance of the inclusion of plaque geometry in models for atherosclerosis.

5.1 Recommendations

The model that we investigated offers opportunities to improve models for atherosclerosis by taking the plaque geometry into account. It can be seen as a step forward to bridge to enormous gap that exists between clinical observations and mathematical modeling. There is also need to take into account the effects of elastic behavior of arteries in the model as arteries have this tendency to regulate themselves to the changing flow conditions. Our current investigations aim at including the elastic properties of the arterial wall in a fashion similar to the methods first proposed by Holzapfel in (Holzapfel and Gasser 2000) and recently improved upon by (van der Broek et al. 2011). Clinical data will remain indispensable to construct increasingly realistic models and to obtain precise values of the model parameters, such that quantitatively predictive models can be realized in the near future.

Bibliography

Abdullah, I. and Amin, N.: 2010, A micropolar fluid model of blood flow through a tapered artery with a stenosis, *Mathematical Methods in the Applied Sciences,* **33(16)** pp. 1910–1923.

Ahmed, S. and Giddens, D.: 1983, Velocity measurements in steady flow through axisymmetric stenoses at moderate reynolds numbers, *J. Biomech.* **16(7)** pp. 505–516.

Arnold, L. and Jones, C.: 1994, Dynamical systems: Lecture notes in mathematics.

Bonert, M., Leask, R. L., Butany, J., Ethier, C., Myers, J., Johnston, K. and Ojha, M.: 2003, The relation between wall shear stress distributions and intimal thickening in the abdominal aorta, *Biom. Eng. Online* **2** *18* .

Bowry, V., Stanley, K. and Stocker, R.: 1992, High density lipoprotein is the major carrier of lipid hydroperoxides in human blood plasma from fasting donors, *Proc. Natl. Acad. Sci. USA 89* pp. 10316–10320.

Brenan, K., Campbell, S. and Petzold, L.: 1996, *Numerical solution of initial-value problems in differential-algebraic equations*, Philadelphia: Society for Industrial and Applied Mathematics.

Bulelzai, M. and Dubbeldam, J.: 2012, Long time evolution of atherosclerotic plaques, *J. Theor. Bio.* **297** pp. 1–10.

Bulelzai, M., Dubbeldam, J. and Lahaye, D.: 2013, Atherosclerotic plaque growth by shear stress dependent low-density lipoprotein transfer: the effect of recirculation, *Submitted to Cardiovascular Engineering and Technology* .

Calvez, V., Ebde, A., Meunier, N. and Raoult, A.: 2009, Mathematical modelling of the atherosclerotic plaque formation, *In: M. Ismail, B. Maury and J.-F. Gerbeau (Eds.), ESAIM: Proceedings,* **28** pp. 1–12.

Caro, C.: 2009, Discovery of the role of wall shear in atherosclerosis, *Arteriosclerosis, Thrombosis, and Vascular Biology, 29(2)* pp. 158–161.

Caro, C., Fitz-Gerald, J. and Schroter, R.: 1971, Atheroma and arterial wall shear observation, correlation and proposal of a shear dependent mass transfer mechanism for atherogenesis, *Proc. R. Soc. Lond. Ser. B Biol. Sci.* **177** pp. 109–159.

Chakravarti, S. and Mandal, P.: 2000, Two-dimensional blood flow through tapered arteries under stenotic conditions, *International Journal of Non-Linear Mechanics* **35** pp. 779–793.

Chatzisis, Y., Jonas, M. and Coskun, A.: 2008, Prediction of the localization of risk coronary atherosclerotic plaques on the basis of low endothelial shear stress: an intravascular ultrasound and histopathology natural history study, *Circulation* **117** pp. 993–1002.

Cheng, C., Tempel, D., Haperen, R., Baan, A., Grosveld, F., Daemen, M., Krams, R. and Crom, R.: 2006, Atherosclerotic lesion size and vulnerability are determined by patterns of fluid shear stress, *Circ. 113* pp. 2744–2753.

Chisolm, G., Hazen, S., Fox, P. and Cathcart, M.: 1999, The oxidation of lipoproteins by monocytes-macrophages, *J. Biol. Chem.* **274** pp. 25959–25962.

Cobbold, C., Sherratt, J. and Mexwell, S.: 2002, Lipoprotein oxidation and its significance for atherosclerosis: a mathematical approach, *Bull. of Math. Bio. 64* pp. 65–95.

Crank, J.: 1984, *Free and moving boundary problems*, Clarendon Press Oxford.

Crowther, M.: 2005, Pathogenesis of atherosclerosis, thrombosis 1, *American Society of Hematology* pp. 436–441.

Dabagh, M., Jalali, P. and Tarbell, J.: 2009, The transport of ldl across the deformable arterial wall: the effect of endothelial cell turnover and intimal deformation under hypertension, *Am J Physiol. Heart Circ. Physiol.* **297(3)** pp. H983–H996.

Davis, N. E.: 2005, Atherosclerosis– an inflammatory process, *J. of Ins. Med. 37* pp. 72–75.

Davis, P.: 1986, Biology of disease; vascular cell interactions with special reference to the pathogenesis of atherosclerosis, *Lab. Invest. 55* pp. 5–24.

de Korte, C. and van der Steen, A.: 2002, Intravascular ultrasound elastography: an overview, *Ultrasonics* **40** pp. 859–865.

Desroches, M., Krauskopf, B. and Osinga, H.: 2008, The geometry of slow manifolds near a folded node, *SIAM J. Appl. Dyn. Syst. 7(4)* pp. 1131–1162.

Dhooge, A., Govaerts, W., Kuznetsov, Y. A., Meijer, H. and Sautois, B.: 2008, New features of the software matcont for bifurcation analysis of dynamical systems, *Mathematical and Computer Modelling of Dynamical Systems, 14(2)* pp. 147–175.

Doedel, E. and Oldman, B.: 2012, Auto-07p:continuation and bifurcation software for ordinary differential equations. available at `http://sourceforge.net/projects/auto-07p/`.

Dormandy, J.: 1970, Clinical significance of blood viscosity, *Annals of the Royal College of Surgeons of England 47(4)* p. 211.

Dumortier, F., Roussarie, R. and Sotomayor, I.: 1991, Generic 3-parameter families of planar vector fields. unfoldings of saddle, focus and elliptic singularities with nilpotent linear parts, *Springer Lecture Notes in Mathematics 1480* pp. 1–164.

Ethier, C.: 2002, Computational modeling of mass transfer and links to atherosclerosis, *Annals of biomedical engineering* **30(4)** pp. 461–471.

Falk, E.: 2006, The pathogenesis of atherosclerosis, *N. Am. Coll. Cardiol. 47 No. 8 (Suppl C)* pp. C7–12.

Fan, J. and Wanatabe, T.: 2003, Inflammatory reactions in the pathogenesis of atherosclerosis, *J. Atheroscl. Thromb.* **10** pp. 63–71.

Fok, P.: 2012, Mathematical model of initimal thickening in atherosclerosis: vessel stenosis as a free boundary problem, *J. Theor. Biol., 314, 23* .

Frisdal, E., Lesnik, P., Olivier, M., Robilard, P., Chapman, M., Huby, T., Guerin, M. and Goff, W. L.: 2011, Interleukin-6 protects human macrophages from cellular cholesterol accumulation and attenuates the pro-inflammatory response, *J. Biol. Chem., M111.264325v1* .

Gazolaz, D., Graneroro-Belinchó, R. and Illera, R.: 2013, The confined muskat problem: differences with the deep water regime, *arXiv:1209.1575v2* .

Gear, C., Kaper, T., Kevrekidis, I. and Zagaris, A.: 2005, Projecting to a slow manifold: Singularly perturbed systems and legacy codes, *SIAM Journal on Applied Dynamical Systems, 4(3)* pp. 711–732.

Gerrity, R.: 1981, Monocytes and atherogenesis, *Am. J. Pathol.* **103** pp. 191–200.

Gijsen, F., Wentzel, J., Thury, A., Mastik, F., Schaar, J., Schuurbiers, J., Slager, C., van der Giesen, W., de Feyter, P., van der Steen, A. and Serruys, P.: 2008, Strain distribution in human coronary arteries relates to shear stress, *Am. J. Physiol. Heart Circ. Physiol.* **295** pp. H1608–H1614.

Goldstein, J. and Brown, M.: 1977, The low-density lipoprotein pathway and its resolution to atherosclerosis, *Annu. Rev. Biochem. 46* pp. 897–930.

Gotlieb, A. I.: 2007, http://www.asip.org/edu/documents/hs/gotlieb-additional notespages.doc.

Guckenheimer, J. and Holmes, P.: 1983, Nonlinear oscillations, dynamical systems, and bifurcations of vector fields, *(Volume 42), Springer-Verlag New York Inc.* .

Guckenheimer, J., Johnson, T. and Meerkamp, P.: 2012, Rigorous enclosure of a slow manifold, *SIAM Journal on Applied Dynamical Systems, 11(3)* pp. 831–863.

Hansson, G. and Libby, P.: 2006, The immune response in atherosclerosis: a double edged sword, *Nat. Immunol.* **6** pp. 508–519.

Holzapfel, G. A. and Gasser, T. C.: 2000, A new constitutive framework for arterial wall mechanics and a comparative study of material models, *J. Elasticity* **61** pp. 1–48.

Hulthe, J., Bokemark, L., Wikstrand, J. and Fagerberg, B.: 2000, The metabolic syndrome, ldl particle size and atherosclerosis, *Atheroscl. Thromb. Vasc. Biol.* **20** pp. 2140–2147.

Ibragimov, A., Neal, C. M., Ritter, L. and Walton, J.: 2005, A mathematical model of atherogenesis as an inflammatory response, *Math Med Biol.* **22** pp. 305–333.

Ismail, Z., Abdullah, I., Mustapha, N. and Amin, N.: 2008, A power-law model of blood flow through a tapered overlapping stenosed artery, *Applied Mathematics and Computation,* **195(2)** pp. 669–680.

Kaper, H. and Kaper, T.: 2002, Asymptotic analysis of two reduction methods for systems of chemical reactions, *Physica D: Nonlinear Phenomena, 165(1)* pp. 66–93.

Khatib, N. E., Genieys, S., Kazmierczak, B. and Volpert, V.: 2009, Mathematical modeling of atherosclerosis as an inflammatory disease, *Phil. Trans. R. Soc. A* **367** pp. 4877–4886.

Khatib, N. E., Genieys, S. and Volpert, V.: 2007, Atherosclerosis initiation modeled as an inflammatory process, *Math. Model. Nat. Phenom.* **2** pp. 126–141.

Khatib, N. E., Génieys, S. and Volpert, V.: 2012, Reaction-diffusion of atherosclerosis development, *J. Math. Biol. 65, 349* .

Koskinas, K., Chatzizisis, Y., baker, A., Edelman, E., Stone, P. and Feldman, C.: 2009, The role of low endothelial shear stress in the conversion of atherosclerotic lesions from stable to unstable plaque, *Curr. Opin. Cardiol.* **24** pp. 580–590.

Krakauer, J.: 2007, The complex dynamics of stroke onset and progression, *Curr Opin Neurol. 20(1)* pp. 47–50.

Krombach, F., Münzing, S., Allmeling, A., Gerlach, J., Behr, J. and Dörger, M.: 1997, Cell size of alveolar macrophages: an interspecies comparison, *Environ. Health Perspect.* **105 Suppl 5** pp. 1261–1263.

Kruth, H., Huang, W., Ishii, I. and Zang, W.: 2002, Macrophage foam cell formation with native low density lipoprotein, *J. Biol. Chem.* **37** pp. 34574–34580.

Kuvin, J. and Kimmelstiel, C.: 1999, Infectious causes of atherosclerosis, *American heart journal, 137(2)* pp. 216–226.

Kuznetsov, Y.: 1996, Elements of applied bifurcation analysis, *Springer Berlin* .

Kuznetsov, Y.: 1999, Numerical normalization techniques for all codim 2 bifurcations of equilibria in ode's, *SIAM journal on numerical analysis, 36(4)* pp. 1104–1124.

Landau, L., Lifchits, E., Landaou, L. and Pitaevski, L.: 1987, *Course of Theoretical Physics, vol.6*, Butherworth-Heinemann.

Lantz, J. and Karlsson, M.: 2012, Large eddy simulation of ldl surface concentration in a subject specific human aorta, *J. Biomech.* **(45)** pp. 537–542.

Levesque, M. and Nerem, R.: 1985, The elongation and orientation of cultured endothelial cells in response to shear stress, *J. Biomech. Eng. 107* pp. 341–347.

Li, Z.-Y., Howarth, S., Tang, T. and Gillard, J.: 2006, How critical is fibrous cap thickness to carotid plaque stability, *Stroke* **37** pp. 1195–1999.

Libby, P., Ridker, P. and Maseri, A.: 2002, Inflammation and atherosclerosis, *Circulation, 105(9)* pp. 1135–1143.

Lipowsky, H.: 2005, Microvascular rheology and hemodynamics, *Microcirculation* **12** pp. 5–15.

Liu, B. and Tang, D.: 2010, Computer simulations of atherosclerotic plaque growth in coronary arteries, *Mol. Cell Biomech. 07* pp. 193–202.

Llodra, J., Angeli, V., Liu, J., Trogan, E., Fisher, E. and Randolph, G.: 2004, Emigration of monocyte-derived cells from atherosclerotic lesions of mice characterizes regressive, but not progressive, plaques, *Proc. Natl. Acad. of Sci.* **101** pp. 11779–11784.

Luscher, T., Tanner, F. and Noll, G.: 1996, Lipids and endothelial function: effects of lipid-lowering and other therapeutic interventions, *Curr. Opin. Lipidol. 7* pp. 234–40.

Mach, F.: 2005, Inflammation is a crucial feature of atherosclerosis and a potential target to reduce cardiovascular events, *Atherosclerosis: Diet and Drugs, A. v. Eckardstein, ed., Springer-Verlag, Berlin* pp. 697–722.

Malek, A., Alper, S. and Izumo, S.: 1999, Hemodynamic shear stress and its role in atherosclerosis, *J. Am Med. Assoc.* **282** pp. 2035–2042.

Maoz, H., Plliack, A., Barak, V., Yatziv, S., Birian, S., Giloh, H. and Treves, A.: 1986, Parameters affecting in vitro maturation of human monocytes to macrophages, *Int. J. Cell Cloning* **4** pp. 167–185.

Mckay, C., Mckee, S., Mottran, N., Mulholland, T. and Wilson, S.: 2005, Towards a model of atherosclerosis, *Available online at Strathclyde University* .

Mittal, R., Simmons, S. and Udaykumar, H.: 2001, Application of large-eddy simulation to the study of pulsatile flow in a modeled arterial stenosis, *J. biom. eng.,* **123(4)** p. 325.

Niehaus, C., Wootton, R., Lewis, R., Nicoll, J., Williams, A., Coltart, D. and Lewis, B.: 1977, Influence of lipid concentrations and age on transfer of plasma lipoprotein into human arterial intima, *The Lancet* **310 (8036)** pp. 469–471.

Nielsen, L.: 1996, Transfer of low density lipoprotein into the arterial wall and risk of atherosclerosis, *Atherosclerosis* **123** pp. 1–15.

Ogunrinade, O., Kameya, G. and Truskey, G.: 2002, Effect of fluid stress on the permeability of the arterial endothelium, *Ann. Biomed. Eng.* **30** pp. 430–446.

Ota, H., Takase, K., Rikimaru, H., Tsuboi, M., Yamada, T. and A. Sato, a. S. T.: 2005, Quantitative vascular measurements in arterial occlusive disease, *Radiographics,* **25(5)** pp. 1141–1158.

Ougrinovskaia, A., Thompson, R. and Myerscough, M.: 2010, An ode model of early stages of atherosclerosis: Mechanisms of the inflammatory response, *Bull. Math. Biol.* **72** pp. 1534–1561.

Parthasarathy, S., Barnett, J. and Fong, L.: 1990, High-density lipoprotein inhibits the oxidative modification of low-density lipoprotein, *Biochim. Biophys. Acta 1044* pp. 275–283.

Pedley, T. and Luo, X.: 1995, *Fluid mechanics of large blood vessels*, Shaanxi People's Press.

Pherson, D. M., Johanson, M., Alvarez, N., Collins, N., Armstrong, S., Kieso, R., Thorpe, J., Marcus, M. and Kerber, R.: 1992, Variable morphology of coronary atheroclerosis: Characterization of atherosclerotic plaque and residual arterial umen size and shape by epicardial achocardiography, *JACC 19* pp. 593–399.

Pozrikidis, C.: 2010, Numerical simulation of blood and interstitial flow through a solid tumor, *J. Math. Biology, 60(1)* pp. 75–94.

Quarteroni, A., Veneziani, A. and Zunino, P.: 2002, Mathematical and numerical modeling of solute dynamics in blood flow and arterial walls, *SIAM J. Numer. Anal. Vol.* **39, No. 5** pp. 1488–1511.

Rappitsch, G. and Perktold, K.: 1996a, Computer simulation of convective diffusion processes in large arteries, *J. Biomech.* **29** pp. 207–215.

Rappitsch, G. and Perktold, K.: 1996b, Pulsatile albumin transport in large arteries: a numerical simulation study, *J Biomech Eng.* **118(4)** pp. 511–519.

Rappitsch, G., Perktold, K. and Pernkopf, E.: 1997, Numerical modeling of shear-dependent mass transfer in large arteries, *Int. J. Numer. Methods Fluids* **25** pp. 847–857.

Ross, R.: 1986, The pathogenesis of atherosclerosis - an update, *N Engl J med 314* pp. 488–500.

Ross, R.: 1993, Atherosclerosis: a defense mechanism gone awry, *Am. J. Pathol.* **143** pp. 987–1002.

Ross, R. and Glomset, J.: 1976a, The pathogenesis of atherosclerosis, *N. Engl. J. Med. 295* pp. 369–373.

Ross, R. and Glomset, J.: 1976b, The pathogenesis of atherosclerosis, *N. Engl. J. Med. 295* pp. 420–425.

Ross, R. and Harker, I.: 1976, Hyperlipidemia and atherosclerosis, *Science* **193** pp. 1094–1100.

Sakllarios, A., Siogkas, P., Tsakanikas, V., Stefanou, K., Michalis, L. and Fotiadis, D.: 2010, Simulation of the effect of tachycardia on atherosclerotic plaque development based on the ldl transport in coronary arteries, *Computing in Cardiology, IEEE* pp. 329–332.

Sandler, M. and Bourne, G.: 1963, *Atherosclerosis and its origin*, Academic Press.

Schwartz, S. and Reidy, M.: 1987, Common mechanism of proliferation of smooth muscle in atherosclerosis, *Hum. Pathol. 18* pp. 240–248.

Shaaban, A. M. and Deurinckx, A. J.: 2000, Wall shear stress and early atherosclerosis: A review, *JKR 174* .

Sheard, R., Ryan, G. and Fouras, A.: 2009, The validity of axisymmetric assumptions when investigating pulsatile biological flows, *ANZIAM Journal, 50* pp. C713–C728.

Slager, C., Wentzel, J., Gijsen, F., Thury, A., der Wal, A. V., Schaar, J. and Serruys, P.: 2005, The role of shear stress in the destabilization of vulnerable plaques and related therapeutic implications, *Nature clinical practice cardiovascular medicine,* **2(9)** pp. 456–464.

Stadius, M., Rowan, R., Fleischhauer, J., Kernoff, R., Billingham, M. and Gown, A.: 1992, Time course and cellular characteristics of the iliac artery response to acute balloon injury. an angiographic, morphometric, and immunocytochemical analysis in the cholesterol-fed new zealand white rabbit, *Arteriosclerosis, Thrombosis, and Vascular Biology, 12(11)* pp. 1267–1273.

Sun, N., Wood, N., Hughes, A., Thom, S. and Xu, X.: 2006, Fluid-wall modeling of mass transfer in an axisymmetric stenosis: effects of shear-dependent transport properties, *Ann. Biomed. Eng.* **34** pp. 1119–1128.

Upchurch, G., Welch, G. and Loscalzo, J.: 1996, Homocysteine, edrf and endothelial function, *Journal of Nutrition* **126**(4), 1290.

van der Broek, C., van der Horst, A., Rutten, M. and van de Vosse, F.: 2011, A generic constitutive model for the passive porcine coronary artery, *Biomech. Model Biomechanobiol. 10* pp. 249–258.

Varghese, S., Frankel, S. and Fischer, P.: 2007, Direct numerical simulation of stenotic flows. part 1. steady flow, *J. Fluid Mech.* **582(1)** pp. 253–280.

Wang, H.: 2001, Analytical models of atherosclerosis, *Atherosclerosis 159* pp. 1–7.

Wieczorek, S., Ashwin, P., Luke, C. and Cox, P.: 2011, Excitability in ramped systems: the compost-bomb instability, *Proceedings of the Royal Society A: Mathematical, Physical and Engineering Science, 467(2129)* pp. 1243–1269.

Xing, X., Baffic, J. and Sparrow, C.: 1998, Ldl oxidation by activated monocytes: characterization of the oxidized ldl and requirement of metal ions, *J. Lipid Res.* **39** pp. 2201–2208.

Yang, N. and Vafai, K.: 2006, Modeling of low-density lipoprotein (ldl) transport in the artery- effects of hypertension, *Int. J. Heat Mass Transfer* **49** pp. 850–867.

Zohdi, T.: 2005, A simple model for shear stress mediated lumen reduction in blood vessels, *Biomech. Model Mechanobiol.* **4** pp. 57–61.

Zohdi, T., Holzapfel, G. and Berger, S.: 2004, A phenomenological model for atherosclerotic plaque growth and rupture, *J. Theor. Biol.* **227** pp. 437–443.

Summary

Atherosclerosis is a disease in which low density lipoproteins (LDL) accumulate in the arterial wall due to an inflammatory response, which is triggered by the oxidation of LDL molecules that are already present in the arterial wall. Progression of atherosclerotic plaques involves many components which includes, macrophages, monocytes, LDL, oxidized-LDL, cytokines etc. Clinical data is scarce for the long term evolution of plaques, therefore, mathematical models provide an alternative to enhance our knowledge in predicting and analyzing the complex processes in the advancement of atherosclerosis. In this thesis, we study different simplified mathematical models and analyse the long term behavior of evolution of plaques. One model we studied, consisted of ordinary differential equations that could be coupled and decoupled to the blood flow. Another model was also developed, which consisted of partial differential equations and that treats the artery wall as a moving boundary problem.

The ordinary differential equations (ODE) model consisted of nonlinear coupled equations for oxidized-LDL, monocytes, macrophages, foam cells and radius of the artery (which can also be translated into an equation for endothelial shear stress). The model is distinguished by model A which is decoupled to the blood flow and model B, which is coupled to blood flow. The model B we call in thesis to be self-consistent system. Both models are time dependent and do not take account of geometry of the artery. Both these models have many parameters, which affect the growth of concentrations in time. A bifurcation analysis was therefore presented in this thesis to understand the impact of varying parameters on the system. For this purpose, a complete codimension two bifurcation analysis was carried out and singularities in the system were discussed. We found that the system, model A, can also have a codimension three bifurcation point (the degenerate Bogdanov-takens point). In model A, bistability and multistability was found to depend on the value of the parameter e. The parameter e is the ingestion rate of oxidized-LDL particles by macrophages in the equation for oxidized-LDL. The regions of stable and unstable equilibria and limit cycles were depicted with the two parameter diagrams. These regions were presented for cases with ingestion rate vs. LDL intake and shear stress vs. LDL intake. A threshold value d_{crit} was found for the LDL particles beyond which occlusion of the plaque seems inevitable. Two other critical parameter values for ingestion rates were also found. These values b_{crit} and e_{crit} were presented along with the Hopf curve as a function of parameters (d,b) and (σ,d), which constitute a critical curve in the system. In model B, the multistability was disappeared and the attachment of blood flow profile stabilized the dynamics of the artery. For understanding the long term response of the suspended system in model B, we have carried out a slow-fast system analysis. This shows that the stable healthy state of $(0,M_0,0,R_0)$ may be perturbed for short amount of times, but

ultimately the suspended system always comes to a stationary point. This all depends on the values of parameters d, b, e. The reduction in radius was found to be proportional to cholesterol intake parameter. For longer times, the radius goes quasi-static suggesting the results to be physically viable.

A complex time dependent moving endothelium model was also presented in an axi-symmetric setting in order to understand the role played by the geometry in the problem. To this end, the Navier-Stokes equations for blood flow were coupled with the convection-diffusion equation for LDL in lumen and a diffusion equation for oxidized-LDL in intima. These equations were coupled to a common boundary (the endothelium) and solved to study the long term effects of recirculation on LDL. The flux of low-density lipoproteins across the endothelium was shown to depend rather strongly on wall shear stress. For the limiting case of Poiseuille flow additional numerical simulations were performed. LDL concentrations and plaque volume were compared with the full model results. It was shown that recirculation leads to larger plaque volumes and is hence detrimental to plaque evolution. Our computations suggest that recirculation leads predominantly to a broader plaque. Comparison with Poiseuille flows also revealed that assuming a Poiseuille flow renders results that compare well with solutions of the full Navier-Stokes model. This implies that a good estimate of plaque progression can be obtained at less expense. It also validates results obtained in ODE model in which Poiseuille flow was implicitly assumed.

For a better mechanical understanding of remodeling of the artery, the stress-strain analysis may also be carried out. For this purpose, fluid-structure interaction (FSI) technique should be applied to the axisymmetric model we proposed.

For a quantitative and realistic model the clinical data is vital to understand the growth of plaques. Such data will remain indispensable to construct increasingly realistic models and to obtain precise values of the model parameters, such that qualitatively predictive models can be realized in near future. Future close collaboration between clinical researchers and applied mathematicians will therefore be essential for progress in the this field.

Samenvatting

Atherosclerose is een ziekte waarbij LDL-cholesterol zich ophoopt in de aderwand. Dit wordt veroorzaakt door een ontstekingsreactie die ontstaat als gevolg van oxidatie van LDL cholesterol dat in de vaatwand is binnen gedrongen .

Het verloop van atherosclerose is een ingewikkeld proces, waarbij zeer veel biochemische componenten een rol spelen, zoals bijvoorbeeld monocyten, macrofagen, cytokinen, LDL en HDL cholesterol, NO en nog een groot aantal andere. Bovendien is er ook nog een biomechanische component die atherosclerose beïnvloedt, namelijk de afschuifspanning op de vaatwand. Al deze interacties leiden tot een complex fenomeen dat bovendien plaatsvindt op een tijdschaal van 15 tot 20 jaar. Deze tijdschaal is veel langer dan de tijdschaal waarop de biochemische processen plaatsvinden en dit maakt atherosclerose-progressie daarom een veel tijdschalen probleem. Hoewel klinische experimenten al een aantal aspecten van atherosclerose aan het licht hebben gebracht, is het nog steeds niet duidelijk hoe de progressie ervan precies in zijn werk gaat. In dit proefschrift hebben we bestudeerd hoe mathematische modellen gebruikt kunnen worden bij het voorspellen van de groei van de karakteristieke plaques die ontstaan als LDL zich in de aderwand ophoopt.

We hebben in dit proefschrift twee simpele modellen ontwikkeld die de ontwikkeling van atherosclerose kunnen voorspellen. Het eerste model gebruikt een eenvoudig gewone differentiaalvergelijkingen model. Het tweede, model bestaat uit een eindige elementen model waarin de Navier-Stokes vergelijkingen op een eenvoudige manier gekoppeld worden aan de groei van de plaque. Het voordeel van het model dat bestaat uit gekoppelde niet-lineaire gewone differentiaalvergelijkingen is dat een bifurcatie analyse kan worden uitgevoerd. Dit is hier gedaan voor het codimensie-twee geval. Onze analyse toont aan dat de dynamica kan worden begrepen uit deze bifurcatie-analyse. Het systeem bevat een Bogdanov-Takens bifurcatie als organizerend punt in het bifurcatiediagram. Het blijkt dat er voor het onstaan van atherosclerose inderdaad een drempelwaarde voor de inname van LDL cholesterol is en dat deze drempelwaarde afhangt van levensduur van de macrofagen. Verder vinden we dat er gebieden zijn in de parameterruimte waar er oscillaties zijn in de macrofaag, monocyt en LDL concentratie. Als er in de toekomst experimenten mogelijk zijn die dergelijke bevindingen kunnen bekrachtigen of weerleggen, geeft deze bifurcatiestudie een extra instrument om het parametergebied waarop het model geldig is af te bakenen.

Het gewone differentiaalvergelijkingen model hebben we vervolgens uitgebreid door dit model op een zelfconsistente manier te koppelen aan de bloedstroming door de ader. Dit aangepaste model is hier bestudeerd door middel van numerieke simulaties en een langzame variëteiten analyse. Deze

berekeningen laten zien dat de reductie in de aderradius afhangt van een aantal parameters, zoals de levensduur van de macrofagen en de snelheid waarmee macrofagen de LDL kunnen wegvangen. Vanuit een mathematisch standpunt is de dynamica in dit systeem erg interessant. Wanneer er geen koppeling is met de bloedstroming blijken er meerdere stabiele evenwichten te bestaan, die in het model met de koppeling aan de bloedstroming weer verdwenen zijn. In het gekoppelde geval wordt de dynamica die uit het ongekoppelde model na voren kwam, successievelijk doorlopen. Dit doet erg denken aan de zogenaamde 'ramped' bifurcaties waarin de bifurcatie parameter langzaam in de tijd verandert en die bijvoorbeeld in de klimaatmodellen een rol spelen.

In het partiële differentiaalvergelijkingen model dat we ontwikkeld hebben, beschouwen we de ontwikkeling van een plaque in een axi-symmetrische setting. We modelleren een plaque waarvan de rand in de tijd beweegt en berekenen met eindige elementen de plaats van de plaque. Op deze manier bestuderen we het effect van recirculatie en separatie van de bloedstroming op de ontwikkeling van plaques in het simpele geval dat alleen LDL het plaque-volume bepaalt. Het blijkt dat recirculatie resulteert in bredere plaques. Een vergelijking met resultaten voor Poiseuille-stroming laat bovendien zien dat de resultaten voor het volledige model en het Poiseuille model goed overeenkomen. Dit betekent dat voor toekomstige simulaties op rekentijd kan worden bespaard, omdat de Poseuille stroming een goede "proxy" is voor het stromingsprofiel in het bloed, in de onderzochte axisymmetrische configuratie.

Om uiteindelijk een kwantitatief wiskundig model te krijgen voor de beweging van de aderwand in de tijd, is een aantal aanpassingen nodig in het huidige model. Ten eerste zal de modelering van de eigenschappen vaatwand moeten worden verbeterd, zodat ook de elasticiteit van de vaatwand kan worden betrokken bij de studie. In het bijzonder kan dan vervorming van de ader aan de buitenkant, zogenaamde "outward remodeling" worden bestudeerd. Verder is een goed contact tussen klinische onderzoekers en wiskundigen essentieel om te zorgen dat de belangrijke effecten worden meegenomen in de modellen en voor de bepaling van de vele parameters die de wiskundige modellen bevatten. Als aan deze voorwaarden voldaan wordt kan er nog grote vooruitgang worden geboekt in het begrijpen en modelleren van de processen die bij de ontwikkeling en progressie van atherosclerose een rol spelen.

Acknowledgments

Many people have contributed to the completion of this thesis, directly or indirectly. Therefore, here I would like to extend my gratitude to those who somehow made it possible for me to finish this thesis. Before, I do so, I remember my parents, Muhammad Hanif Khan & Raheem Khatoon, who will always remain in my good memories. May they live in peace! ab-sit-omen.

When I came to The Netherlands, I was fascinated with the people and culture around. I loved it! I would like to thank Johan who helped me follow my goal not only in the capacity of a supervisor but also as a teacher and friend. He really helped me come to a level of scientific aptitude which I lacked when I joined TUD. I would like to thank him for our research discussions, and for carefully reading my papers. What a fascinating and unforgettable experience it was working in TUD for my Phd. As none of this would have been possible without the generous help of the group of Mathematical Physics in general and Johan in particular.

Furthermore, I thank two senior researchers of our department, Wim van Horssen, and Prof. A.W. Heemink for their professional and critical guidance over the time. I would like to thank people from numerical analysis group who guided us with tough calculations. I must name Prof. C. Vuik, Duncan van der Heul and Domenico Lahaye for their support to our numerical results. I also like to thank Dr. Hil Meijer from TU Twente and Dr. Domenico Lahaye who helped me in bifurcation analysis and Comsol analysis respectively and devoted some of their time in the production of this thesis. Kees Lemmens has helped me a lot to work in my office by his support on different facets of Linux, and other computer assistance which was very much technical for me. Franca post and CICAT must be thanked as they helped us administratively and remained only one email away to assist us. I must thank our secretaries Evelyn Sharabi (note the name in Urdu!), Dorothée Engering, and T. Steeneken who assisted me in all official matters and also nice lunches in lunch meetings (of course the annual trips and Christmas buffet as well). I appreciate and thank my room-mates Maria, Sevetlana, Syed, Morteza Hassanabadi and Xiaoyan Wei for their time and help to work in my office. I also thank colleagues from our mathematics department that includes Rafae, Umer Altaf, Sandilo, Haider, Rajab, Budiarto, Mariam, Abdul, Fahim, Nick, Mohit, Wei, and others who all, have been a great company. I would like to thank precious friends whom I met with, and now it seems, we are friends forever. These valuable friends have given me so many parties, so many outside tours and so much time I have spent that it will be difficult to forget a single friend. These friends include Faisal (man having heaven in his mind),

Seyab (the coolest Gengiz Khan), Laiq (the passionate traveler), Devender (the party boy), Cheema (the ABBU), Fakhar (the cool mind), Imran (the generous man), Kazmi (the humblest man), Humayun (the great man), Iftikhar (the lovely bird), Rafiullah (the serious man), Bilal (the singer), Faisal Karim (the player!), Abdul (the sweet melody), Sarfaraz Muneer (the IKKA), Sajad (the golden man), Ahson Jabbar (the rebellion), Rajab (the jolly man), Haider (the courageous man), Fahim (the cricketer), Nick (the fighter), Zubair (the hunk with beard), Tabish (the finisher), Usama (the President), Umer Ijaz (the Bro) and others (Pardon if I forget anyone here!). Muneerah, my especial thanks to you for bringing love and passion in my life. You have been a great friend and yes, who can forget those delicious mexican meals!

On this note, I also like to mention my previous teachers Prof.Dr. Zakaullah Khan and Prof.Dr. Noor Mustafa Sheikh who created interest in me, to pursue higher studies. I must praise the encouragements from my family members, Bajjo (divine), Aapi (rhythmic), Bi aapa (endurance), Bhai jan (ahm ahm!), Tahir bhai (ahm ahm!), Asif (the ultimate dignity) and all kids of our home (all shonu paras!). I thank my dearest friends who kept in touch with me from Pakistan, they include, Ghayor (the furious), Kashif (the furious), Fahad (the coolness), Habib (the logic), Umair (the Einstein), Hussein Mangi (the lover), Asim Soomro (the passionate), Pir Tanveer (the kindness) and others.

“Nobody ever figures out what life is all about, and it doesn’t matter. Explore the world. Nearly everything is really interesting if you go into it deeply enough.”– Richard P. Feynman

M.A.K. Bulelzai
TU Delft
November 18, 2013

Curriculum Vitae

M. Atif Khan Bulelzai was born in Hyderabad, Pakistan on September 28, 1978. He finshed his secondary education in his native city. He moved on to follow a university bachelors degree in Mathematics from Institute of Mathematics and Computer Science, University of Sindh, Jamshoro, Pakistan. After completing B.Sc.(Hons) in Mathematics in 2000, he subsequently completed his masters degree (M.Sc.) in Mathematics from University of Sindh, Jamshoro, Pakistan in 2002. He started teaching at Isra schools and The city school in Pakistan susequently. He joined Quaid-e-Awam university as Lecturer in Mathematics in the department of Basic Sciences and related studies on January 07, 2005. He started his Phd formally on November 01, 2008 in the Delft Institute of Applied Mathematics in Delft Technical University under supervision of Dr. J.L.A. Dubbeldam.